공학박사 학위논문

Data-Based Evaluation and Updating of Bridge Reliability Considering Traffic Environment and Strength Degradation

교통환경 및 강도저하를 고려한 데이터 기반 교량 신뢰도 평가 및 업데이팅

2021년 8월

서울대학교 대학원

건설환경공학부

김 지 환

Data-Based Evaluation and Updating of Bridge Reliability Considering Traffic Environment and Strength Degradation

교통환경 및 강도저하를 고려한 데이터 기반 교량 신뢰도 평가 및 업데이팅

지도교수 송 준 호

이 논문을 공학박사 학위논문으로 제출함

2021년 8월

서울대학교 대학원

건설환경공학부

김 지 환

김지환의 공학박사 학위논문을 인준함

2021년 8월

위 원 장 김 호 경

부 위 원 장 송 준 호

위 원 이 해 성

위 원 이 영 주

위 원 강 원 희

Abstract

A bridge is subjected to various kinds of loads from the environmental conditions, and changes in its condition and performance, such as structural degradation due to aging over its service life. Therefore, in efforts regarding bridge maintenance, it is essential to continuously monitor these changes in conditions and evaluate the bridge reliability accordingly. Among the various types of loads, one of the most uncertain loads in the general environment condition, excluding those caused by disasters such as wind and earthquake load, is the traffic load. Therefore, it is important to accurately estimate traffic loads by considering uncertainty through probabilistic methods for the purpose of the design and condition evaluation of bridges. However, most studies have focused on elaborate modeling of strength degradation and deterioration processes to consider the strength degradation of bridge members, while paying relatively less attention to the traffic load effects on the bridge reliability. Therefore, this dissertation aims to evaluate the bridge reliability by sophisticated estimation of not only the strength of bridge members but also the traffic load effects on the members. Specifically, the dissertation presents a new framework for evaluating and updating reliability over the service life of post-tensioned concrete (PSC) box girder bridges by considering flexural strength degradation due to corrosion of strands, and changes in traffic load effects caused by traffic environment changes.

First, to estimate the traffic loads while reflecting the diverse conditions of the traffic environment of the bridge, a comprehensive probabilistic model for bridge

traffic load is developed based on the WIM data collected in three sites (Gimcheon, Sunsan, and Waegwan) of South Korea. Key variables are identified and then probabilistic models for them are developed based on statistical studies, theories of transportation engineering, and the analysis of WIM data representing the traffic environment. For a congested traffic flow, microsimulation models are introduced to consider changes in the lane and speed of vehicles. Numerical examples rigorously verify the developed model and confirm that the multiple presence factor of the current design code is conservative. In addition, a simple parametric study shows that the developed model can quantitatively evaluate the effect of changes in the key variables on the traffic load effects because all variables in the developed model are parameterized.

Second, a Bayesian updating methodology is proposed to update traffic load effects by using in-service traffic data based on the changing traffic environment over time. Gaussian-inverse gamma distribution, Bayesian linear regression, and Gibbs sampling are used for Bayesian inference. A hyper-parameter setting method is proposed that considers the degrees of belief in the prior model and the measurement accuracy of new observations. Through numerical investigations, the proposed updating methodology is verified. Next, updating examples confirm that the proposed methodology can quantitatively evaluate the effect of changes in the traffic environment on the traffic load effects of the bridge, and the accuracy of estimated traffic load effects can be improved in the specific bridge (the 2nd Jindo Bridge) whose information is insufficient to estimate traffic loads.

Third, a new design live load model for long-span bridges in South Korea is

proposed by incorporating the diverse traffic environment into the bridge design. The traffic environments of long-span bridges in Korea were investigated and the classification was proposed for two important variables (heavy vehicles and traffic congestion). For each traffic environment condition, traffic flow simulations were conducted to calculate the live load samples, upon which a design lane load model and multiple presence factor are proposed. The live load effects are calculated using the influence line of the actual cable-stayed bridge based on the new proposed live load model and compared to the live load effects from the Korean Highway Bridge Design Code-Cable-supported Bridges. Furthermore, a final unified design live load model is proposed which covers short- to long-span bridges, and statistical characteristics of live loads and live load effects are investigated.

Lastly, the time-dependent reliability of the PSC box girder bridges over the service life is evaluated through elaborate modeling of the corrosion of strands and using the developed bridge traffic load estimation techniques. Various variables related to corrosion are considered to describe strength degradation, and classification of the corrosive environment is proposed. Two sections (positive and negative moment) of Hwayang-Jobal Bridge are selected as application examples. The traffic load effect (bending moment) of the target section is estimated based on the traffic information around the example bridge and the assumed scenarios of traffic environment change. The flexural strength of the girder is calculated through an iterative method with considering strength degradation due to corrosion. Ultimate limit state 1 is used as the limit state, and a total of 22 random variables are used for time-dependent reliability evaluation. To efficiently calculate the time-dependent

reliability, the subset simulation and a recently proposed structural reliability method that combines FORM and sampling-based methods are used. The time-dependent reliability of the bridge over 100 years is evaluated to investigate the effects of corrosion and traffic load on reliability. These examples show that not only corrosion of steel strands but also the traffic load is an important factor in evaluating reliability. In addition, the reliability is updated using the data and information obtained through inspection and monitoring. Based on this result, maintenance strategies to satisfy the target level of reliability are established.

The data-based bridge reliability evaluation and updating framework that considers traffic environment and strength degradation proposed in this dissertation is expected to contribute to enhancing bridge condition evaluation technology and establishing optimized maintenance strategies.

Keyword : Bridge reliability evaluation, Weigh-In-Motion, Vehicular live loads, Traffic loads, Time-dependent reliability, Bayesian updating, Design live load model, Korean Highway Bridge Design Code (LRFD), Multiple presence factor, Traffic environment, Data-based, Strength degradation, Corrosion of strands, PSC box girder bridges.

Student Number: 2015-22922

Table of Contents

List of Figures

List of Tables

Chapter 1. Introduction

1.1. Motivation

Reliability-based methods are widely used when designing bridges and assessing the performance of bridges in operation to ensure their safety and serviceability nowadays. This approach can consider various uncertainties from many factors related to bridge safety such as earthquake, traffic load, strength degradation, and corrosion. When evaluating the reliability of a bridge, the first thing to be defined is the limit state function, which is a criterion to judge whether the performance of the bridge is achieved or not. This function is mainly composed of two components. The first component is the load applied to bridges. Bridges are inherently subjected to various loads from environments over their service life, typically dead, traffic, earthquake, and wind load. The second component is the strength or the so-called resistance, which indicates the capacity of the structure against the load (demand) and includes stress, flexural strength, shear strength, fatigue strength, etc. The load and strength are not fixed values during the service life of bridges, and rather vary continuously due to diverse factors and surroundings. Therefore, it is essential to precisely estimate the load and strength during the service life of the bridge for more cost-effective design, and accurate assessment or prediction of the actual in-use condition of the bridge.

In the last two decades, with the development of sensor technologies and structure safety inspection, a lot of data and information related to load and strength

have been collected. Based on these data, many methods have been developed to precisely estimate and predict load and strength. Furthermore, bridge reliability evaluation has been performed using estimated load and strength (Darmawan and Stewart, 2007; Guo et al., 2016; Tu et al., 2019). However, most of these studies consider the strength degradation in-depth by focusing on the deterioration and corrosion phenomenon while, another important component, loads have been relatively neglected. Many studies lack the sophistication to model and estimate loads that are critical for bridge reliability so far.

Particularly, among many kinds of loads, the traffic load (or so-called normally live load in design codes) is an important load component that should be considered in the ultimate, fatigue, and serviceability limit state because it is constantly applied in general situations unlike loads caused by disasters such as earthquakes and typhoons. Traffic load is significantly affected by the traffic environment of the bridge, so it has naturally a lot of uncertainty and variability. Recently, Weigh-In-Motion (WIM) systems have been widely used to obtain various types of data related to traffic environments, such as vehicle characteristics and traffic flow patterns. In structural engineering, many researchers and engineers have studied bridge traffic loads using WIM data nowadays.

These studies can be divided into two main categories. The first studies are about the accurate estimation of traffic load effects of bridges in operation based on related traffic information and data collected during their service life. Many studies have been conducted in this regard (a detailed literature review is provided in Section 2.1) but previous studies still miss or do not properly take into account several key

variables that are essential in estimating the traffic load effects. In addition, the developed traffic load models are specialized for a certain span length of a bridge (short or long), and therefore cannot cover all the bridges from short-span to long-span types. Thus, a comprehensive bridge traffic load model should be developed which can reflect the actual traffic environment of bridges and is applicable regardless of bridge length and type.

In addition, it is noted that the traffic environment of a bridge may change over its service life, which can affect the traffic load effects significantly. It means that changes in the traffic environment need to be considered for accurate estimation of the traffic loads on in-use bridges. Accordingly, an updating methodology is required to update the parameters of the probabilistic model of bridge traffic loads based on new observations and information obtained through continuous monitoring of the traffic environment of the bridge.

The second studies are about the development of new design live load models or calibration of existing live load models based on traffic data and information collected in diverse regions and over a long period. Recently, two reliability-based bridge design codes were introduced in South Korea which are the Korean Highway Bridge Design Code (MOLIT, 2016a) and Korean Highway Bridge Design Code-Cable-supported Bridges (MOLILT, 2016b). These are called KHBDC and KHBDC-CB respectively in this dissertation. The former code is for short- and medium-span bridges and the latter code is for long-span bridges.

The design live load models of both design codes have been newly defined based on two studies (Hwang, 2008; Hwang and Kim, 2015). These design live load

models consist of design truck load, lane load, and multiple presence factor (MPF). KHBDC and KHBDC-CB use the same design truck load as shown in Figure 1.1.

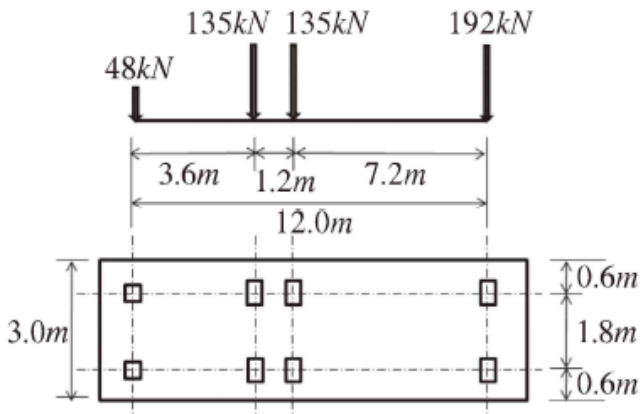

Figure 1.1 Design truck load for KHBDC and KHBDC-CB (MOLIT, 2016a)

The design truck has four axles whose loads are 48, 135, 135, and 192 kN, while spacings are 3.6, 1.2, and 7.2m. Two design lane load models exist in codes as shown in Table 1.1 and Table 1.2. In Table 1.1, L is the span length of bridges, while L_I in Table 1.2 denotes the loaded length of bridges, defined as the sum of the unfavorable parts of the influence line that increases the maximum traffic load effect. KHBDC adopts the design lane load model 1 whereas KHBDC-CB adopts the design lane load model 1 and 2 both and recommends using the one which produces larger live load effects between the two models. Lastly, the same MPFs are used for KHBDC and KHBDC-CB as provided in Table 1.3.

Table 1.1 Design lane load model 1

$L \leq 60\text{m}$	$w = 12.7\ \text{kN/m}$
$L > 60\text{m}$	$w = 12.7 \times \left(\frac{60}{L}\right)^{0.10}\ \text{kN/m}$

Table 1.2 Design lane load model 2

$L_I \leq 60\text{m}$	$w = 12.7\ \text{kN/m}$
$L_I > 60\text{m}$	$w = 12.7 \times \left(\frac{60}{L_I}\right)^{0.15}\ \text{kN/m}$

Table 1.3 Multiple presence factor for KHBDC and KHBDC-CB

Number of loaded lanes	Multiple presence factors
1	1.0
2	0.9
3	0.8
4	0.7
≥ 5	0.65

In addition to the design live load model of South Korea, AASHTO HL-93 (AASHTO, 2012) and Eurocode Load model 1 (LM1) (ECS, 2003) are briefly introduced as representative live load models in this section. In AASHTO HL-93, the design truck has three axles whose loads are 35.6, 142.3, and 142.3 kN. The first axle spacing is 4.3m while the second axle spacing varies from 4.3m to 9.1m. Also, the design tandem has two axles each of which has a loading of 111.2 kN and a 1.2 m-long axle spacing. The design lane load is 9.34 kN/m per lane regardless of the loaded length of bridges. The multiple presence factors are defined as in Table 1.4 (AASHTO, 2012). Basically, design live load models of AASHTO and KHBDC are defined similar way.

Table 1.4 Multiple presence factors of AASHTO HL-93

Number of loaded lanes	Multiple presence factor
1	1.2
2	1.0
3	0.85
> 3	0.65

Table 1.5 Eurocode LM1

Location	Tandem system Axle loads (kN)	UDL (Uniformly distributed load) system (kN/m^2)
Lane number 1	300	9
Lane number 2	200	2.5
Lane number 3	100	2.5
Other lanes	0	2.5
Remaining area	0	2.5

On the other hand, Eurocode LM1 is defined significantly differently from KHBDC and AASHTO HL-93 as shown in Table 1.5. Instead of using MPFs, Eurocode LM1 defines different axle loads (corresponding to design truck in KHBDC) and UDL (corresponding to lane loads in KHBDC) depending on the location of the lane. Most of the design live load models including KHBDC, AASHTO HL-93, and Eurocode LM1 introduced above, were developed to target short- and medium span bridges (shorter than span length of 200 m) while there is relatively few design live load models for long-span bridges and several related studies are still underway (detailed literature review is provided in Section 4.1). In Korea, although the design live load model has been developed based on recent research (Hwang and Kim, 2015), the model is overestimated based on simple traffic jam scenarios (full stop situation) to estimate maximum live load effects for conservatism. Therefore, to reduce excessive conservatism and reflect various traffic

environments of bridges, it is necessary to develop a new design live load model for long-span bridges in Korea.

Finally, in order to evaluate the reliability during the service life of bridges, the aforementioned changes in traffic loads, as well as the strength degradation due to deterioration phenomena, should be considered. However, previous studies have not evaluated and updated the bridge reliability in practical ways by taking into account the test results and data that can be obtained through structure safety inspections and sensors (detailed literature review is provided in Section 5.1). Therefore, a framework for evaluating and updating the bridge reliability using data and information obtained over the service life of bridges is required.

1.2. Objectives and scope

The dissertation aims to develop a framework for data-based evaluation and updating of bridge reliability during the service life of bridges. Specifically, among various loads and strength degradation due to deterioration processes, this dissertation focuses on estimations of traffic loads and strength degradation due to corrosion of strands through sophisticated modeling and methods. To this end, the following tasks are performed for data-based evaluation and updating of bridge reliability based on traffic environment and strength degradation.

First, to accurately estimate the traffic load effects on bridges, a comprehensive probabilistic traffic load model for bridges is developed which can reflect the unique traffic environment of the bridge. Although many related studies have been

conducted using WIM data which contain traffic information, limitations still exist that are mentioned in Section 1.1. Therefore, in this dissertation, several key random variables representing the traffic condition of bridges are identified and described by detailed probabilistic models to properly consider the uncertainty of the traffic environment. These models are elaborately developed based on theories of transportation engineering and statistical investigations of highway WIM data measured in three regions of South Korea. Numerical examples are provided to validate the developed model and compare it to bridge design codes.

Second, the dissertation aims to develop an updating methodology to update the parameters of the probabilistic model of bridge traffic loads based on new observations and information obtained through continuous monitoring of the traffic environment of the bridge. However, most of the previous studies have estimated the traffic load effects assuming no significant variation in traffic volume and other characteristics of the traffic environment. To address this, a Bayesian inference methodology to directly update the parameters of the probabilistic model of bridge traffic loads based on new observations regarding the traffic environment is proposed.

Third, as explained in Section 1.1, design live load model in South Korea especially for long-span bridges is necessary to be studied more rigorously to reduce excessive conservatism. Thus, this dissertation aims to propose a new design lane load model and multiple presence factor (MPF) for long-span bridges based on simulated traffic congestion scenarios through the developed probabilistic traffic load model which can consider diverse traffic conditions of bridges.

Lastly, to accurately evaluate and update the reliability of bridges over the

service life, changes in traffic load effects and strength degradation are considered. Among strength degradation of bridge members due to many causes, this dissertation focuses on the flexural strength degradation due to corrosion of steel strands, and post-tensioned concrete (PSC) box girder bridge is used as an example bridge. Time-dependent reliability is evaluated using the estimated flexural strength and traffic load effects based on (1) corrosion-related data collected from the current practice of structure safety inspection, and (2) the traffic environment data obtained through WIM systems and traffic investigation.

Additionally, applicable bridge types for each developed method and model in this dissertation are clearly stated here in advance. The probabilistic model and updating methodology for bridge traffic loads can be applied regardless of the length and structural type of the bridge. The proposed design live load model for long-span bridges can be applied to bridges with a span length longer than 200m. In addition, a design live load model for short- and medium-span bridges whose span length is shorter than 200 m is also described in the dissertation. The method for estimating flexural strength degradation due to strand corrosion is applicable to PSC box girder bridges with tendons. The proposed time-dependent reliability evaluation framework can be applied to all bridge types if the major strength degradation phenomenon of the target bridge can be precisely modeled.

1.3. Organization of the dissertation

The organization of the dissertation is as follows. Chapter 2 develops a comprehensive probabilistic bridge traffic load model based on WIM data and numerical examples for estimation of traffic load effects are provided. Chapter 3 proposes a Bayesian updating methodology for traffic loads that can consider the changing traffic environment. Then, updating examples of traffic load effects using in-service WIM data of actual bridge are presented. In Chapter 4, a new design live load model for long-span bridges is proposed according to the traffic environment classification. In addition, statistical characteristics of live loads and live load effects are investigated. Chapter 5 provides a framework to evaluate and update the time-dependent reliability of PSC box girder bridges considering traffic environment and strength degradation due to corrosion of strands. Then, numerical examples are provided for maintenance based on time-dependent reliability updating. Finally, Chapter 6 provides major findings of this dissertation and recommendations for further study.

Chapter 2. A Comprehensive Probabilistic Bridge Traffic Load Model Based on Weigh-In-Motion (WIM) Data

2.1. Introduction

Precise estimation of the load effects on bridges is critical so that the required levels of safety and serviceability can be assured. In particular, traffic loads require special attention because they are being applied continuously to the bridge and show large uncertainties and considerable variability. These uncertainties mostly arise from the traffic environment of the bridge location. Therefore, the site-specific traffic conditions of the bridge should be considered in estimating the traffic load effects. However, most bridges have been designed based on the conservative design live load model in codes that cannot take into account the unique traffic conditions of bridges. Thus, there are pressing research needs for developing a probabilistic framework facilitating accurate estimation of site-specific traffic loads, which eventually helps ensure the safety and serviceability of bridges and reduce the costs of bridge construction and maintenance (O'Connor and Enevoldsen, 2009).

For the probabilistic modeling of uncertain site-specific traffic environments of a bridge, it is essential to collect data that effectively describe these environments. Recently, Weigh-In-Motion (WIM) systems have been widely used to obtain various types of data related to traffic environments, such as vehicle characteristics and traffic flow patterns. Although the main purpose of WIM systems is to determine

whether passing trucks are overloaded based on the measured axle weights and gross vehicle weight (GVW), WIM data sets also include the vehicle length, vehicle class, passing time, and velocity, among other factors. To take advantage of this useful information about the site-specific conditions of traffic environments, many governments or owners of bridges and roads have installed WIM systems at important highways and bridges to collect large amounts of WIM data continuously.

Using these large amounts of WIM data, a lot of studies have employed the Monte Carlo simulation (MCS) approach to simulate various traffic scenarios to estimate the maximum traffic load effects. At the time when computing power was limited and the collected WIM data lacked, several studies focused on short-span bridges based on simple scenarios using assumed headway or distances between vehicles (Nowak, 1993; Vrouwenvelder and Waarts, 1993). However, recent advances in computing power and a lot of collected WIM data from many regions have enabled the simulation of traffic scenarios similar to real traffic patterns, e.g. modeling headway in probabilistic ways using data (O'Brien and Caprani, 2005; Enright and O'Brien, 2013), microsimulation models for traffic flow (Kesting et al., 2007). After that, the current MCS approach which can generate samples of vehicles and traffic patterns for a long period has been robustly established by many studies (Caprani et al., 2008; Enright and O'Brien, 2013; Enright et al., 2013; O'Brien et al., 2015; Caprani et al., 2016; Lu et al., 2016; Ruan et al., 2017; Lu et al., 2017). It has been shown that such a long-run computational simulation of traffic load effects can result in highly accurate extrapolation (O'Brien et al., 2015).

The general procedure of the MCS approach is illustrated in Figure 2.1. As the

first step of the procedure, the measured WIM data must be calibrated and cleaned, as WIM systems may have some measurement errors and are thus sensitive to environmental conditions such as the variation of temperature. Second, to construct a simulation model of traffic loading, key random variables representing the traffic environment of a bridge are identified and fitted to probabilistic models such as Gaussian, lognormal, and Gaussian mixture model. Then, using the developed simulation model with appropriate parameter values of the key random variables, MCS is performed to generate artificial WIM data for the time period of interest. Next, the traffic load effects on the bridge, e.g., the moment, shear force, tension, and axial force, are calculated using the influence lines of the target bridge and the artificial WIM data. These calculated load effects are extrapolated to estimate those during the service life of a bridge or a return period of interest. Finally, target traffic load effects can be used to evaluate the performance of bridges in operation or calibrate live load demands in the design code.

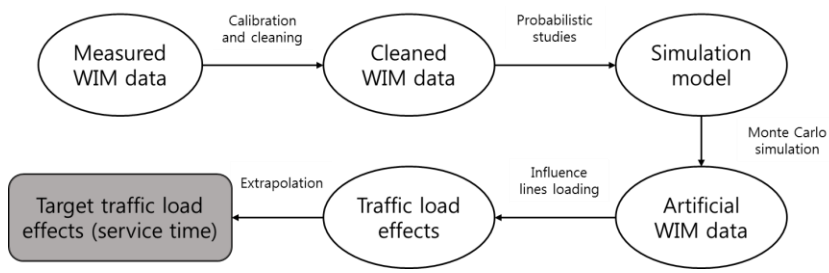

Figure 2.1 General procedure of the Monte Carlo simulation approach to estimate the traffic load effects on a bridge

In addition, many researchers have paid attention to the different dominant traffic flows according to the span length of the bridge. For a short-span bridge, the free flow state is the dominant traffic flow. This is because many vehicles cannot exist simultaneously on short-span so the weight of a few heavy trucks results in large traffic load effects. O'Brien and Enright (2011) modeled bridge loading from traffic in two same-direction lanes for short-span bridges by considering significant patterns of correlation of heavy trucks. Enright and O'Brien (2013) developed the MCS method of extreme traffic loading on short and medium span bridges by modeling headway sophisticatedly. On the other hand, for a long-span bridge, the congested traffic flow state is dominant because the number of vehicles passing over a long bridge determines the traffic load effects (Buckland, 1981). In the case of traffic congestion, the changes in speed and lane of vehicles should be elaborately modeled. To address this, microsimulation models for describing the traffic congestion were introduced for estimation of bridge traffic loads (O'Brien et al., 2015; Caprani et al., 2016; Carey et al., 2018; Guo and Caprani, 2019).

In addition to these studies, other studies using WIM data have been conducted. traffic load models of several design codes were developed and calibrated based on widely collected WIM data (Nowak, 1995; Nowak et al., 2010; Kwon et al., 2011; Hwang et al., 2012; Zhao and Tabatabai, 2012; Enright et al., 2013; Tabatabai et al., 2017), and site-specific traffic load effects such as the moment, shear force, and tension were calculated using the influence lines of bridges and extrapolated to estimate the maximum load effects over the service life of bridges (O'Connor and O'Brien, 2005; Caprani et al., 2008; Enright and O'Brien, 2013; O'Brien et al., 2015;

Caprani et al., 2016; Ruan et al., 2017). Fatigue reliability assessment and first passage probability of the deflection of a bridge have been investigated based on WIM data (Lu et al., 2016; Lu et al., 2017). Bridge Weigh-In-Motion (B-WIM) technologies have been studied using sensors and structural health monitoring systems (Seo et al., 2013; Lydon et al., 2017; O'Brien et al., 2018). Extrapolation methods to obtain exact extreme traffic load effects have been studied (O'Brien et al., 2015; Zhou et al., 2016).

However, previous studies still miss or do not properly take into account several key variables that are essential in estimating the traffic load effects, e.g., differences in the headway caused by the lanes and vehicle types, heavy vehicle ratio, and the occurrence frequency of traffic congestion, among others. These variables need to be parameterized using appropriate probabilistic models to consider the site-specific conditions of traffic environments on bridges. Moreover, existing studies are specialized for a certain span length of a bridge (short or long), and therefore the model cannot cover all the bridges from short-span to long-span types.

Therefore, this chapter develops a comprehensive probabilistic traffic load model for bridges based on WIM measurements. The developed model employs the aforementioned MCS approach but with significant improvements. Most importantly, key random variables representing the traffic condition of bridges are identified and described by detailed probabilistic models, which are elaborately established based on theories of transportation engineering and statistical investigations of WIM data. These comprehensive modeling processes enable us to handle general span lengths (short and long) as well as multi-lane.

2.2. Description of WIM data

This study uses the WIM data collected on the highway of three sites in South Korea by Korea expressway corporation, i.e., Gimcheon, Sunsan, and Waegwan, over the period from February to December, 2013. The measured data of each lane describe uni-directional traffic flow. Table 2.1 shows the details of the WIM data. The "perfect" traffic records in Table 2.1 indicate that all lanes of WIM data were continuously recorded for 24 hours without missing or erroneous data. Each site has multiple lanes, one of which is defined as the truck lane where heavy vehicles such as dump trucks and trailers mainly pass. The traffic loads on this lane occupy a large portion of the total traffic loads on a bridge. Although these data have been already calibrated by the data management institution, they are further processed in this study to eliminate unreliable data which might cause inaccurate estimation of the traffic load effects. For this process, this study adopts some guidelines from Sivakumar et al. (2011) as well as the author's judgment based on the vehicle information of South Korea and safety distance in the cleaning process. Some of the rules used in the process are summarized as follows:

1) The difference between the measured Gross vehicle weight (GVW) and the sum of axle weights should be less than 10%.
2) GVW should be greater than 0.8 tons and less than 100 tons.
3) Vehicle length should be greater than 2 m and less than 36 m.
4) Each vehicle type has lower and upper bounds on vehicle length and GVW.
5) The smallest proportion of axle weight to GVW must exceed 5 percent.
6) Headway should be longer than 0.3 seconds.

To develop a comprehensive probabilistic model from which one can simulate traffic flow and compute traffic loads, two types of models are developed respectively describing (1) vehicle characteristics, e.g., axle weight, and spacing of vehicles, and (2) traffic flow characteristics representing the pattern of traffic flow on a bridge. In the following sections, details of the two groups of probabilistic models are provided.

Table 2.1 Details of used WIM data

Sites	Gimcheon	Sunsan	Waegwan
Number of lanes	3	2	4
Average daily traffic of all lanes (vehicles/day)	17,885	29,484	53,595
Average daily truck traffic in the truck lane (vehicles/day)	2,405	4,307	3,483
Number of days with “perfect” traffic records	205	221	246

2.3. Probabilistic models for vehicle characteristics

2.3.1 Vehicle type

The WIM measurement systems installed at the three sites automatically classify the passing vehicles into a total of 12 types following the guidelines provided by the Ministry of Land, Infrastructure, and Transport (MOLIT) of South Korea. The guidelines are established in terms of the number of axles and the types of vehicles such as a car, bus, truck, semi-trailer, and full-trailer. The classification of 12 vehicle types is shown in Figure 2.2. Furthermore, additional sub-vehicle types are introduced to accurately generate characteristics of each vehicle type in MCS. For

example, the position of the maximum axle spacing (see Figure 2.3 for an example in which the first axle spacing is the maximum) is different among the same type of vehicles, especially for the vehicle types 6, 8, 10, and 11. To address this, three sub-vehicle types are introduced to those types as described in Table 2.2.

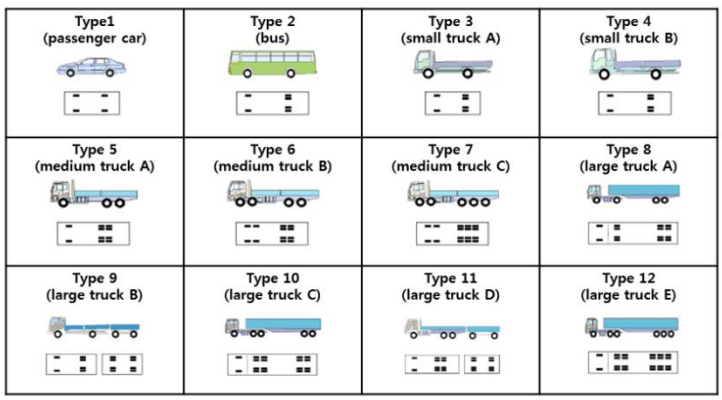

Figure 2.2 The classification of 12 vehicle types used in South Korea (MOLIT)

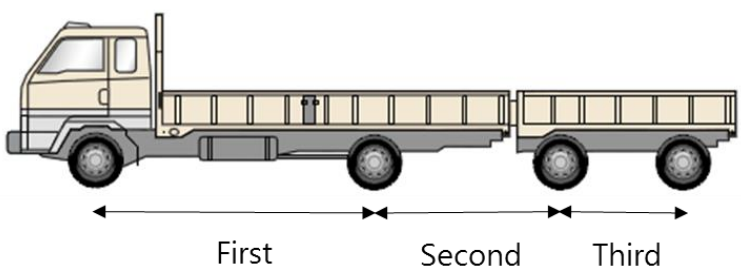

Figure 2.3 Example of the position of the maximum axle spacing (MOLIT)

Table 2.2 Sub-classifications of vehicle types

Position of the maximum axle spacing	Sub-vehicle type
First	6-1, 10-1, 11-1
Second	6-2, 8-1, 10-2, 11-2
Third	8-2, 10-3

2.3.2 Axle weight and spacing

Based on the measured WIM dataset, this study focuses on the following four key variables to describe the vehicle characteristics: GVW (Gross vehicle weight, i.e., the sum of the axle weights), the proportion of axle weight, total axle spacing, and the proportion of axle spacing. The actual value of axle weight and spacing can be calculated by distributing the GVW and total axle spacing according to the corresponding proportion. In all vehicle types, these four variables exhibit large uncertainties, which should be modeled by probability distributions. In addition, histograms of these variables generally show multiple peaks (See Figure 2.4) and thus do not follow one of typical unimodal probability distribution models such as Gaussian, lognormal, or Gamma distributions. In previous studies, these random variables were described by a variety of distribution models such as Gaussian distribution, Weibull distribution (Kennedy et al., 1992), Gaussian mixture model (GMM) (Enright et al., 2013; Enright and O'Brien 2013; Lu et al., 2017) and empirical distributions (Nowak, 1995; Nowak et al., 2010; Kwon et al., 2011; Hwang et al., 2012).

Among many probabilistic models used in the literature, GMM is selected to capture multiple peaks of the distributions of vehicle characteristics because it is a parametric distribution model which can adjust parameters to represent different traffic environments based on new measurements, unlike empirical distributions. In this study, the parameters of GMMs are estimated by the Expectation-Maximization (EM) algorithm (Bilmes, 1998). The optimal number of components of the GMM could be identified from the dataset, i.e., selecting the number of components based

on entropy criterion such as Akaike information criterion (AIC) and Bayesian information criterion (BIC), or adaptively during the parameter estimation process (Celeux and Soromenho, 1996; Zivkovic, 2004). However, the number of components is pre-selected based on not only AIC but also a visual inspection of the histogram and understanding of the physical conditions of vehicle characteristics variables in this study because in some cases, AIC decreases as the number of components increases. Therefore, in those cases, first, this study uses the number of peaks in the histogram as the number of GMM components and compares the shape of probability density function (PDF) and cumulative distribution function (CDF) of the original dataset with those of the GMM fitted by the EM algorithm. If such comparison is not good enough in the visual comparison, the number of the GMM components is increased by one to check the PDF and CDF again. Using this visual inspection and AIC, all four key variables of vehicle characteristics are modeled by GMMs which include at most four components. For example, Figure 2.4 shows that the GMM using two components can effectively describe the axle spacing random variable, which does not follow a typical unimodal distribution model.

Additionally, after fitting the variables using GMM, the Kolmogorov-Smirnov test (K-S test), which is one of the goodness-of-fit tests, is performed to quantitatively assess how suitable the GMM is for vehicle characteristics variables. The K-S test with a significance level of 0.05 for a total of 34 variables (17 vehicle types including sub-types × 2 variables including GVW and total axle spacing) is conducted. The results show that GMM is accepted for all GVW variables while the GMM is rejected for all total axle spacing variables. This is because total axle

spacing data are discretized more than GVW due to the specifications of vehicles. Hence, this study compares CDF of raw data and fitted GMM as shown in Figures 2.5 and 2.6 for additional verification. The results confirm the GMM is appropriate for total axle spacing variables.

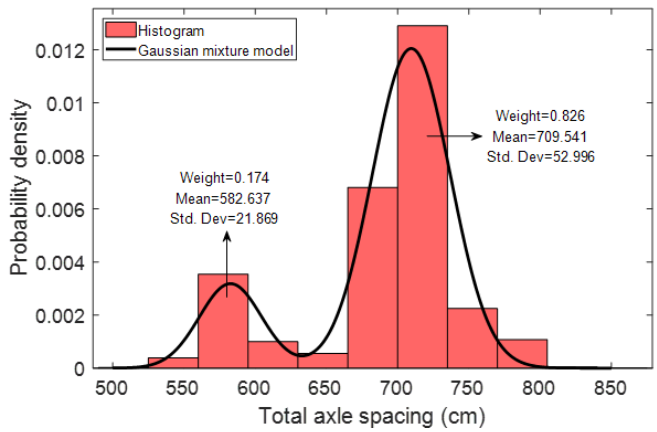

Figure 2.4 Histogram of total axle spacing of Type 5 vehicles and fitted Gaussian mixture model

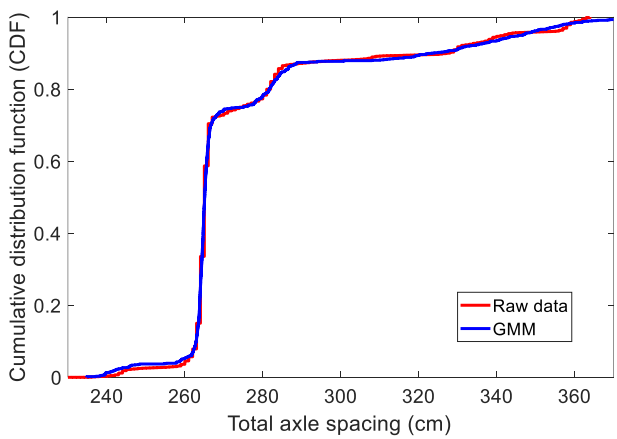

Figure 2.5 Comparison of empirical CDF of raw data and fitted GMM about total axle spacing of Type 3

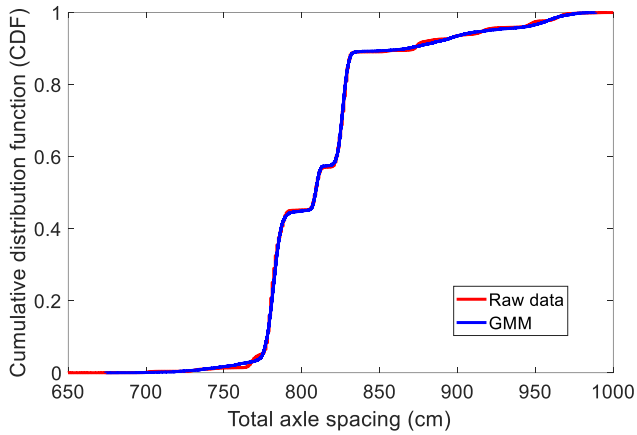

Figure 2.6 Comparison of empirical CDF of raw data and fitted GMM about total axle spacing of Type 7

Furthermore, to accurately generate the WIM data for vehicle characteristics variables during MCS, statistical correlations between these random variables are considered. In some of the previous studies, correlation relationships between axle loads are modeled using copula functions (Crespo-Minguillón and Casas, 1997; Srinivas et al., 2006; Tabatabai et al., 2017). These studies used rank correlation coefficients which are obtained through ranking rather than the actual values of data. However, it is noted that rank correlation is not enough to accurately generate these WIM data. To overcome this limitation, the linear correlation between random variables is considered by constructing Nataf distribution models (Liu and Der Kiureghian, 1986). Specifically, a Nataf distribution model relates the correlation coefficient between the original random variables, ρ_{ij} and that for the corresponding standard Gaussian random variables, ρ'_{ij} by an integral equation

$$\rho_{ij} = \int_{-\infty}^{\infty}\int_{-\infty}^{\infty}\left(\frac{x_i-\mu_i}{\sigma_i}\right)\left(\frac{x_j-\mu_j}{\sigma_j}\right)\varphi_2(z_i,z_j;\rho'_{ij})dz_i dz_j \quad (2.1)$$

where x_i and x_j are the original random variables, μ and σ respectively denote their means and standard deviations, and z_i and z_j are the corresponding standard Gaussian variables for which the Nataf distribution model is constructed. The correlation coefficient ρ'_{ij} can be obtained by numerically solving Eq. (2.1) for the given correlation coefficient ρ_{ij}, means, and standard deviations of the original variables which can be estimated from the measured WIM data. To generate correlated samples of the vehicle characteristics in MCS, standard Gaussian random variables z_i are first generated based on the correlation coefficient matrix $\mathbf{R}' = [\rho'_{ij}]$. Then the generated standard Gaussian variables are transformed to the original random variables by $x_i = F_{X_i}^{-1}[\Phi(z_i)]$ where $F_{X_i}(\cdot)$ is the cumulative distribution function (CDF) of the original random variable and $\Phi(\cdot)$ is the standard Gaussian CDF. When following this procedure, for some vehicle types, the correlation coefficient matrix $\mathbf{R}' = [\rho'_{ij}]$ did not satisfy the positive semi-definite condition. This is because the non-typical probabilistic distributions of original random variables may cause a large difference between ρ_{ij} and ρ'_{ij} (Liu and Der Kiureghian, 1986). In such cases, approximate values satisfying the positive semi-definite condition are introduced by the author's judgment.

2.4. Probabilistic models for traffic flow characteristics

To represent the traffic flow characteristics, probabilistic models are developed for four key random variables - traffic volume, speed of vehicles, ratio of vehicle types, and headway. These random variables are so highly interrelated that the

probabilistic models should be developed carefully based on the measurement data as well as theories of transportation engineering.

2.4.1 Traffic volume and speed

In transportation engineering, it is widely known that traffic volume and speed have the highly interrelated relationship described by a macroscopic traffic flow model of the area, e.g., Greenshield's model. This model is known to be fairly accurate despite its simplicity (Adolf, 1990). According to the model shown in Figure 2.5(a), the average speed and traffic volume in a certain time period can have one of the two possible traffic flow states: "free traffic flow" and "congested traffic flow" states. In the free traffic flow, the vehicle is independent of the passing car ahead while, in the congested traffic flow, the vehicle is significantly influenced by the car ahead. This relationship between average speed and traffic volume is observed in the WIM data measured at the three sites as shown in Figures. 2.7(b), 2.7(c), and 2.7(d), where traffic volume on the x-axis is the number of vehicles passing during 5-minute intervals, and the y-axis represents the average speed of passing vehicles during the same time intervals. Based on the theories which were confirmed by measured WIM data, the two traffic flow states are carefully incorporated into the developed model. It is also noted from the WIM data that traffic congestion does not occur every day. In Sunsan data, traffic congestion occurred for 39 days during the measurement period while Waegwan experienced it only 5 days and Gimcheon did not experience traffic congestion at all. To incorporate these characteristics into the traffic load model systematically, probabilistic models of the

traffic volume and average speed are developed as described below.

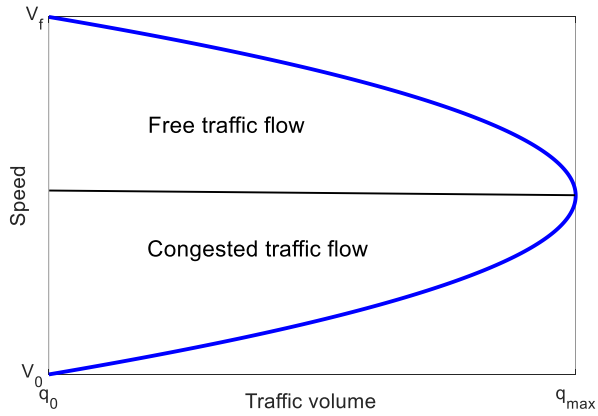

(a) Greenshield's model

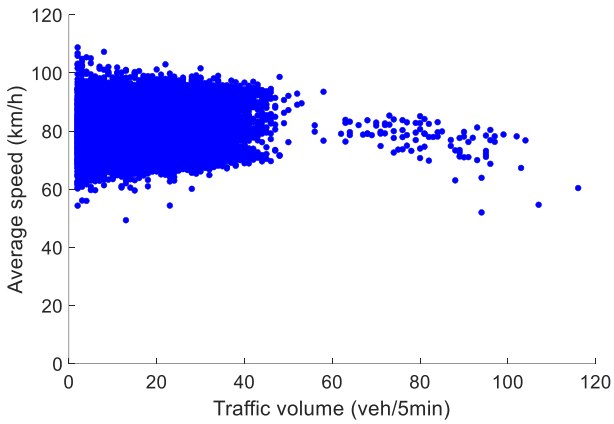

(b) The truck lane of Gimcheon

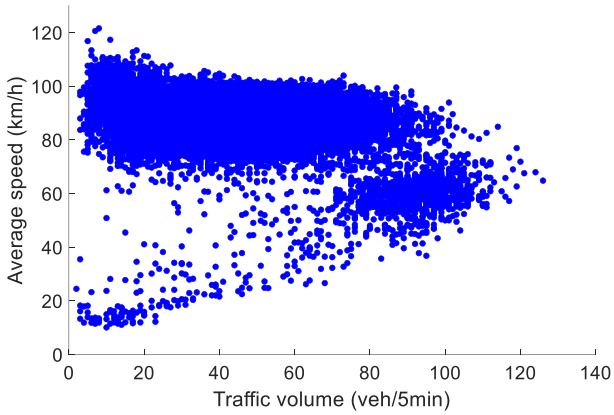

(c) The truck lane of Sunsan

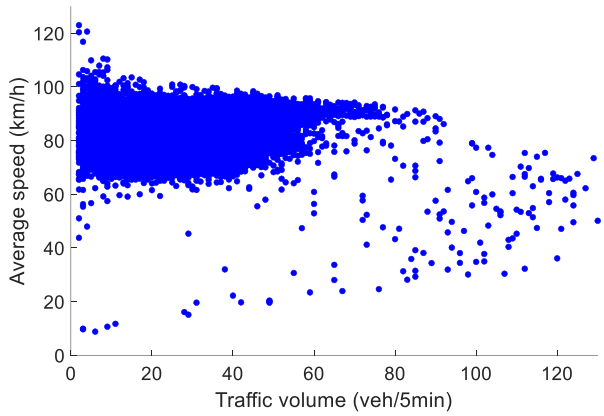

(d) The truck lane of Waegwan

Figure 2.7 Traffic volume-speed relationship

First, it is noted that the traffic volume varies significantly with hours, days, and months. To consider these temporal variations, the traffic volume data is obtained from measured WIM data over each hour in the unit of veh/5 min, not the veh/hour that is widely being used in the literature. This is because the duration of congested traffic flow is usually less than one hour, so if the time interval is too long, the congested and free traffic flow might co-exist in the same time interval. This may result in a significant overestimation of the estimated average speed in congested traffic flow, which may lead to inaccurate modeling of the vehicle speed. Another reason for measuring traffic volume per 5-minute interval is that it generally takes less than five minutes for vehicles to pass a bridge. Also, traffic volume is modeled separately depending on the state of traffic flow, i.e., congested or free traffic flow. Specifically, traffic volume is modeled through GMM by dividing it into data measured on the day of traffic congestion and data measured on the day of no traffic

congestion. GMM is used again because the data of traffic volume at every given hour show multiple peaks in general and do not follow typical distributions. Second, to deal with the speed of vehicles, the average speed data (per each of the 5-minute intervals) are categorized in terms of congested or free traffic flow and separately fitted by GMM.

To take into account the relationship between the traffic volume and speed (shown in Figure 2.7), these GMM models of average speed are developed for each group of traffic volumes (grouped by 20 veh/5 min intervals), not for each traffic volume (1 veh/min intervals). Because the data is not enough to model the average speed for each traffic volume (1 veh/5 min interval) and too many probabilistic models will be established. In addition, because calculated traffic volumes from WIM data naturally have errors and the average speed data have a lot of variabilities as shown in Figure 2.7. The reason why selecting 20 veh/5 min intervals is that the average speed data in the same group of traffic volume (20 veh/5 min interval) have similar values (can be found in Figure 2.7) and the number of probabilistic models required is not excessive. After fitting the variables using GMM, the K-S test with a significance level of 0.05 is conducted again to quantitatively assess how suitable the GMM is for traffic volume and speed variables. The GMM is not rejected for around 83% of variables which confirms GMM is appropriate to fit traffic volume and speed variables.

Additionally, to incorporate the aforementioned randomness of traffic congestion occurrences, this study introduces the probability of the daily occurrence of traffic congestion into the probabilistic model of traffic flow characteristics. This

probability is calculated as the total number of days with congestion divided by the total number of days with WIM measurements, and used in MCS as follows: If a random number generated based on the probability of daily congestion occurrences indicates that traffic congestion occurs on a given day, the traffic volume and average speed are randomly generated for each 5-minute interval based on the conditional GMM of traffic volume and average speed given the congested traffic flow. Otherwise, the conditional distribution given free traffic flow is used instead.

2.4.2 Ratio of vehicle types

In simulating the 12 vehicle types in Figure 2.2, it is important to note that the relative ratios of the vehicle types change over time. Especially, the temporal change of the heavy vehicle ratio, which causes significant impacts on traffic load effects, is carefully investigated. Vehicle types 5 to 12, which cover medium and large trucks, are defined as the heavy vehicles in this study. The heavy vehicle ratio is estimated from the measured WIM data on all lanes at three sites for each hour of the day, and day of the week as shown in Figure 2.8. It is noteworthy that the heavy vehicle ratio is particularly higher at night and dawn than during daytime on a weekday while the ratio stays low from Saturday afternoon to Sunday evening. The other two sites have the same trend in their truck lanes. The reason for this phenomenon is that drivers of heavy trucks usually travel at night to speed up the shipment by avoiding the high traffic volume and take rest on holidays. This hourly variation of heavy vehicle ratio (fitted with the Gaussian distribution) is incorporated into the developed probabilistic model. After fitting the heavy vehicle ratios using Gaussian distribution,

the K-S test with a significance level of 0.05 is performed and the results show that Gaussian distribution is not rejected for all heavy vehicle ratios except the ones in the car lane which have values close to 0. However, this study judges that it is acceptable to use the Gaussian distribution for heavy vehicle ratio in the car lanes. Because it has a minor effect on estimating the maximum traffic load effects due to low heavy vehicle ratios.

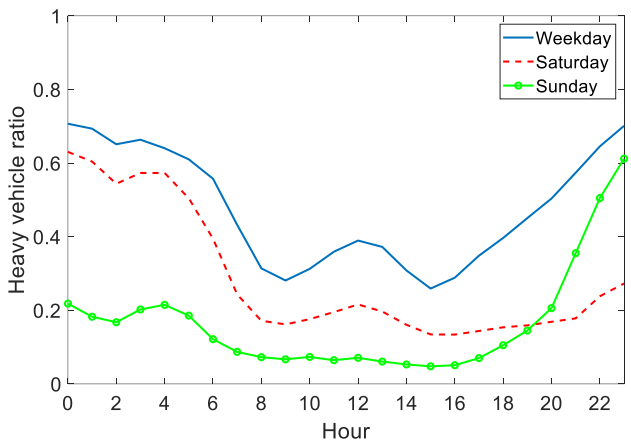

Figure 2.8 Heavy vehicle ratio on the truck lane from WIM data at Sunsan

2.4.3 Headway

The fourth key random variable, headway is defined as the distance or time between two consecutive passing vehicles. Headway is an important component in the modeling and simulation of traffic flow. In general, headway shows a large degree of uncertainty caused by the traffic volume, driving habits, truck platoon, safety distance, interactions between vehicles, among other factors. Many studies have been carried out to establish headway models based on measured data and

statistical studies. Exponential, uniform, gamma, and lognormal distributions are often used, while other studies rely on a deterministic model based on safety distance rules and measurement data (O'Brien and Caprani, 2005). Among these models, one of the simplest and widely used models is the exponential distribution, a natural choice especially when vehicle arrival events can be assumed as independent events forming a Poisson process. However, simulations from exponential distribution can produce headway values close to zero, which is impossible in an actual traffic flow. To resolve this issue, shifted exponential distribution based on an assumed minimum headway value is used (Cowan, 1975). In recent studies, three piecewise quadratic curves were used to fit the empirical CDF for headways smaller than 4 seconds for traffic volume groups (with 20 veh/hour intervals) while shifted exponential distribution was used for headways larger than 4 seconds (O'Brien and Caprani, 2005; Enright and O'Brien, 2013).

The histogram of the headway data shows that the bin height (frequency) keeps increasing until a certain threshold between 2.5~5 seconds and starts decreasing at larger headway than the threshold (can be found in Figure 2.9). Thus, headways larger than the threshold can be described by shifted exponential distribution derived from a Poisson process under the assumption that the driving of the rear vehicle is independent of that of the front vehicle. On the other hand, headways smaller than the threshold are modeled by GMM, rather than general probability distributions. This is because 1) the driving of the rear vehicle is relatively significantly affected by that of the front vehicle, 2) the headways have large uncertainties, and 3) no specific shapes are shown in the histogram. Hence, when constructing probabilistic

models for the headway, the threshold should be determined first. This study performs the K-S test about three candidate thresholds of 3, 4, and 5 seconds after the fitting process to determine the threshold value. Table 2.3 shows K-S test results for candidate threshold values. Since the acceptance rate is the lowest in the case of 3 seconds and the acceptance rate is similar in the case of 4 and 5 seconds, 4 seconds that are used in previous studies are selected as the threshold value in this study.

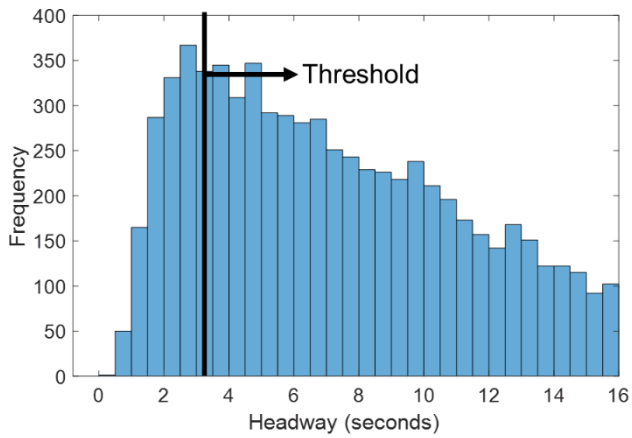

Figure 2.9 Histogram of headway data (30 veh/5 min) at the truck lane of Sunsan

Table 2.3 Acceptance rate of the K-S test according to threshold values of headway

	3 seconds	4 seconds	5 seconds
Shifted exponential distribution	83.5%	89.5%	91.2%
GMM	96.2%	97.8%	96.9%

After determining the threshold value, headway is classified into two cases of "small" (shorter than 4 sec) and "large" (longer than 4 sec). The small headways are fitted with the Gaussian mixture model for traffic volume groups (with 20 veh/5 min intervals) which are the same intervals for speed variables. The large headways are

modeled by shifted exponential distribution based on the aforementioned Poisson process assumption, whose parameters are estimated by maximum likelihood estimation for each traffic volume group. The probability distribution function of the shifted exponential distribution used in this study, $f(x;\lambda)$ is defined as

$$f(x;\lambda) = \begin{cases} \frac{1}{\lambda}\exp\left\{-\left(\frac{x-4}{\lambda}\right)\right\}, & x \geq 4 \\ 0 \quad , & otherwise \end{cases} \tag{2.2}$$

where λ is the parameter of the shifted exponential distribution. The relationship between the estimated parameter λ and the corresponding traffic volume is identified and fitted by the power series function of the traffic volume.

In generating the artificial WIM data by MCS, the headway is generated as follows. For a generated traffic volume value, the percentage of small headway is predicted. For this purpose, linear regression models are developed to predict the percentage for each traffic volume group (with 20 veh/hour intervals) as shown in Figure 2.10. This percentage is used to determine which type of headway, i.e., small or large, is to be generated given the traffic volume in the MCS. It is found that the percentage of small headway increases as the traffic volume increases because the increased traffic volume naturally causes adjacent vehicles to have a shorter distance between them given a constant duration of the traffic flow.

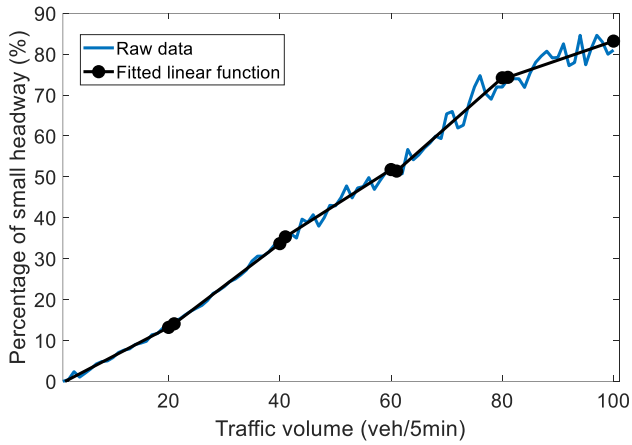

Figure 2.10 Predicting percentage of small headway for a given traffic volume at the truck lane of Gimcheon

This study also considers the effects of different driving habits given the types of vehicles. It is reported in the literature that drivers of cars and trucks have significantly different driving behaviors, which naturally leads to differences in headway. Therefore, the influence of trucks should not be ignored when modeling the headway (Aghabayk et al., 2012). In order to address this, the percentage of small headway cases and parameters of the GMM model, and the shifted exponential distribution explained above are estimated separately for the following four cases:

1) Case 1: Rear vehicle: A light vehicle, Front vehicle: A light vehicle
2) Case 2: Rear vehicle: A heavy vehicle, Front vehicle: A light vehicle
3) Case 3: Rear vehicle: A light vehicle, Front vehicle: A heavy vehicle
4) Case 4: Rear vehicle: A heavy vehicle, Front vehicle: A heavy vehicle

A “light” vehicle is defined as vehicle type 1 to 4, while types 5 to 12 are considered as “heavy” vehicles. Figure 2.11 shows the CDFs of the fitted Gaussian

mixture model for the truck lane of Sunsan when the traffic volume is 20~40 veh/5 min. The CDFs of the four cases are significantly different from each other. The results for the other traffic volumes and lanes show the same tendency identical to that in Figure 2.11, that is, Cases 1 and 2 (in which the front vehicle is light) have a smaller headway than Cases 3 and 4 (in which the front vehicle is heavy). This stems from the fact that the driver tends to be careful when the vehicle ahead is a heavy vehicle, and it takes a longer time for all axles of the front vehicle (heavy vehicle) to pass, as its length is longer than a light vehicle.

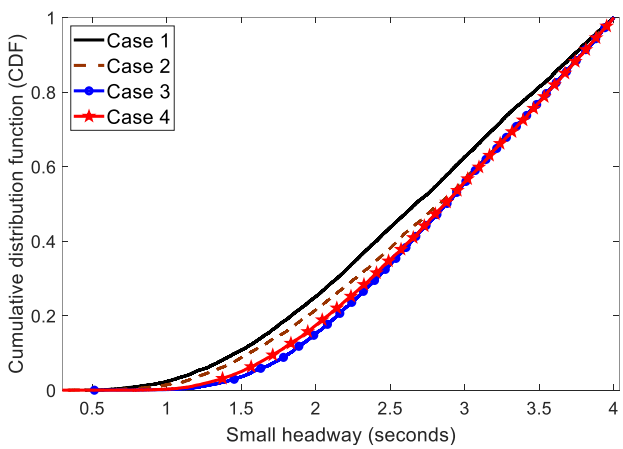

Figure 2.11 The Gaussian mixture model CDF of small headway (20~40 veh/5 min) from the truck lane of Sunsan

In addition, it is observed that the parameter λ in the shifted exponential distribution and the percentage of small headway is significantly affected by the total ratio of heavy vehicles (i.e., the ratio over the total measurement period) in each lane. To address this, the lanes are categorized in terms of the total ratio values as follows:

1) Car lane: first lane of Gimcheon, first lane of Sunsan, first and second lane of Waegwan
2) Middle lane: second lane of Gimcheon, third lane of Waegwan
3) Truck lane: third lane of Gimcheon, second lane of Sunsan, fourth lane of Waegwan

The total ratio of heavy vehicles in the car lane is lower than 0.01 while the truck lane's total ratio exceeds 0.5. Those for the middle lane are between 0.01 and 0.5. To show the difference between the three-lane categories, Figures 2.12(a) and 2.12(b) show the parameter of the shifted exponential distribution, λ, and the percentage of small headway for three categories in Case 4 (in which both the rear and front vehicles are heavy vehicles). Among the four aforementioned cases of rear and front vehicle combinations, Case 4 particularly shows noticeable differences between lane categories. As shown in Figure 2.12(b), the car lane and middle lane have higher percentages of small headway than the truck lane, indicating that the headway of heavy trucks in the car and the middle lane is smaller than that of the truck lane. To analyze this difference, the characteristics of heavy vehicle drivers are investigated and categorized into two types. The first type refers to those who drive heavy vehicles in groups, in which heavy vehicles move close to each other, and thus have relatively small headway. For the second type, those who drive alone, the heavy vehicles move freely and thus have relatively large headway. Therefore, due to the nature of the truck lane, heavy vehicles mainly use the truck lane whether driving alone or in groups, so it causes a relatively large headway. On the other hand, when heavy vehicles need to use the car or middle lane, they usually move in groups,

resulting in a higher percentage of small headway compared to the percentage of the truck lane.

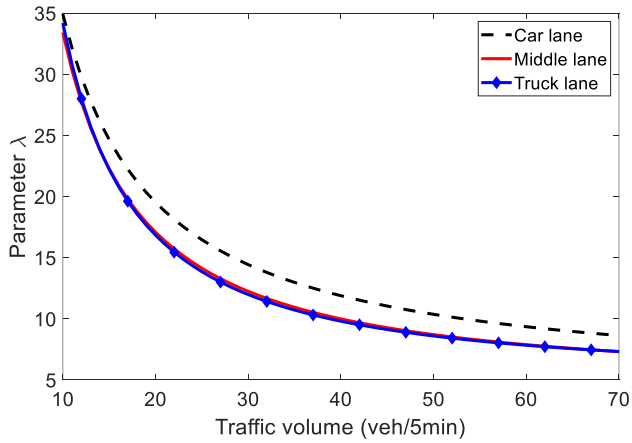

(a) The parameter λ of the shifted exponential distribution

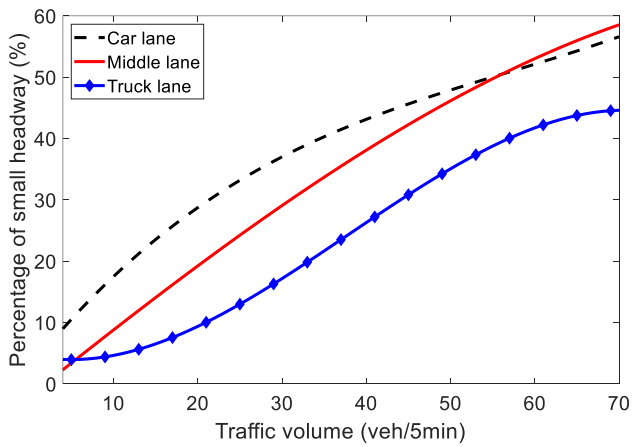

(b) The percentage of small headway

Figure 2.12 Fitted parameters in headway model of three-lane categories

2.4.4 Generation of artificial WIM data using Monte Carlo simulation

After developing probabilistic models for key random variables, artificial WIM data on each lane are generated by MCS based on the developed models with

adjusted parameters considering each lane's traffic environment. However, there exists a significant correlation between lanes in actual traffic flow, especially in traffic congestion. It is observed from the WIM data that all lanes should have similar traffic volume and average speed when congested traffic flow occurs. To consider this interaction, a simple method is proposed during MCS as follows. First, artificial WIM data of all lanes are generated independently and the sections of WIM data representing traffic congestion in the truck lane are identified. Next, the WIM data generated for the other lanes at the same time duration are re-generated based on the average speed and the traffic volume of the identified sections of the truck lane. As a result, the generated WIM data at the other lanes can be appropriately modified to consider the correlation between lanes. The results show that the proposed simple method can improve the accuracy of the traffic load effect estimation, especially for long-span bridges where the congested traffic flow tends to dominate (Kim and Song, 2018).

The procedure for generating artificial WIM data is illustrated by a flow chart in Figure 2.13. First, the state of traffic flow of the given day is determined whether or not traffic congestion occurs on the day based on the probability of the daily occurrence of traffic congestion. Then, the traffic volume and heavy vehicle ratio for 5 minutes are generated for the given hour. Next, the average speed during 5 minutes and the vehicle type are generated according to the generated traffic volume and the state of traffic flow. Then, the vehicle characteristic variables and the headway are generated. Through this procedure, WIM data are continuously generated until 5 minutes pass. After 5 minutes, the traffic volume is generated again and this process

is repeated until one day is covered. After one day, the state of flow for the next day is determined and the above process is repeated until the target period is achieved.

After generating WIM data, traffic flow should be simulated using generated WIM data to calculate the traffic load effect of the bridge member. For this, two traffic flow simulation methods are used. The first one is assuming the driving lane and speed of vehicles do not change in free traffic flow. In most bridges in South Korea, drivers are not allowed to change lanes during driving and the vehicle speed generally does not vary much when passing bridges especially for free traffic flow. Therefore, it is assumed that generated vehicles keep driving in the same lane until they exit the bridge with maintaining the generated speed (average speed) during free traffic flow. This method is a relatively simple and low-computational cost method. The second method is to consider the change in lane and speed of vehicles during congested traffic flow using microsimulation models. This method requires high computational cost but can simulate more accurate congested traffic flow and will be explained in more detail in Section 2.4.5.

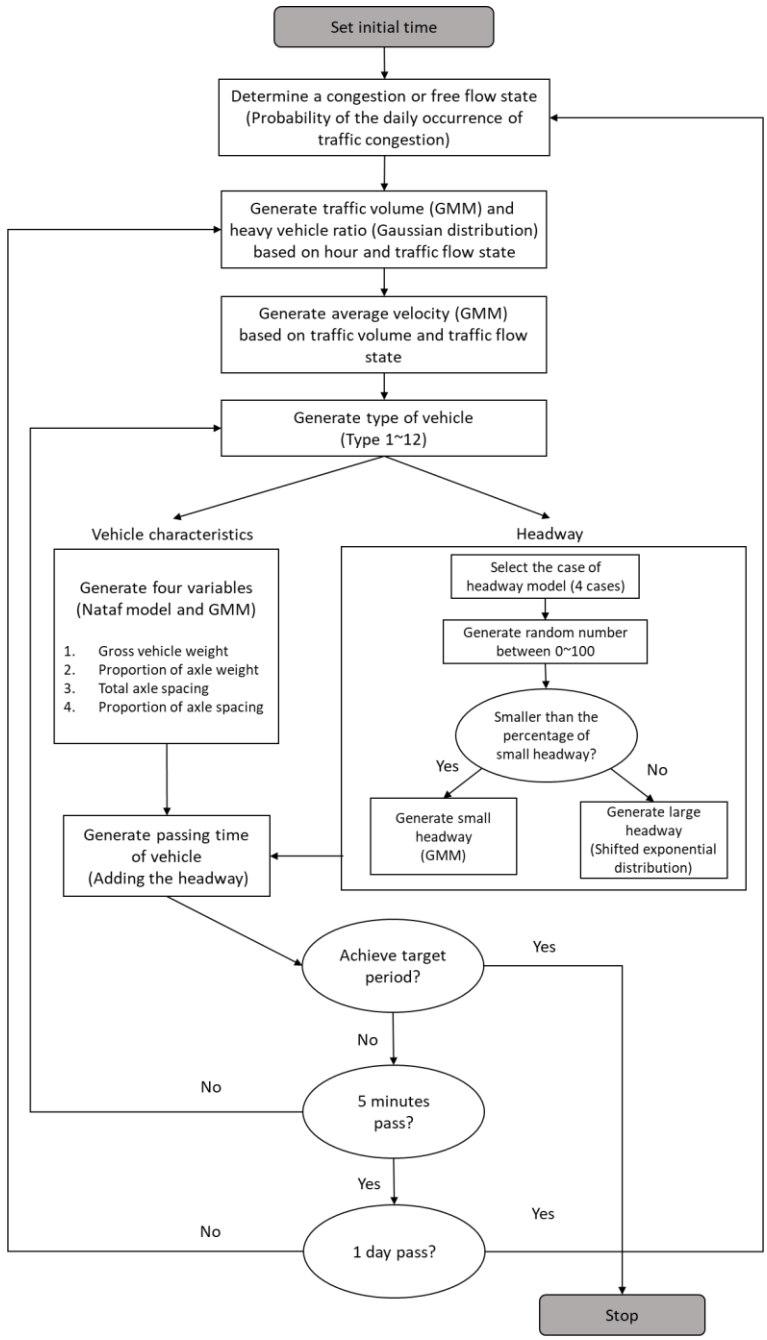

Figure 2.13 Flow chart for generating artificial WIM data based on the WIM-based probabilistic bridge traffic load model

2.4.5 Microsimulation models for congested traffic flow

In the case of traffic congestion, the speed of vehicles changes frequently, especially during the stop-and-go waves condition (O'Brien et al., 2015). In addition, lane changes should be considered, as car drivers tend to move away from heavy vehicles, which causes heavy vehicles to gather in the truck lane during traffic congestion (Caprani et al., 2016). To address this, some researchers used microsimulation models for describing traffic congestion (O'Brien et al., 2015; Caprani et al., 2016; Carey et al., 2018; Guo and Caprani, 2019). The microsimulation models are also employed in this dissertation to simulate the congested traffic flow more accurately.

First, the Intelligent Driver Model (IDM) (Treiber et al., 2000) is used as a speed change model in this study. This model takes into account the change in the speed of each vehicle by the acceleration model

$$\frac{dv(t)}{dt} = a\left\{1 - \left(\frac{v(t)}{v_0}\right)^4 - \left(\frac{s^*(t)}{s(t)}\right)^2\right\} \tag{2.3}$$

where a is the maximum acceleration, v_0 and $v(t)$ respectively denote the desired and current speed, and $s(t)$ is the current gap to the front vehicle. The term $s^*(t)$ is defined as follows to represent the desired minimum gap between two adjacent vehicles:

$$s^*(t) = s_0 + max\left\{Tv(t) + \frac{v(t)\Delta v(t)}{2\sqrt{ab}}, 0\right\} \tag{2.4}$$

where s_0 is the minimum jam distance (bumper-to-bumper), T is the safe time headway, $\Delta v(t)$ represents the speed difference between the current and the front

vehicles, and b is the comfortable deceleration. To simulate the traffic flow on a bridge, the speed of each vehicle is calculated at each time step (0.25 s) using its acceleration calculated by Eqs. (2.3) and (2.4). Further details of this model can be found in Treiber et al. (2000) and O'Brien et al. (2015).

To consider lane changes of vehicles while simulating traffic flow, this study uses the MOBIL model (Kesting et al., 2007), which allows the vehicles to change the driving lane when satisfying the so-called incentive criteria. Because the South Korean government adopts a designated lane system that allows drivers to change the driving lane from the right lane (slow lane) to the left lane (fast lane) only, the asymmetric rule of the MOBIL model is used. In detail, the following two equations are used as incentive criteria:

$$\begin{gathered} For\ right\ to\ left\ lane: \\ \tilde{a}_c(t) - a_c(t) > \Delta a_{th} + \Delta a_{bias} + p(a_n(t) - \tilde{a}_n(t)) \end{gathered} \tag{2.5}$$

$$\begin{gathered} For\ left\ to\ right\ lane: \\ \tilde{a}_c(t) - a_c(t) > \Delta a_{th} - \Delta a_{bias} + p\left[\left(a_n(t) - \tilde{a}_n(t)\right) + \left(a_o(t) - \tilde{a}_o(t)\right)\right] \end{gathered} \tag{2.6}$$

where the tilde indicates the situation after assuming the lane change, the subscript *c* means a current vehicle, the subscript *o* means the following vehicle of the current car (in the current lane), and *n* is the new following vehicle of the current car after the current car changes the driving lane (in the target lane to change). The threshold Δa_{th} represents minimum benefits to be exceeded for the driver when selecting change of lane, Δa_{bias} is the incentive to drive in the right lane, and p is the politeness factor to express driver aggressiveness. The incentive criteria are calculated for each vehicle on a bridge at every time step (0.25 s) considering the vehicle's acceleration and various parameters to determine whether the lane is

changed or not during the simulation of traffic flow. More details on the MOBIL model can be found in Kesting et al. (2007) and Caprani et al. (2016). To perform the microsimulation for congested traffic flow using the two models above, this study uses the model parameters in Table 2.4 based on Caprani et al. (2016) and vehicle data of South Korea. To simulate the congested traffic flow, the target bridge is located on a long road, and the safe time headway T increases gradually after a certain part to decrease the speed of vehicles (Kesting et al., 2007). The safety time headway is a parameter that controls the severity of traffic congestion, e.g. When we increase T more, vehicle speed decrease more. Therefore, the values of T corresponding to the average speed during congestion from MCS should be identified to adequately combine microsimulation models with the developed probabilistic model of bridge traffic loads. Figure 2.14 shows the investigated safe time headway values. They are similar to those presented in the literature (Caprani et al., 2016) that can describe the various traffic congestion states, e.g. stop and go waves (SGW), oscillatory congested traffic (OCT), and homogeneous congested traffic (HCT). It is also noted that traffic congestion does not occur from the beginning of microsimulation, so the traffic load effects should be calculated after simulating traffic flow for more than at least 20 minutes.

Table 2.4 Model parameters for the IDM and MOBIL models

	Light vehicles (type 1~4)	Heavy vehicles (type 5~12)
Desired speed v_0	120 km/h ($\pm$20%)	80 km/h ($\pm$10%)
Safe time headway, T	1.6 s	1.6 s
Maximum acceleration, a	0.73 m/s^2	0.73 m/s^2
Comfortable deceleration, b	1.67 m/s^2	1.67 m/s^2
Minimum jam distance, s_0	2 m	2 m
Politeness factor, p	0.1	0.1
Changing threshold, Δa_{th}	0.2	0.2
Bias for the right lane, Δa_{bias}	0.1	0.1
Maximum safe deceleration, b_{safe}	4 m/s^2	4 m/s^2
Front overhang	1 m	1.6 m
Rear overhang	1 m	2.5 m

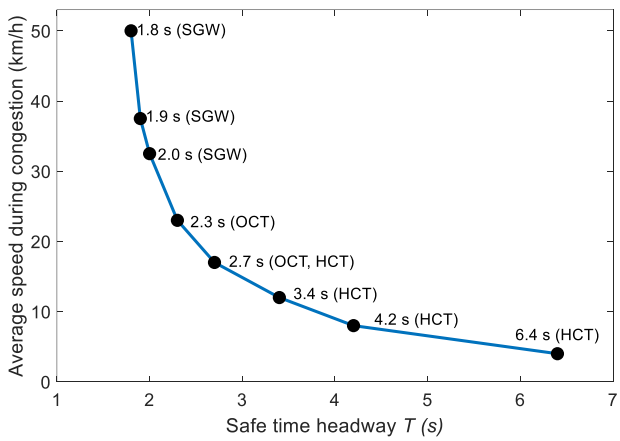

Figure 2.14 The safe time headway T corresponding to average speed during congested traffic flow

2.5. Verification of the developed model

Before estimating the traffic load effects for a bridge, the probabilistic model for traffic loads developed in this chapter is verified. The developed model is verified in terms of the total load on a bridge instead of other load effects computed from the influence lines. This is because the influence lines of bridges have highly diverse and

unique shapes depending on the elements, structural types, and length of bridges such that the verification using a particular set of influence lines would not ensure general validity. Moreover, the total load on a bridge has been used to calculate the Uniformly Distributed Load (UDL) in design codes (design lane load) and were often used to evaluate the traffic load effect on a bridge in many previous studies (Nowak et al., 2010; Buckland, 1981; Vrouwenvelder and Waarts, 1993; ECS, 2003). Considering the computational cost and the fact that traffic congestion does not occur often at Gimcheon and Waegwan, the average speed method is used to simulate traffic flow for verification. It is also assumed that the traffic volume does not vary notably for the remaining service life of the bridge.

By MCS, a total of 10 sets of artificial WIM data are generated at each lane for one year, and a total load of each lane is calculated every 0.2 seconds by simulating the traffic flow for imaginary multi-lane bridges at Gimcheon (3 lanes), Sunsan (2 lanes), and Waegwan (4 lanes). The total load on the bridge is calculated by summing up the loads computed for the individual lanes at the same time points. Among the calculated total loads on the bridge, the daily maximum total loads are selected because they are important in estimating the maximum traffic load over the service life of bridges through an extrapolation process. The daily maximum total loads from actual WIM data are also computed for comparison with those from the generated WIM data in a Gumbel probability paper.

To demonstrate the applicability of the developed model to general span lengths of bridges, two span length cases: 40m (short-span) and 800m (long-span) are investigated for the verification. The daily maximum values, often used for

extrapolation to longer periods, are plotted in Gumbel probability papers (see Figures 2.15, 2.16, and 2.17) to clearly show the extreme values at tail parts. The empirical CDFs show variability at the upper ends of the curves caused by the low likelihoods of extreme events. Overall, the daily maximum total loads show good overall agreements with those by actual WIM data for both short- and long-span bridges at all three sites. In addition, to analyze the comparison results in Figures 2.15, 2.16, and 2.17 quantitatively, the K-S test with a significance level of 0.05 is performed to check whether daily maximum total loads data from generated WIM data and those from actual WIM data belong to the same probability distribution. Table 2.5 shows the results of the K-S test for two span length cases at the three sites.

For three cases, it is confirmed that daily maximum total loads data from generated WIM data and those from actual WIM data do not follow the same probability distribution. This might be attributed to the local biases arising from the headway and vehicle characteristic models because these probabilistic models are developed by using data from all three sites. Moreover, 10 daily maximum total loads sets are obtained by generated WIM data, whereas only one daily maximum total load set is obtained by actual WIM data. Therefore, it is difficult to have almost the same values on the tail side where a lot of variabilities inherently exist. Hence, this study checks that a similar annual maximum total loads value (maximum value of the daily maximum total loads set) by actual WIM data exists among the annual maximum total loads values by generated WIM data for verification. Because this study ultimately aims to obtain maximum traffic load effects over the service life, so the annual maximum value is more important than daily maximum values. The

minimum errors between annual maximum total load by generated WIM data and annual maximum total load by actual WIM data are calculated and the results are provided in Table 2.6. All minimum errors are below 5%, which implies that generated WIM data can produce maximum traffic load effects similar to maximum traffic load effects by actual WIM data. These results presented in this section confirm the validity of the comprehensive probabilistic bridge traffic load model developed in this study for the purpose of estimating the traffic load effects on a bridge.

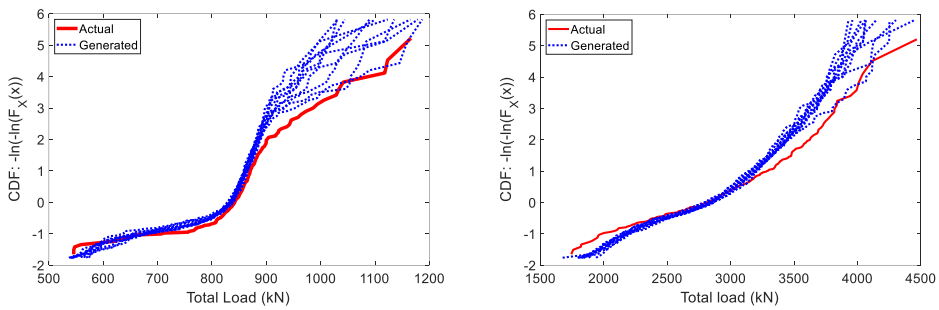

(a) Span length: 40m (b) Span length: 800m

Figure 2.15 Gumbel probability paper of daily maximum total load on bridge at Gimcheon

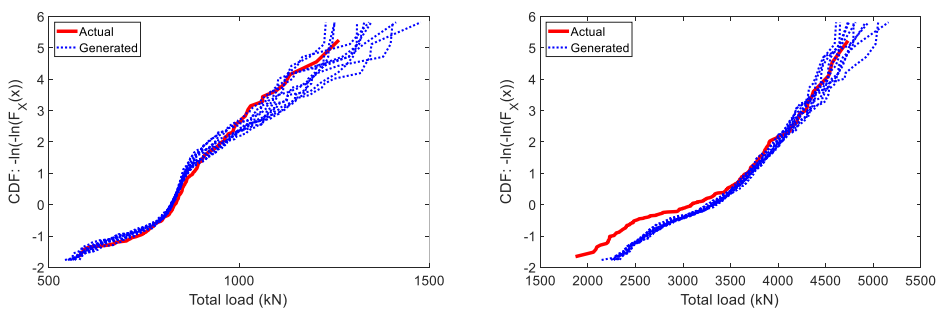

(a) Span length: 40m (b) Span length: 800m

Figure 2.16 Gumbel probability paper of daily maximum total load on bridge at Sunsan

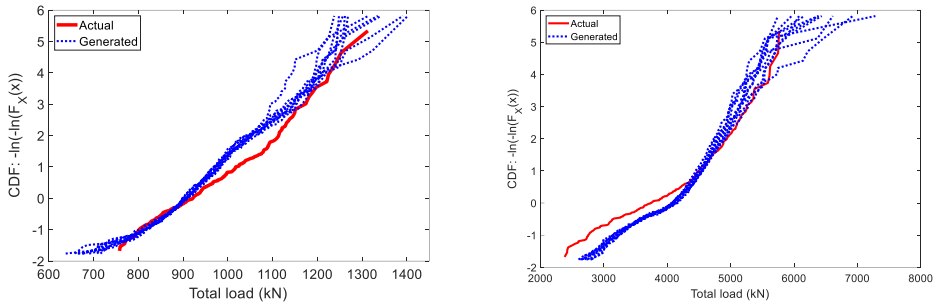

(a) Span length: 40m (b) Span length: 800m

Figure 2.17 Gumbel probability paper of daily maximum total load on bridge at Waegwan

Table 2.5 Results of the K-S test for daily maximum total loads data

Span length / Sites	40 m	800 m
Gimcheon	Reject	Reject
Sunsan	Not reject	Not reject
Waegwan	Reject	Not reject

Table 2.6 Minimum errors between annual maximum total load from generated WIM data and annual maximum total load from actual WIM data

Span length / Sites	40 m	800 m
Gimcheon	0.03%	0.18%
Sunsan	-0.94%	-0.24%
Waegwan	-1.38%	4.05%

2.6. Numerical examples

2.6.1 Estimation of traffic load effects of Incheon Grand Bridge

The maximum traffic load effects over the service life of a bridge are estimated using the developed model and the influence lines of bridges. The Incheon Grand Bridge, one of the long-span bridges in South Korea, is selected for the investigation.

The Incheon Grand Bridge is 21.38 km long and connects Yeongjong Island with the city of Incheon. In this study, a finite-element (FE) model of the cable-stayed bridge part (see Figure 2.18) is established using MATLAB®. The total length and main span length of the model are 1,480 m and 800 m respectively. The input information used for the FE model development, e.g., 3D coordinates of nodes, material/section properties, and dead loads of the bridge, was provided by the Korea Bridge Design & Engineering Research Center for academic use. The FE model considers the nonlinear behavior of cables, and it is assumed that the influence lines do not vary with the transverse position of each vehicle.

Several influence lines are obtained based on the FE model and examined through comparison with those from an existing model developed independently by the Korea Bridge Design & Engineering Research Center (Hwang and Kim, 2015). Two influence lines are selected to estimate the traffic load effects: the tension of a cable #52 and the moment of a girder #250, which is located at 685 m points from the column on the far left (see Figure 2.18 for the locations). Figure 2.19 shows the two influence lines of the Incheon Grand Bridge. The negative values of the influence line of the tension do not mean that the cable is actually under compression because the influence line shows the variation of tension caused by the traffic loads. The actual tension of the cable can be calculated by adding the tension caused by the dead load of the bridge.

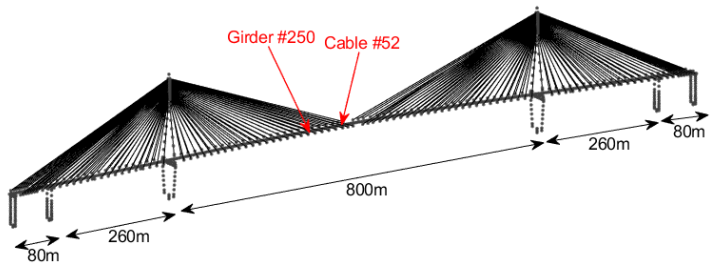

Figure 2.18 Finite element model of the cable-stayed bridge part of the Incheon Grand Bridge

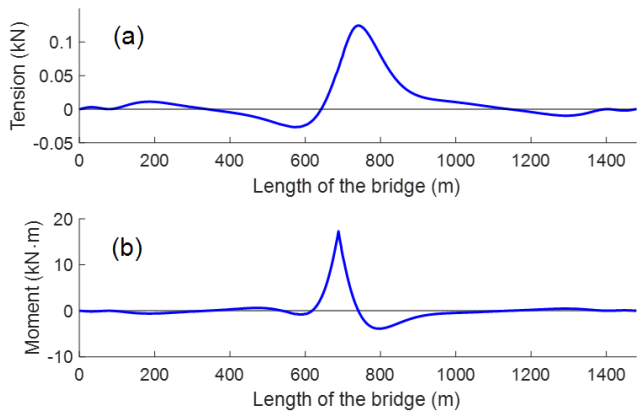

Figure 2.19 Influence lines of the Incheon Grand Bridge: (a) Tension of a cable #52, and (b) Moment of a girder #250

The Incheon Grand Bridge has two-way six lanes (three lanes in each direction). Because the WIM data used in this study are only uni-directional, the traffic load effects are calculated for three lanes using uni-directional artificial WIM data. Because no WIM data sets are available for the Incheon Grand Bridge, the three lanes of WIM data from Gimcheon site are used instead in this example. Artificial WIM data for each lane are generated by MCS with the appropriate parameter values of random variables representing the traffic environment of each lane at Gimcheon. The traffic load effects (tension, moment) of each lane are calculated using the

generated WIM data and the influence lines. Subsequently, the total traffic load effects on the bridge are obtained by summing up the load effects on the three lanes at the same time points. Before the target traffic load effects are estimated, this study compares the daily maximum traffic load effects (tension and moment) from the developed model with those from actual WIM data as described above for verification. Figure 2.20 shows the comparison results, which again demonstrate the validity of the developed model for traffic loads on bridges.

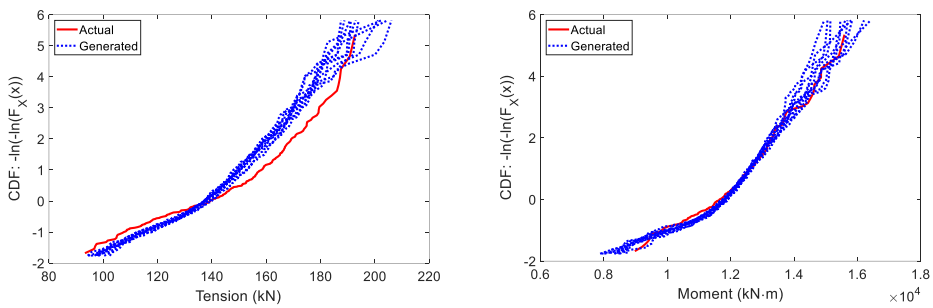

(a) Tension of a cable (cable #52) (b) Moment of a girder (girder #250)

Figure 2.20 Gumbel probability paper of daily maximum traffic load effects

2.6.1.1 Extrapolation

In various efforts to design and evaluate bridges, it is important to accurately predict the maximum traffic load effects during the service life or a return period of possible events, e.g., exceeding a certain threshold of load effects. This study uses extreme value theory, block maximum method, and return period to extrapolate the traffic load effects to obtain them for such a long period.

For applications of extreme value theory, let us consider a sequence of independent and identically distributed random variables, $x_1, x_2 \cdots, x_n$ having a

common CDF $F(\cdot)$. In this study, such a sequence can represent maximum traffic load effects for *n* time intervals. The CDF of the maximum value from a sequence of $x_1, x_2 \cdots, x_n$, denoted by M_n, is derived as

$$\begin{aligned} \Pr(M_n < z) &= \Pr(x_1 < z, x_2 < z, \cdots, x_n < z) \\ &= \Pr(x_1 < z) \times \cdots \times \Pr(x_n < z) = F(z)^n \end{aligned} \tag{2.7}$$

When the distribution *F* is unknown and it is difficult to estimate the type of the distribution from the available data, the extrapolation by Eq. (2.7) may produce the inaccurate distribution of M_n. As *n* increases, i.e., for a long time period, it is known that the distribution of M_n asymptotically converges to one of the three types of extreme value distributions, Gumbel, Fréchet, and Weibull distributions according to Fisher–Tippett–Gnedenko theorem (Gnedenko, 2018). The three types of extreme value distributions can be described by the CDF of generalized extreme value (GEV) distribution (Gumbel, 1958)

$$G(x; \mu, \sigma, \xi) = \begin{cases} \exp\left[-\left\{1 + \xi\left(\frac{x-\mu}{\sigma}\right)\right\}^{-\frac{1}{\xi}}\right], & \xi \neq 0 \\ \exp\left\{-\exp\left(-\frac{x-\mu}{\sigma}\right)\right\}, & \xi = 0 \end{cases} \tag{2.8}$$

where μ, σ, and ξ respectively denote the parameters describing the location, scale, and shape of the distribution. If $\xi = 0$, the GEV distribution means the Gumbel distribution. The cases $\xi > 0$ and $\xi < 0$ respectively represent Fréchet and Weibull distribution.

According to the extreme value theory, maximum load effects can be described by GEV distributions as long as appropriate data sets are available to estimate the parameters of GEV distribution. In this study, the GEV parameters are obtained by

the block maximum method as follows. A long series of data sets are divided by "blocks" having the same duration. The maximum value from each block is obtained to estimate the parameters of GEV distribution based on the set of maximum data (Gnedenko, 2018). Many studies used hourly, daily, weekly, and annual maximum traffic load data to fit the GEV distribution (O'Brien et al., 2015). This study calculates the *annual* maximum tension and moment of the Incheon Grand Bridge using artificial long-period WIM data. Data covering a long duration are needed to accurately capture the extreme events during the service life of a bridge and reduce the variability of the target traffic load effects (Enright and O'Brien, 2013). Thus, artificial WIM data are generated by MCS for a 100-year duration to calculate a total of 100 annual maximum tensions and moments. These maximum values are fitted with GEV distribution using maximum likelihood estimation as shown in Figure 2.21.

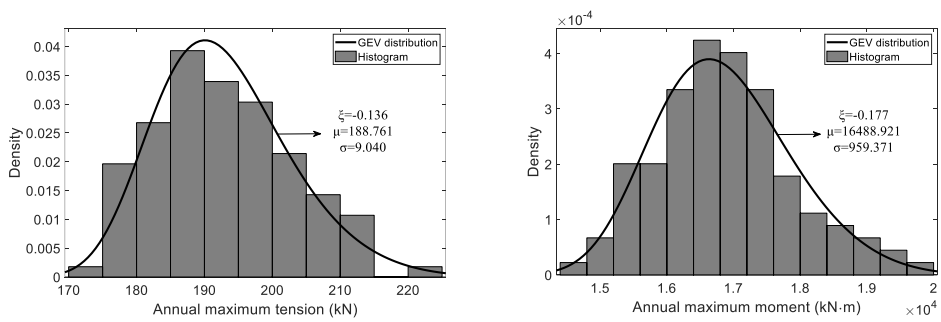

(a) Tension of a cable (cable #52) (b) Moment of a girder (girder #250)

Figure 2.21 Histogram and fitted GEV distributions of annual maximum total traffic load effects

In bridge design codes, the live load is often defined in terms of a return period. Return period is defined as an average time interval between two exceedance events over a given threshold value. Specifically, if the probability of event exceeding a certain threshold value z is p, the return period $R(z)$ is defined as (Ang and Tang, 1975)

$$R(z) = \frac{1}{p} \tag{2.9}$$

For example, an event with the 100-year return period means that the probability p of exceeding the threshold z in any one year is 1/100 (Ang and Tang, 1975). Therefore, the target traffic load effects x_T can be calculated using the return period and the distribution of the annual maximum traffic load effects as follows.

$$x_T = G^{-1}(1-p) = G^{-1}\left\{1 - \frac{1}{R(z)}\right\} \tag{2.10}$$

The target traffic load effects x_T estimated by this method represent so-called return period value. Return period value is the value that has the highest probability of an event exceeding this value occurring once during the return period., e.g. service life of bridges. In the following subsection, using Eq. (2.10) and the return period defined in each design code, the target traffic load effects by artificial WIM data are calculated and compared with those in design codes.

2.6.1.2 Comparison with the live load model in design codes

For comparison, two bridge design codes: KHBDC-CB and AASHTO HL-93 which are already described in Chapter 1 are used. KHBDC-CB calculates the live load effects as the larger value between 1) the effect of one design truck, and 2) the

combined effects of reduced design truck (75%) and the design lane load. In AASHTO HL-93, the live load effects are calculated as the maximum value of 1) the combined effect of the design tandem and the design lane load, and 2) the combined effect of one design truck and the design lane load.

The maximum tension of a cable #52 and the moment of a girder #250 are calculated by use of the design lane loads and MPF of KHBDC-CB and AASHTO HL-93. The maximum traffic load effects from KHBDC-CB and AASHTO HL-93 are based on return period values (the same way to obtain target traffic load effects in this study) of traffic loads over defined each return period (100 years for KHBDC-CB and 75 years for AASHTO HL-93). For comparison, the target tension and moment are estimated by fitted GEV distribution of annual maximum traffic load effects and Eq. (2.10) with return periods explained above. The results are shown in Tables 2.7 and 2.8 where the "ratios" are calculated by dividing the traffic load effects from the developed model by those from the bridge design code. It is noted that target tension and moment are quite lower than those from the codes.

Table 2.7 Comparison with 100-year total maximum traffic load effects by KHBDC-CB (with MPF considered)

	KHBDC-Cable-supported Bridges	Developed model	Ratio
Tension (kN)	546.62	219.64	0.40
Moment (kN·m)	34,832.55	19,468.36	0.56

Table 2.8 Comparison with 75-year total maximum traffic load effects by AASHTO HL-93 (with MPF considered)

	AASHTO HL-93	Developed model	Ratio
Tension (kN)	602.95	218.22	0.36
Moment (kN·m)	36,243.85	19,342.15	0.53

To investigate the reason for the differences, target traffic load effects on the truck lane are calculated without considering MPF. The results in Tables 2.9 and 2.10 show that the traffic load effects are now much more similar. According to Fu et al. (2013), MPF is mainly influenced by average daily truck traffic (ADTT), span length, and the number of lanes although there have been not many studies related to this topic. They showed that MPF in design codes is highly conservative, and proposed MPF for short- and medium-span bridges (Fu et al., 2013). Therefore, the results in this example indicate that MPF in bridge design codes is making a significant difference between actual traffic load effects and those in design codes. Although comparison results can differ significantly depending on site-specific conditions and shape of influence lines, the results at least raise pressing needs for careful studies on MPF and this topic will be handled in Chapter 5.

Table 2.9 Comparison with 100-year maximum total traffic load effects on the truck lane by KHBDC-CB (without considering MPF)

	KHBDC-Cable-supported Bridges	Developed model	Ratio
Tension (kN)	227.76	178.54	0.78
Moment (kN·m)	14,513.56	14,281.35	0.98

Table 2.10 Comparison with 75-year maximum traffic load effects on the truck lane by AASHTO HL-93 (without considering MPF)

	AASHTO HL-93	Developed model	Ratio
Tension (kN)	283.74	175.92	0.62
Moment (kN·m)	17,055.93	14,232.88	0.83

Additionally, to identify the influence of microsimulation models on estimating traffic load effects in the congested traffic flow, the 100-year maximum traffic load effects are calculated and compared to those from the method using average speed which is the first method explained in Section 2.4.5. The traffic environment of Sunsan is used because traffic congestion occurs frequently. Two traffic load effects, i.e. tension and moment using the same influence lines of the Incheon Grand Bridge (Figure 2.19), are estimated as shown in Table 2.11. The results show that the traffic load effects increase by 5~10% when using microsimulation models. This is because the method assigning the average speed to each vehicle uses the overestimated headway data in traffic congestion and does not consider the change of driving lanes. The effects of microsimulation on traffic load estimations were studied in detail by Lipari (2013).

Table 2.11 Comparison of traffic flow simulation method using estimated 100-year maximum traffic load effects

	Average speed	Micro simulation	Rate of change	KHBDC
Tension (kN)	242.06	259.53	7.21%	409.96
Moment (kN·m)	15,294.72	16,358.66	6.95%	26,124.21

2.6.2 Parametric study

The developed traffic load model could be used as a generic model, i.e., a base model representing a wide range of traffic conditions, which can be later customized for a specific site by adjusting parameters of key variables based on available information or through Bayesian updating with the WIM data collected at the location. To investigate the potential of developing such a generic probabilistic traffic load model, the following parametric study is performed.

First, the 100-year maximum traffic load effects are estimated while varying the total ratio of heavy vehicles (introduced for the headway model above), which is a key variable regarding the overall traffic environment of the bridge. For the truck lane of Gimcheon, where the total ratio of heavy vehicles is 53% according to the WIM data, the traffic load effects are estimated by the developed model with all parameters of variables in the simulation model unchanged except for the total ratio of heavy vehicles. To vary the ratio, the mean and standard deviation of the hourly heavy vehicle ratio, which is fitted by a Gaussian distribution, are scaled. Just as in Section 2.6.1, after 100 years of artificial WIM data sets are generated, the tension of a cable #52 and the moments of a girder #250 are obtained using the influence lines of the Incheon Grand Bridge. The 100-year target traffic load effects are estimated using GEV distributions of the annual maximum tension and moment. The results are shown in Figure 2.22.

As the total ratio of heavy vehicles increases from 0.1 to 0.7, the 100-year maximum tension and moment increase by 71.9 and 23.8 percent, respectively. Although the influence can differ depending on the shape and characteristics of the

influence lines, it is observed that the total ratio of heavy vehicles can have a significant impact on the extreme traffic load effects. As shown in this brief case study, the comprehensive probabilistic traffic load model developed in this study is expected to provide effective means of various parametric studies on traffic loads and their effects on bridges.

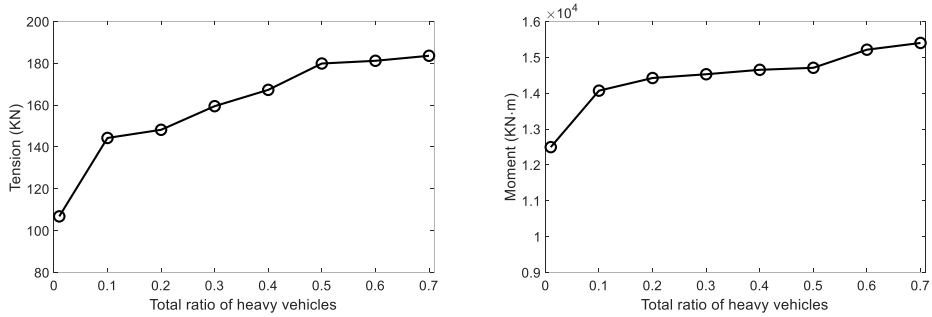

(a) Tension of a cable (cable #52) (b) Moment of a girder (girder #250)

Figure 2.22 100-year maximum traffic load effects estimated according to change of the total ratio of heavy vehicles

2.7. Summary

This chapter developed a comprehensive probabilistic traffic load model based on Weigh-In-Motion (WIM) data collected from three highway sites in South Korea for accurate estimations of the traffic load effects on bridges. To simulate the traffic flow on a bridge by the Monte Carlo simulation approach, essential key random variables representing the site-specific conditions of traffic environments of the bridge were identified and incorporated into the model. In the probabilistic model for vehicle characteristics, four random variables (Gross vehicle weight, axle weights, total axle spacing, and axle spacing) were fitted to Gaussian mixture models and statistical correlations between these variables were fully considered using the

Nataf model. The probabilistic model for traffic flow also featured four key random variables: traffic volumes, speed, the ratio of vehicle types, and headway. These variables were incorporated into the model based on probabilistic studies and theories of transportation engineering. Additionally, a simple method was proposed to take into account the interaction between multiple lanes.

To verify the developed traffic load model, the daily maximum total loads on the bridge were calculated from generated WIM data and compared to those from actual WIM data. These results showed good agreements in both short- and long-span cases at all three sites. Next, maximum traffic load effects for a long period on the Incheon Grand Bridge were estimated using its influence lines. The 100- and 75-year maximum traffic load effects (tension of a cable, moment of a girder) were estimated by extrapolation process and compared with the design loads of two design codes (KHBDC-CB, AASHTO HL-93). The estimated traffic load effects were significantly lower than those by the design code, which might be attributed to highly conservative multiple presence factors (this topic will be addressed in Chapter 5). A case study was also conducted to explore the potential of the developed model to be used as a generic probabilistic traffic load model that can be customized to site-specific conditions. The 100-year traffic load effects were estimated while varying the parameters of a key variable (total ratio of heavy vehicles) to show the influence of the parameter changes on estimating site-specific traffic load effects.

Chapter 3. Bayesian Updating Methodology for Traffic Loads Using In-Service Data of Traffic Environment

3.1. Introduction

In Chapter 2, a comprehensive probabilistic model for bridge traffic loads that can reflect the various traffic environment of bridges are developed. However, the traffic environment of a bridge may change over its service life, which can affect the traffic load effects significantly. For example, a reduction in traffic volume due to the construction of new highways or bridges in the surroundings may result in a decrease in traffic load effects. On the other hand, if many factories are constructed nearby, which causes increasing the volume of cargo transportation and in turn, the traffic loads can increase. Therefore, these changes in the traffic environment must be considered for accurate estimation of the traffic loads on in-use bridges. This naturally requires a methodology to update the parameters of the probabilistic model of bridge traffic loads based on new observations and information obtained through continuous monitoring of the traffic environment of the bridge.

While most of the previous studies have estimated the traffic load effects assuming no significant variation in traffic volume and other characteristics of the traffic environment, some studies considered the future growth of traffic volumes in terms of the annual growth rate, interval traffic-growth model, or non-stationary Bayesian method (O'Brien et al. 2014; Lu et al., 2017a; Lu et al., 2017b; Yu et al.,

2019). Also, Leahy et al. (2015) estimated the site-specific bridge traffic load effects using Bayesian statistics with Gross vehicle weight (GVW) data from 19 sites as prior knowledge. Yu et al. (2019) and Yu and Cai (2019) proposed a Bayesian method to predict the traffic load effects with direct updates based on the measured strain response. However, the traffic load effects of all members of the bridge cannot be updated through direct measurements such as strain because of limitations in the number of sensors and their locations. Besides, it is impossible to identify which factors quantitatively change the traffic load effects. Therefore, if observations or information about the changes in individual variables of traffic environment from the WIM system and traffic investigation, e.g. traffic volume, axle weight, speed are available, direct updating of the corresponding distribution parameters would be more effective and intuitive. Since such an updating process can reflect the degree of change in each traffic environment variable, the traffic load effects can be estimated more accurately and quantitatively. This would enable us to identify the impacts of the changed variables on the traffic load effects on bridges as well.

Thus, this chapter aims to develop a Bayesian inference methodology to directly update the parameters of the probabilistic model of bridge traffic loads based on new observations regarding the traffic environment. Bayesian inference, a method of statistical inference to quantify the uncertainty of parameters, obtains the posterior probability distribution by combining the existing information represented by a prior model with newly measured data (Ang and Tang, 2007; Box and Tiao, 2011). This method enables us to continuously update traffic load effects on bridges by estimating the parameters of the posterior distribution affected by the changes in the

surroundings based on WIM data. Besides, it is often impossible to obtain sufficient WIM data in estimating traffic loads on bridges because of challenges in continuous WIM data acquisition. In such cases, by using the indirect information about the traffic around the bridge and the generic probabilistic model of bridge traffic loads as a prior model, Bayesian updating can estimate the traffic load effects on that particular bridge more reasonably and accurately.

3.2. Bayesian updating methods

The probabilistic distributions of the random variables used in the developed traffic load model in Chapter 2 can be divided into three main categories: (1) the Gaussian distribution used to represent the heavy vehicle ratio, (2) the linear regression model used to represent the percentage of small headway, and (3) the Gaussian mixture model (GMM) employed to represent the variables of vehicle characteristics (axle weight, axle spacing), speed, small headway, and traffic volume. These probabilistic models are developed based on theories of transportation engineering and statistical investigations. This study proposes a suitable Bayesian inference method for each of the three models as described in this section.

3.2.1 Bayesian inference and conjugate prior

Bayesian inference generally refers to statistical analysis that infers the posterior distribution of the target parameter based on the prior information and new observations. In Bayesian inference, the parameters θ in the probability distribution

are treated as random variables rather than fixed values, and are expressed as follows in terms of hyper-parameters ν:

$$\theta \sim p(\theta|\nu) \tag{3.1}$$

Based on the Bayes' theorem, the posterior probability distribution can be calculated by updating the prior distribution with newly available observations $\boldsymbol{X} = \{x_1, x_2, \dots, x_n\}$, which is expressed as

$$p(\theta|\boldsymbol{X},\nu) = \frac{p(\boldsymbol{X}|\theta)p(\theta|\nu)}{p(\boldsymbol{X}|\nu)} = \frac{p(\boldsymbol{X}|\theta)p(\theta|\nu)}{\int p(\boldsymbol{X}|\theta)p(\theta|\nu)d\theta} \propto p(\boldsymbol{X}|\theta)p(\theta|\nu) \tag{3.2}$$

where $p(\boldsymbol{X}|\theta)$ is the conditional probability density of $\boldsymbol{X}$ given θ, which is called the likelihood function.

It is generally challenging to calculate the integral in the denominator of Eq. (3.2), termed the normalizing constant. To facilitate this calculation, the concept called a conjugate prior distribution was introduced by Raiffa and Schlaifer (1961). If the conjugate prior distribution corresponding to the given likelihood is chosen, the posterior distribution follows the same type of distribution for the prior, and its distribution parameters can be calculated by closed-form formulas, i.e. without calculating the integral. To make use of these computational merits, the three Bayesian inference methods proposed in the following sections use conjugate priors.

3.2.2 Method 1: Gaussian-inverse-gamma distribution for Gaussian distribution

In the probabilistic model developed for bridge traffic loads, heavy vehicle ratios are represented by Gaussian distribution. When the two parameters of Gaussian distribution (mean μ and variance σ^2) are to be updated, the Gaussian-

inverse-gamma (N-Γ^{-1}) distribution can be used as the conjugate prior. The probabilistic distributions of the two parameters are expressed as

$$\mu|\sigma^2 \sim N\left(\mu_0, \frac{\sigma^2}{\lambda}\right),\ \sigma^2 \sim \Gamma^{-1}(\alpha, \gamma) \tag{3.3}$$

where μ_0 and λ are the hyper-parameters of the prior distribution of the mean parameter μ (which is conditional distribution given σ^2), and α and γ are the hyper-parameters of the prior distribution of the variance parameter σ^2. The joint probability density function (PDF) of the Gaussian-inverse-gamma distribution is defined as

$$\begin{aligned} p(\theta|\nu) &= f(\mu, \sigma^2|\mu_0, \lambda, \alpha, \gamma) \\ &= \frac{\gamma^\alpha \sqrt{\lambda}}{\Gamma(\alpha)\sqrt{2\pi\sigma^2}}\left(\frac{1}{\sigma^2}\right)^{\alpha+1} \exp\left(-\frac{2\gamma + \lambda(\mu - \mu_0)^2}{2\sigma^2}\right) \end{aligned} \tag{3.4}$$

When a set of n observations $\boldsymbol{X} = \{x_1, x_2, \ldots, x_n\}$ is obtained, the likelihood function $p(\boldsymbol{X}|\theta)$ can be calculated by

$$\begin{aligned} p(\boldsymbol{X}|\theta) = \prod_{i=1}^{n} p(x_i|\,\mu, \sigma^2) &\propto \prod_{i=1}^{n} \frac{1}{\sigma} \exp\left[-\frac{1}{2\sigma^2}(x_i - \mu)^2\right] \\ &\propto \frac{1}{\sigma^n} \exp\left[-\frac{1}{2\sigma^2}\sum_{i=1}^{n}(x_i - \mu)^2\right] \end{aligned} \tag{3.5}$$

Using the prior distribution $p(\theta|\nu)$ in Eq. (3.4) and the likelihood function $p(\boldsymbol{X}|\theta)$ in Eq. (3.5), the posterior probability distribution $p(\theta|\boldsymbol{X}, \nu)$ in Eq. (3.2) can be calculated as the same form of the prior distribution, i.e. Gaussian-inverse-gamma distribution, whose hyper-parameters are updated as follows (Bernardo and Smith, 2009):

$$\mu_0 \to \frac{\lambda\mu_0 + n\bar{x}}{n+\lambda}, \qquad \lambda \to \lambda + n, \qquad \alpha \to \alpha + \frac{n}{2},$$
$$\gamma \to \gamma + \frac{1}{2}\left(ns^2 + \frac{\lambda n(\bar{x} - \mu_0)^2}{n+\lambda}\right) \tag{3.6}$$

where $\bar{x}$ and s^2 are the sample mean and sample variance from $\boldsymbol{X}$, respectively. In summary, the posterior probability distribution of the parameters μ and σ^2 can be obtained by updating the hyper-parameters of the conjugate prior distribution.

3.2.3 Method 2: Bayesian linear regression for linear regression model

Headway is one of the critical variables that characterize traffic flow on bridges. To generate the headway between two adjacent vehicles given traffic volume, the percentage of "small" headway (smaller than 4 seconds), which is used as an important criterion regarding whether generating small or large headway in MCS, was introduced in Chapter 2. The percentage of small headway given traffic volume is expressed by a linear regression model for each of the traffic volume ranges as shown in Figure 2.10 and the equation for the linear regression model is given by

$$y_i = \beta_0 + \beta_1 x_{i1} + \epsilon_i = \boldsymbol{x_i}\boldsymbol{\beta} + \epsilon_i, \qquad \epsilon_i \sim N(0, \sigma^2) \tag{3.7}$$

where y_i, $i = 1, \dots, n$ is the response variable representing the percentage of small headway in this study, $\boldsymbol{x}_i$ is 1×2 predictor row vector denoting the traffic volume, $\boldsymbol{\beta}$ is 2×1 vector of the regression model parameters, and ϵ_i is independent and identically distributed Gaussian random variable representing the model error. Assuming homoscedasticity, the variance of ϵ_i, σ^2 is assumed to be constant over $\boldsymbol{x}_i$.

When the error term ϵ_i follows a Gaussian distribution and an appropriate conjugate prior distribution is assumed, the posterior distribution for a linear regression model can be analytically calculated. This updating method is called Bayesian linear regression. Naturally, this study employs Bayesian linear regression to update the parameters of the linear regression models that were developed to predict the percentage of small headway for a given traffic volume. A Gaussian-inverse-gamma distribution is selected again as a conjugate prior distribution but unlike Eq. (3.3), bivariate Gaussian distribution is used instead of univariate because the prediction vector consists of two random variables. In detail, the conjugate priors of the regression parameters $\boldsymbol{\beta}$ are given by

$$\boldsymbol{\beta}|\sigma^2 \sim N(\boldsymbol{\mu}, \boldsymbol{\Lambda}),\ \sigma^2 \sim \Gamma^{-1}(\alpha, \gamma) \tag{3.8}$$

where $N(\boldsymbol{\mu}, \boldsymbol{\Lambda})$ represents the bivariate Gaussian distribution with the mean vector $\boldsymbol{\mu} = \begin{pmatrix}\mu_0 \\ \mu_1\end{pmatrix}$ and covariance matrix $\boldsymbol{\Lambda} = \sigma^2\boldsymbol{\lambda}^{-1} = \sigma^2\begin{pmatrix}1/\lambda & 0 \\ 0 & 1/\lambda\end{pmatrix}$ (a conditional distribution given the other parameter σ^2). The diagonal matrix form indicates that β_i and β_j $(i \neq j)$ are assumed to be uncorrelated (O'Hagan, 2004).

When n datasets $(\boldsymbol{y}, \boldsymbol{X})$, consisting of $n\times1$ vector $\boldsymbol{y}$ and $n\times2$ matrix $\boldsymbol{X}$, are measured, the corresponding likelihood function is expressed as

$$p(\boldsymbol{y}|\boldsymbol{X}, \boldsymbol{\beta}, \sigma^2) \propto \frac{1}{\sigma^n}\exp\left[-\frac{1}{2\sigma^2}(\boldsymbol{y} - \boldsymbol{X}\boldsymbol{\beta})^{\mathrm{T}}(\boldsymbol{y} - \boldsymbol{X}\boldsymbol{\beta})\right] \tag{3.9}$$

Using the conjugate prior in Eq. (3.8) and the likelihood function $p(\boldsymbol{X}|\theta)$ in Eq. (3.9), the posterior probability distribution $p(\boldsymbol{\beta}, \sigma^2|\boldsymbol{y}, \boldsymbol{X})$ is calculated as follows based on Bayes' theorem:

$$
\begin{aligned}
p(\boldsymbol{\beta}, \sigma^2|\boldsymbol{y}, \boldsymbol{X}) &\propto p(\boldsymbol{y}|\boldsymbol{X}, \boldsymbol{\beta}, \sigma^2) p(\boldsymbol{\beta}|\sigma^2) p(\sigma^2) \\
&\propto \frac{1}{\sigma^n} \exp\left[-\frac{1}{2\sigma^2}(\boldsymbol{y} - \boldsymbol{X}\boldsymbol{\beta})^{\mathrm{T}}(\boldsymbol{y} - \boldsymbol{X}\boldsymbol{\beta})\right] \\
&\quad \frac{1}{\sigma^2} \exp\left[-\frac{1}{2\sigma^2}(\boldsymbol{\beta} - \boldsymbol{\mu})^{\mathrm{T}} \boldsymbol{\lambda} (\boldsymbol{\beta} - \boldsymbol{\mu})\right] \frac{1}{\sigma^{2(\alpha+1)}} \exp\left(-\frac{\gamma}{\sigma^2}\right)
\end{aligned} \tag{3.10}
$$

After further derivations (O'Hagan, 2004), the hyper-parameters in Eq. (3.8) are updated as follows:

$$
\begin{aligned}
&\boldsymbol{\mu} \to (\boldsymbol{\lambda} + \boldsymbol{X}^{\mathrm{T}}\boldsymbol{X})^{-1}\left(\boldsymbol{X}^{\mathrm{T}}\boldsymbol{X}\widehat{\boldsymbol{\beta}} + \boldsymbol{\lambda}\boldsymbol{\mu}\right), \quad \boldsymbol{\Lambda} \to \sigma^2(\boldsymbol{\lambda} + \boldsymbol{X}^{\mathrm{T}}\boldsymbol{X})^{-1} \\
&\alpha \to \alpha + \frac{n}{2}, \quad \gamma \to \left[\gamma^{-1} + \frac{1}{2}\left(\boldsymbol{y} - \boldsymbol{X}\widehat{\boldsymbol{\beta}}\right)^{\mathrm{T}}\left(\boldsymbol{y} - \boldsymbol{X}\widehat{\boldsymbol{\beta}}\right)\right. \\
&\qquad \left. + \frac{1}{2}\left(\widehat{\boldsymbol{\beta}} - \boldsymbol{\mu}\right)^{\mathrm{T}}(\boldsymbol{\lambda} + (\boldsymbol{X}^{\mathrm{T}}\boldsymbol{X})^{-1})^{-1}\left(\widehat{\boldsymbol{\beta}} - \boldsymbol{\mu}\right)\right]^{-1}
\end{aligned} \tag{3.11}
$$

where $\widehat{\boldsymbol{\beta}} = (\boldsymbol{X}^{\mathrm{T}}\boldsymbol{X})^{-1}\boldsymbol{X}^{\mathrm{T}}\boldsymbol{y}$ is the estimate of $\boldsymbol{\beta}$ obtained by minimizing the sum of squared residuals. The updated parameters of the linear regression model in Eq. (3.11) make it possible to improve inference on the percentage of small headway in the probabilistic model.

3.2.4 Method 3: Gibbs sampling for Gaussian mixture model

A Gaussian mixture model (GMM) consists of multiple Gaussian densities, which is suitable for representing random variables with multiple peaks or modes. Therefore, in the probabilistic model of bridge traffic load, various random variables showing multiple peaks, i.e. axial weight, axle spacing, traffic volume, average speed, and small headway, are described by GMM. The PDF of a GMM is described as

$$
f(x|\boldsymbol{\theta}) = \sum_{j=1}^{J} \pi_j f_j\left(x\middle|\mu_j, \sigma_j^2\right) \tag{3.12}
$$

where $\boldsymbol{\theta} = \{(\pi_1, \ldots, \pi_J), (\mu_1, \sigma_1^2), \ldots, (\mu_J, \sigma_J^2)\}$ represents the distribution parameters of GMM, π_j is the relative weight of the *j*-th Gaussian component,

satisfying $0 < \pi_j < 1$ and $\sum_{j=1}^{J} \pi_j = 1$, and $f_j(x|\mu_j, \sigma_j^2)$ is the PDF of the *j*-th Gaussian distribution whose parameters are μ_j and σ_j^2.

To facilitate the parameter estimation of a GMM model, a classification vector $Z = (z_1, \dots, z_n)$ consisting of latent variables z_i is introduced unlike the other cases in Sections 3.2.2 and 3.2.3. This is because a GMM model has weight parameters, unlike other probability distributions. The assignment of the latent variable, $z_i = j$ means that the *i*-th observation is classified into the *j*-th component (Bilmes, 1998). Therefore, it is impossible to obtain the posterior probability distribution of all parameters as closed form at once. Thus, this study adopts Gibbs sampling, one of the Markov Chain Monte Carlo simulation (MCMC) methods, to update the parameters of GMM. This method is widely used particularly when it is more difficult to extract a sample directly from the joint distribution of parameters than from the conditional probability distribution of the parameters of interest given the values of the other parameters (Gelfand, 2000). So, it is required to obtain the conditional posterior probability distribution of each parameter before performing the Gibbs sampling.

Since each component of GMM is Gaussian distribution with mean μ_j and variance σ_j^2, the Gaussian-inverse-gamma distribution shown in Eqs (3.3) and (3.4) is used as a conjugate prior distribution of the parameters of each Gaussian distribution. Therefore, the posterior distribution of the Gaussian distribution for *j*-th component given *n* samples $\boldsymbol{X} = \{x_1, x_2, \dots, x_n\}$ is derived as

$$\mu_0 \to \frac{\lambda\mu_0 + n_j\bar{x_j}}{n_j + \lambda}, \qquad \lambda \to \lambda + n_j, \qquad \alpha \to \alpha + \frac{n_j}{2},$$
$$\gamma \to \gamma + \frac{1}{2}\left(n_j s_j^2 + \frac{\lambda n_j\left(\bar{x_j} - \mu_0\right)^2}{n_j + \lambda}\right) \tag{3.13}$$

The mathematical form of the result is similar to that in Eq. (3.6). The difference from Eq. (3.6) is that n_j denotes the number of samples classified into *j*-th component, and the sample mean $\bar{x_j}$ and sample variance s_j^2 of each *j*-th component are used instead.

As for the weight parameter $\boldsymbol{\pi} = (\pi_1, \ldots, \pi_J)$, the likelihood function of $\boldsymbol{\pi}$ is a multinomial distribution that represents the probability of the number of samples belonging to each component when samples are observed (Gauvain and Lee, 1994). So, a Dirichlet distribution can be used as a conjugate prior distribution as follows:

$$\boldsymbol{\pi} = (\pi_1, \ldots, \pi_J) \sim D(\tau_1, \ldots, \tau_J),$$
$$f(\boldsymbol{\pi}|\boldsymbol{\tau}) = \frac{\Gamma(\tau_1 + \cdots + \tau_J)}{\Gamma(\tau_1)\cdots\Gamma(\tau_J)} {\pi_1}^{\tau_1 - 1} \cdots {\pi_J}^{\tau_J - 1} \tag{3.14}$$

where $\tau = (\tau_1, \ldots, \tau_j)$ is the hyper-parameters of a Dirichlet distribution. Following Bayes' theorem in Eq. (3.2), the posterior distribution of a Dirichlet distribution π is derived as

$$\boldsymbol{\pi}|\boldsymbol{X} \sim D\left(\tau_1 + \sum_{i=1}^{n} I(z_i = 1), \tau_2 + \sum_{i=1}^{n} I(z_i = 2), \ldots, \tau_J + \sum_{i=1}^{n} I(z_i = J)\right) \tag{3.15}$$

where $I(\cdot)$ is the indicator function that gives 1 if the statement is true and zero otherwise. It is noted that the function is calculated based on the classification vector $Z = (z_1, \ldots, z_n)$ describing the GMM component to which the corresponding sample y_i belongs. To obtain the classification vector Z, the posterior probability

t_{ij}, i.e. the probability that the *i*-th sample belongs to the *j*-th component is calculated as

$$t_{ij} = p(z_i = j|x_i) = \frac{\pi_j f_j\left(x_i|\mu_j, \sigma_j^2\right)}{\sum_{j=1}^{J} \pi_j f_j\left(x_i|\mu_j, \sigma_j^2\right)} \tag{3.16}$$

In summary, using the conditional posterior probability distribution of the parameters as explained above, the following four steps are repeated to generate samples representing the updated distribution of the GMM parameters (Franzén, 2008):

- **Step 1**: Generate a sample for the variance σ_j^2, $j = 1,2,\dots,J$ from the posterior inverse gamma (Γ^{-1}) distribution in Eqs. (3.3) and (3.13) with updated hyper-parameters α and γ, given $\boldsymbol{X}$ and $Z = (z_1, \dots, z_n)$.
- **Step 2**: Generate a sample for the mean μ_j, $j = 1,2,\dots,J$ from the posterior Gaussian distribution in Eqs. (3.3) and (3.13) with updated hyper-parameters μ_0 and λ, given $\boldsymbol{X}$, $Z = (z_1, \dots, z_n)$, and the new sample of variance σ_j^2 from Step 1.
- **Step 3**: Generate samples for the component weights in $\boldsymbol{\pi} = (\pi_1, \dots, \pi_J)$ from the posterior Dirichlet distribution in Eqs. (3.14) and (3.15) with updated hyper-parameters $\tau_1, \dots, \tau_J$ given $\boldsymbol{X}$ and $Z = (z_1, \dots, z_n)$.
- **Step 4**: Calculate the new classification vector $Z = (z_1, \dots, z_n)$ based on the new posterior probability t_{ij} in Eq. (3.16) which is calculated using $\boldsymbol{X}$ and new samples of parameters $\pi = (\pi_1, \dots, \pi_J), (\mu_1, \sigma_1^2), \dots, (\mu_J, \sigma_J^2)$ from Steps 1, 2, and 3.

It is noted the initial steps of the sampling process showing the lack of convergence, i.e. so-called burn-in period (Gelman et al., 2013), are discarded.

To demonstrate the results by Gibbs sampling for the GMM model, the first axle spacing in type 7 vehicle is updated by artificially generated observations. Figure 3.1 shows the CDF of the prior (original) GMM, posterior (updated) GMM, and the cumulative frequency diagram of the observations. Figure 3.2 shows the trace plots of the samples of the weight parameters $\boldsymbol{\pi} = (\pi_1, \ldots, \pi_4)$ of the four components. It is shown that the samples of the parameter represent the posterior probability distribution after around 30 iterations. Since the probabilistic distributions for random variables that use the three Bayesian updating methods described above were independently developed, there is no need to consider additional conditional dependencies when carrying out Bayesian updating.

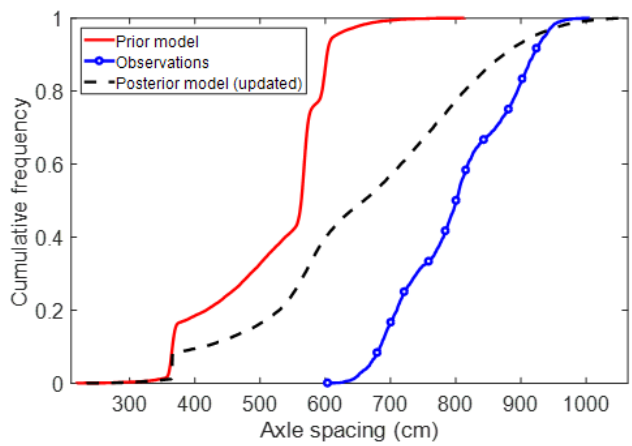

Figure 3.1 The CDFs of prior (original) and posterior (updated) probability distribution, and cumulative frequency diagram of the observations

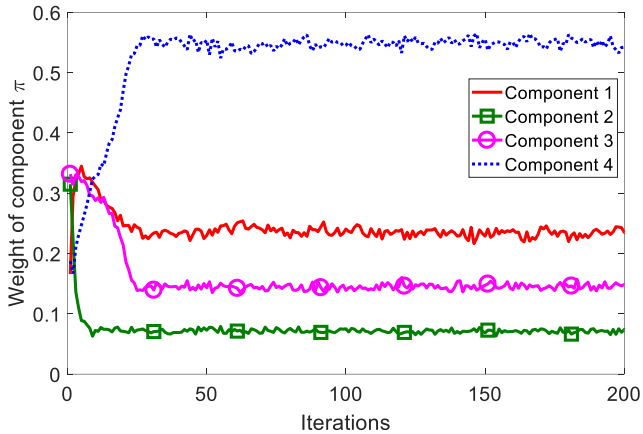

Figure 3.2 The trace plot of the sample of weight parameter $\boldsymbol{\pi}$

3.2.5 Setting the hyper-parameter of the prior model

Before updating the parameters of the probabilistic model of bridge traffic loads using new WIM data or traffic information, the hyper-parameters of the prior models should be set in advance. In Bayesian inference, in order to incorporate the prior knowledge and data into the prior model, hyper-parameters are often determined subjectively based on individual judgments (Gelman et al., 2013). The prior information and data related to the traffic loads on the target bridge are relatively reliable when data are measured in the surroundings, or accumulated over a long period of time. By contrast, the prior information can be less reliable if data are measured for a short period of time, measurement lacks accuracy, or assumptions must be introduced due to the lack of data. Therefore, hyper-parameters of these cases should be set differently in each case to reflect how much belief we have in the prior information used.

In this study, all three Bayesian methods use Gaussian-inverse-gamma

distribution. Eqs. (3.4), (3.11), and (3.13), which are updating equations of the hyper-parameters, show that the hyper-parameters of the posterior model are updated based on the relative size of the hyper-parameter of the prior model with respect to the number of new observations n. Therefore, to obtain a reasonable posterior model, hyper-parameters of the prior model should be specified based on the number of new observations n. These corresponding hyper-parameters are generally interpreted as the effective number of observations in the case of exponential family distributions (Bishop, 2006). So, if we already know the number of data in a prior model, we can use it as hyper-parameters. However, if a prior model is assumed because no data are available or if the measurement accuracy of the prior data and the new observations are different, the hyper-parameter values of the prior model should be determined based on individual judgments on prior knowledge and data. This study introduces the degree of belief of the prior model as a concept to indicate how reliable the prior model is, and uses the relative degrees of belief of the prior model and new observations to quantify and adjust hyper-parameters of the prior model as illustrated in Figure 3.3.

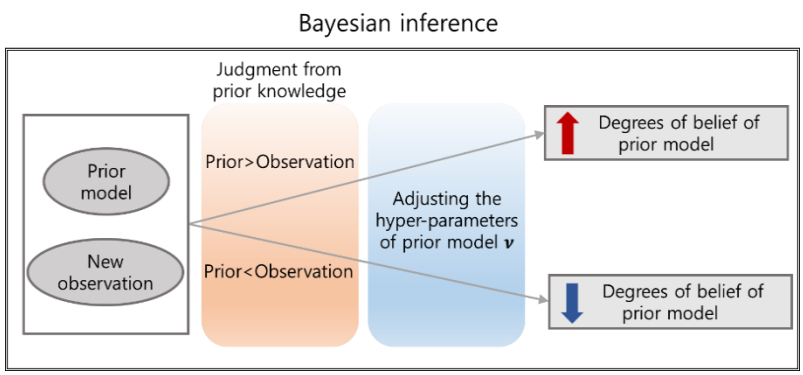

Figure 3.3 Setting the hyper-parameters for Bayesian inference

For a specific example, when the prior data and new observations are measured for the same period (one year) with the same WIM system on the bridge, it is reasonable to give the same degrees of belief to the prior model and new observations. On the other hand, when the prior data were measured for two years and new observations are measured for one year with the same WIM system on the bridge. It is reasonable to give twice higher degrees of belief to the prior model than those of new observations. For concise expressions, in this dissertation, the relative ratio of the degrees of belief of the prior model to those of new observations R_{belief} is introduced instead of presenting all the values of the hyper-parameter of the prior distributions. For example, if the hyper-parameters are set such that the degrees of belief of the prior model and new observations are equal, the corresponding R_{belief} is defined as 1. When degrees of belief of the prior model are twice higher than those of new observations, the ratio R_{belief} is defined as 2. In other words, in terms of effective sample size (Bishop, 2006), the assumption that the ratio R_{belief} is 1 implies that the prior model has an equivalent sample size of new observations while the ratio R_{belief} of 2 means that the prior model has a twice larger sample size than those of new observations.

Using this concept, let us consider the updating hyper-parameters of Gaussian-inverse-gamma distribution in Eq. (3.6). It is noteworthy that λ and α, which are the hyper-parameters of the prior model, and n and $n/2$, which are associated with the number of new observations, serve as weights for the prior model and new observations, respectively in Eq. (3.6). So, if the hyper-parameters of the prior model

for each updating are set as follows based on the number of new observations *n* and the ratio R_{belief}:

$$\mu_0 = \mu_{prior}, \lambda = R_{belief} n, \alpha = \frac{R_{belief} n}{2}, \gamma = \frac{R_{belief} n s_{prior}^2}{2} \tag{3.17}$$

The hyper-parameters of the prior model for each updating are updated as follows:

$$\mu_{\text{update}} = \frac{R_{belief}\mu_{prior} + \bar{x}}{R_{belief} + 1}, \quad \lambda_{update} = R_{belief} n + n,$$

$$\alpha_{update} = \frac{R_{belief} n + n}{2}, \tag{3.18}$$

$$\gamma_{update} = \frac{R_{belief} n s_{prior}^2}{2} + \frac{1}{2}\left[n s^2 + \frac{R_{belief} n \left(\bar{x} - \mu_{prior}\right)^2}{R_{belief} + 1}\right]$$

where μ_{prior} and s_{prior}^2 are the mean and variance of the prior model, and $\bar{x}$ and s^2 are the mean and variance of the new observations. It is noted that the updated mean μ_{update} is calculated by R_{belief} without the number of new observations n. This implies that the relative ratio of the degrees of belief of the prior to those of new observations is important in the updating examples. Using the same way, the hyper-parameters of other prior models (Linear regression model and GMM) can be updated to reflect the relative degrees of belief of the prior model and new observations.

Furthermore, when the measurement accuracy is different among data sets related to the variables of traffic environment, e.g. traffic volume, axle weight, and vehicle types, the hyper-parameters can be set differently during Bayesian inference to reflect the effects of the measurement accuracy of related data. Lastly, as the updating proceeds, the degrees of belief of the updated model which are used as the

prior model in the next Bayesian updating stage should be increased because the data have been sequentially accumulated and assimilated into the updated model enhancing its credibility.

It should be noted that the hyper-parameter setting method presented in this section is just one of many methods. Depending on situations of a given Bayesian updating problem and the judgment of the experts, the hyper-parameters can be set up in different ways, which means that updating results might vary depending on engineering judgments when performing Bayesian updating. Therefore, studies are needed to secure objectivity when updating traffic load effects. For this, it is required to verify objectivity through performing diverse traffic load update examples considering factors such as measurement period and convergence speed. Specific examples and explanations related to hyper-parameter settings are provided in the numerical examples in Sections 3.3 and 3.4.

3.3. Numerical investigations of the updating methodology

This section demonstrates and investigates the proposed updating methodology using real WIM data. To this end, the developed probabilistic model of bridge traffic loads (Chapter 2) is updated by WIM data measured in South Korea to check if the traffic load effects estimated by the updated model converge to those calculated by the new observations.

A probabilistic model of bridge traffic loads, whose parameters are determined based on the truck lane data of Gimcheon is used as a prior model while the actual WIM data of the truck lane at Sunsan are used as new observations. For verification

in a more general setting, total loads on a bridge, which are often used to develop the design live load model, are calculated in this investigation rather than using the influence lines of a particular bridge. In calculating total loads, two span lengths are considered: short-span bridge (60m) and long-span bridge (500m). Each time the probabilistic model of bridge traffic loads is updated by a year-long WIM data from Sunsan, 10 sets of one-year-long traffic flows are generated by MCS of the updated model to calculate the corresponding traffic load effects. The daily maximum traffic load effects by the 10 MCS flows are averaged to consider the variability in traffic flows. The average daily maximum total loads are compared with those directly calculated by the new observations to check if the model is converging to the traffic load effects from the WIM data at Sunsan as the number of updates increases. The updated model is used as the prior model of the next Bayesian updating. The average daily maximum total loads are plotted on the Gumbel probability paper as shown in Figure 3.4. In this investigation, the hyper-parameters of the prior model are set to have the relative ratio of the degrees of belief R_{belief} as 1 (the degrees of belief of the prior model and new observations are equal).

In both cases, the average daily maximum total loads on the bridge are initially increased and then decreased gradually as the updating proceeds. The curves eventually converge to that calculated by the new observations at around the 10th updating. As the Bayesian updating progresses, meaningful differences occur in the two variables: the traffic volume increases and the ratio of heavy vehicles decreases. Since the increase in the total loads due to the increase of traffic volume are greater than the decrease in the total loads caused by the reduction of heavy vehicle ratio, so

the total loads experience a significant increase in the beginning. But as the updating progresses, the difference between these effects decreases, and eventually, the updated total loads converge to those from observations.

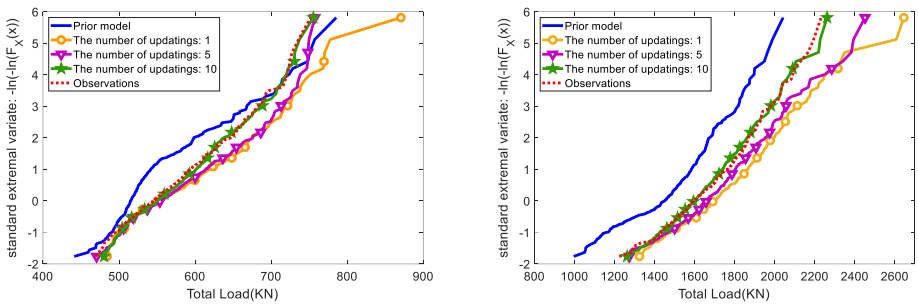

(a) Span length: 60m (b) Span length: 500m

Figure 3.4 Gumbel probability paper of average daily maximum total loads on the bridge (the relative ratio of the degrees of belief: 1)

Next, the same calculations are performed but with different relative degrees of belief of the prior model to investigate the effect of the hyper-parameters. In the first case, the degrees of belief of the prior model are set to half of the degrees of belief of the observations (R_{belief} is 0.5) by adjusting hyper-parameters, and in the second case, the degrees of belief of the prior model are set to twice than those of the observation (R_{belief} is 2) by adjusting hyper-parameters. Figures 3.5 and 3.6 show the results of updated traffic load effects when the relative ratio of the degrees of belief are 0.5 and 2, respectively. In the first case, the updated traffic load effects converge to the traffic load effects from observations around the 7th updating, while the convergence is achieved at around the 15th updating in the second case. This shows that the higher the degrees of belief of the prior model are, the more slowly

the probabilistic model is updated by new observations. These numerical examples confirm that the proposed updating methodology effectively updates the probabilistic model of bridge traffic loads through Bayesian inference using new observations representing the real traffic environment of the bridges available.

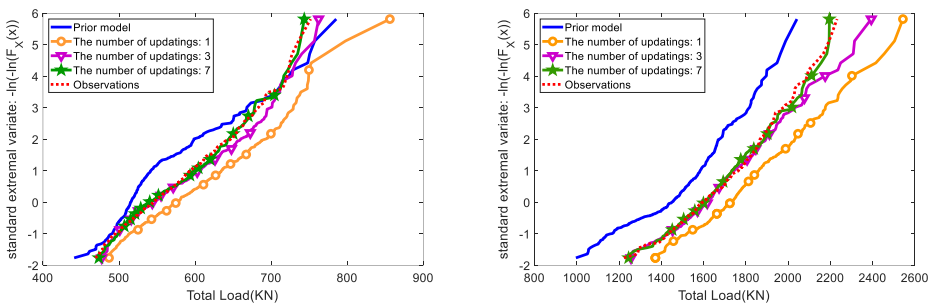

(a) Span length: 60m (b) Span length: 500m

Figure 3.5 Gumbel probability paper of average daily maximum total loads on the bridge (the relative ratio of the degrees of belief: 0.5)

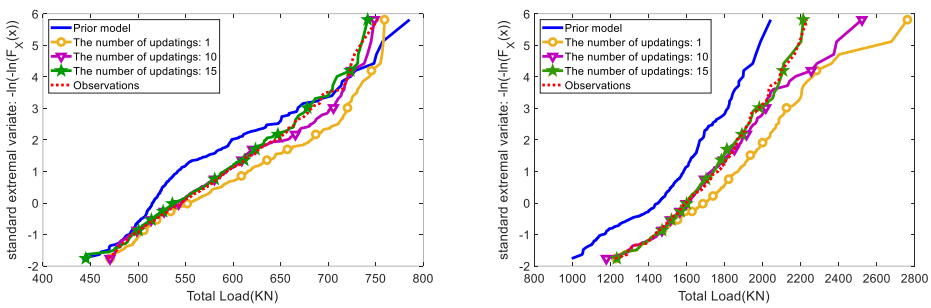

(a) Span length: 60m (b) Span length: 500m

Figure 3.6 Gumbel probability paper of average daily maximum total loads on the bridge (the relative ratio of the degrees of belief: 2)

3.4. Updating examples of applications to cable-stayed bridges

The proposed updating methodology is applied to update the probabilistic model of traffic loads on two cable-stayed bridges in South Korea using assumed scenarios of traffic environment changes and the WIM data measured from the bridge. Section 3.4.1 investigates the changes in the traffic load effects on the Incheon Grand Bridge resulting from the assumed scenarios of traffic environment changes in the surroundings. In Section 3.4.2, the traffic load effects on the 2nd Jindo Bridge are updated by incomplete WIM data measured from the same bridge during a short time period.

3.4.1 Updating traffic load effects using scenarios of traffic environment changes: Incheon Grand Bridge

The target bridge in this section is the Incheon Grand Bridge in South Korea. The finite element (FE) model representing the cable-stayed part explained in Chapter 2 is used again to calculate the traffic load effects. For each type of load effects (axial force of a tower, moment of a tower, moment of a girder, and tension of a cable), the bridge members showing the maximum design live load effect are selected for the investigation. Figure 3.7 shows the finite element model and the locations of the selected bridge members.

Two assumed scenarios of traffic environment changes are used to perform Bayesian updating of the traffic load effects. The first scenario represents the restriction of overweight vehicles. An effective way to ensure the safety of the bridge is to prevent overweight vehicles from passing over the bridge by means of

monitoring and restrictions. In fact, many countries have restricted overweight vehicles by setting standards of overweight vehicle permits. Nevertheless, many overweight vehicles still pass on bridges. Therefore, this example estimates how much of the traffic load effects will be reduced if the perfect restriction of overweight vehicles is enforced for the bridge.

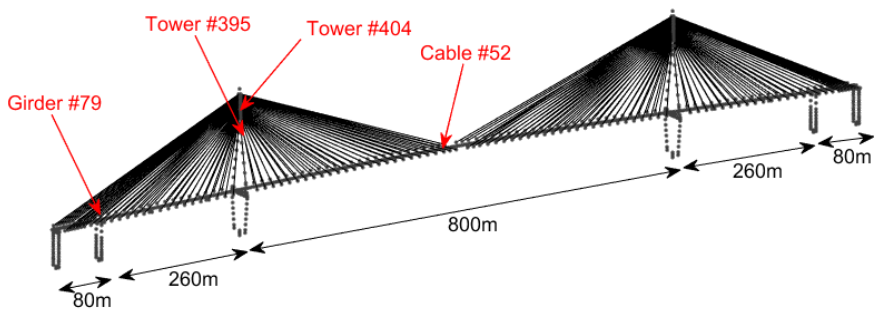

Figure 3.7 FE model of Incheon Grand Bridge and critical members selected for updating traffic load effects

In South Korea, overweight vehicles are being restricted by the following criteria: the gross vehicle weight (GVW) should be less than 40 tons and each axle weight should be less than 10 tons. Thus, these conditions are imposed when generating the GVW and axle weight variables from the WIM-based probabilistic model of bridge traffic loads. A total of 100 sets of one-year-long traffic flows are generated to calculate the traffic load effects using the influence lines of selected members in Figure 3.8. Next, the 100-year maximum traffic load effects are estimated through extrapolation explained in Section 2.6.1.1. Table 3.1 shows the results of the Bayesian updating.

It is seen that the traffic load effects on the bridge decrease by 10 to 20%

through perfect restriction of overweight vehicles. The differences in the reductions over the load effect types are caused by the shapes of the influence lines. The results demonstrate that the probabilistic model of bridge traffic loads can be updated by data and information regarding the axle weights to facilitate prediction of the changes in the traffic load effects, which helps decision-making processes regarding the criteria for overweight vehicles, and whether certain vehicles should be allowed to pass the bridge or not.

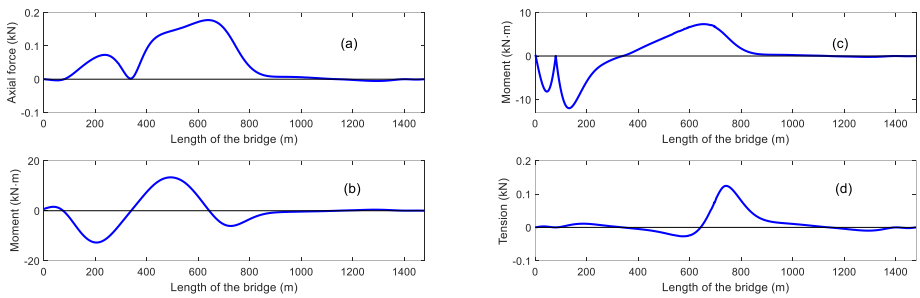

Figure 3.8 Influence lines at the selected bridge members of the Incheon Grand Bridge: (a) axial force of a tower #395, (b) moment of a tower #404, (c) moment of a girder #79, and (d) tension of a cable #52

Table 3.1 Estimated 100-year maximum traffic load effects assuming perfect restriction of overweight vehicles

	Prior	Updated	Reduction (%)
Axial force of a tower #395 (kN)	519.92	467.55	10.07
Moment of a tower #404 (kN· m)	29,934.25	25,258.99	15.62
Moment of a girder #79 (kN· m)	19,705.74	15,299.23	22.36
Tension of a cable #52 (kN)	230.22	200.41	12.95

The second scenario representing a change in the traffic environment is that new roads and bridges are built around the bridge, resulting in 20% reduction in the heavy vehicle ratio and 40% reduction in the traffic volume of the bridge. The influence lines of the Incheon Grand Bridge in Figure 3.8 are used again to calculate the traffic load effects. The WIM data generated from the probabilistic bridge traffic load model in Chapter 2 with reduced heavy vehicle ratio and traffic volume are used as "new" observations. With these observations and the prior model, Bayesian updating is performed until the results converge to a certain extent while the hyper-parameters are adjusted for each updating to gradually increase the degrees of belief of the updated model (the prior model in the next updating) linearly from the relative ratio 1 to 2.2 (see Section 3.2.5 regarding the meaning of the relative ratio). The reason for increasing the degrees of belief of the updated model is that the credibility of the updated model increases as new observations are assimilated with the updated model as the updating progresses. For each update, a total of 100 sets of one-year-long traffic flows are generated to calculate the corresponding traffic load effects. Finally, the 100-year maximum traffic load effects are extrapolated as shown in Figure 3.9.

After more than 10 updatings, the reductions in the updated traffic load effects converge to the amount of reduction in the traffic load effects calculated based on new observations (17-25%). Each traffic load effect has a different level of reduction due to the shape of the influence line. In the event of such a change in the traffic environment on existing bridges, prediction on the traffic load effects can be obtained by using the developed updating methodology to assess the influence of the

change on the demands and reliability of existing bridges.

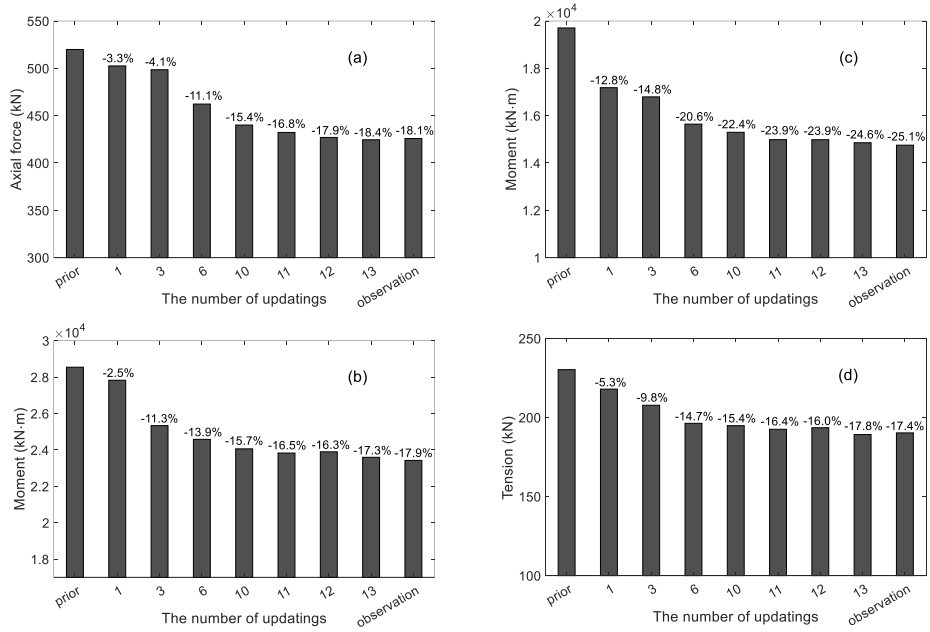

Figure 3.9 Estimated maximum 100-year traffic load effects, updated by the reduction of traffic volume and heavy vehicle ratio by a change in the traffic environment: (a) axial force of a tower #395, (b) moment of a tower #404, (c) moment of a girder #79, and (d) tension of a cable #250

3.4.2 Estimation of site-specific traffic load effects using in-service WIM data: The 2nd Jindo Bridge

To demonstrate the estimation of site-specific traffic load effects on bridges by the proposed updating methodology, the in-service WIM data measured on the 2nd Jindo Bridge from May to August, 2019 are used. A total of 4 Bayesian updatings are carried out using one-month-long data each time to improve the accuracy of the estimated traffic load effects. The bridge is 484 m long and connects the city of Mokpo to Jindo island. A finite element (FE) model of the bridge is developed with SAP2000 as shown in Figure 3.10. The influence lines of the selected members are

shown in Figure 3.11.

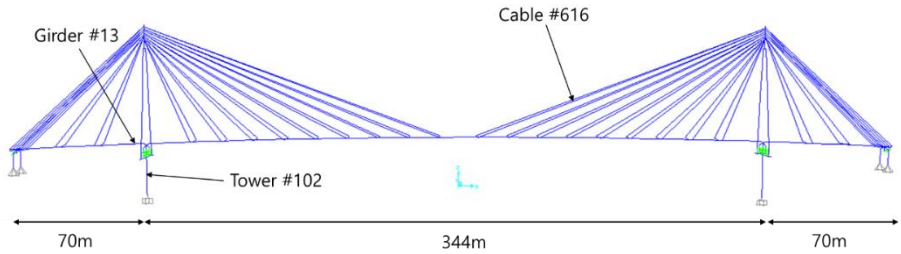

Figure 3.10 FE model of the 2nd Jindo Bridge and the members selected for estimating traffic load effects

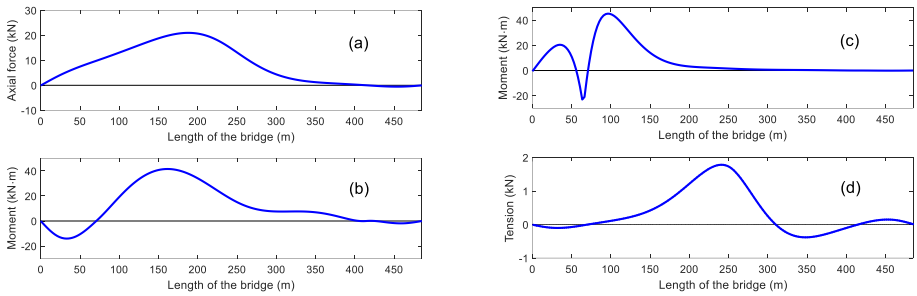

Figure 3.11 Influence lines of the 2nd Jindo Bridge: (a) axial force of a tower #102, (b) moment of a tower #102, (c) moment of a girder #13, and (d) tension of a cable #61

The in-service WIM data alone are not enough for precise estimation of the traffic load effects due to the short measurement period and incompleteness. Therefore, this study employs the generic probabilistic model of bridge traffic loads in Chapter 2 as a prior model and updates it based on the WIM data. The measured in-service WIM data consist of the following five variables: *1) Headway, 2) Heavy vehicle ratio, 3) Traffic volume, 4) Axle weight, and 5) Speed*

For these variables, the parameters are continually updated using the measured data while the other variables are generated using the same parameters as the existing

prior model. Before proceeding with Bayesian updating, the parameters of the prior model i.e., generic probabilistic model of bridge traffic loads, are first set up with indirect traffic information of surroundings of the bridge and reasonable assumptions.

The headway model is applicable to most bridges because it was developed based on the theories of transportation engineering and general driving habits. Therefore, existing parameters of the prior model for headway are used to represent the headway in this example. As for the traffic volume and heavy vehicle ratio, this study refers to the regular traffic investigation data collected over the last five years. These were measured on the road near the 2nd Jindo Bridge once a year for 24 hours on a selected day. However, since the data used to investigate the traffic volume and the ratio of vehicle types are expressed by direction, i.e. not by lane, it is necessary to distribute vehicles over each lane of the bridge. The lane distribution of vehicles is determined based on the lane usage ratio through the literature (Caprani et al., 2016; Witczack and El-Basyouny, 2004) and the analysis of WIM data used in Chapter 2 (more details are covered in Section 4.3.1). Types 5 to 12 vehicles (Heavy vehicles) are distributed to the left and right lane by the ratio 1:9, and the others (type 1~4) are distributed by the ratio 7:3. The parameters of the prior model are set based on the result of the lane distribution of vehicles. In the case of variables of vehicle characteristics, the same model parameters of axle spacing as the prior model are used because data are not available while the model parameters of axle weight are updated with in-service data. The speed is fixed at 70 km/h according to a speed limit sign on the exit of the bridge. The occurrence probability of traffic congestion is assumed to be zero because the bridge is not located in an urban area.

Next, the hyper-parameters of the prior model should be set up. There are a total of five variables which will be updated in this example and each variable has different measurement accuracy and different degree of belief in the prior model. Based on the method for setting hyper-parameter of the prior model described in Section 3.2.5, the degree of belief in the prior models of five variables are assumed as follows:

headway > *axle weight* > *traffic volume* = *heavy vehicle ratio* > *speed*

The headway is given the highest degree of belief because the driver's behavior does not vary over bridges. The prior model of the axle weight is considered also reliable because it is established from three sites in Korea for a one-year-long period each. The speed is assumed to be a constant value, so it is given the lowest degree of belief. The variables with the second-lowest degree of belief are the traffic volume and heavy vehicle ratio which are determined based on investigation data of the surrounding road, which were measured over a short period.

Additionally, in this example, the degrees of belief of the updated model, i.e. the prior model of the next round, are gradually increased over the four rounds of Bayesian updating to reflect the accumulation of measured data into the updated model. According to the specifications of the WIM system, the measurement accuracy for speed data is 99% or higher while that for the traffic volume and heavy vehicle ratio is 95% or higher. As for the axle weight, the accuracy is 85 to 90%. For headways, although accuracy is greater than 99%, it is the least accurate variable because the minimum unit of measurement is only 1 second. To summarize, the measurement accuracy for five variables are expressed as follows:

speed>axle weight>traffic volume=heavy vehicle ratio>headway

Based on the information about the degree of belief in the prior model and measurement accuracy described above, the degree of belief of the updated model for each variable through hyper-parameter adjustment for each updating round as shown in Figure 3.12 (expressed in the relative ratio of the degrees of belief). For speed, the updating starts with the relative ratio of 0.1 but increases up to 2 at the fourth round, which is the largest increase among the four variables. As for the headway, the relative ratio is 3 initially and increases to 3.5, which is the smallest increase.

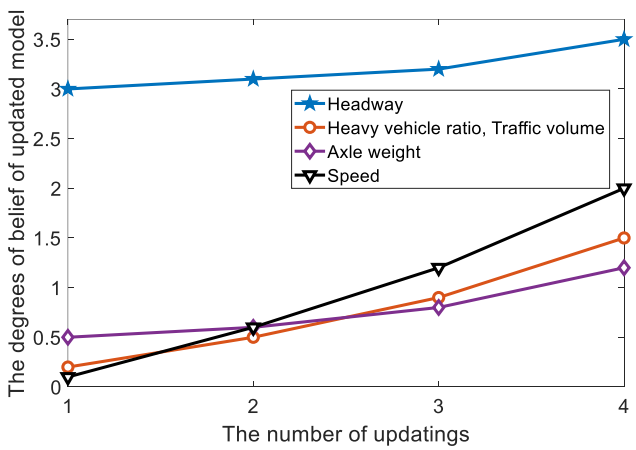

Figure 3.12 The changes of degree of belief of the updated model for each variable as updating progresses

After setting up the prior model and its hyper-parameters, the probabilistic model of bridge traffic loads is updated four times using a one-month-long dataset each time. For example, gross vehicle weight and traffic volume are updated by Gibbs sampling as shown in Figure 3.13, and so are other variables by using the

proposed Bayesian updating methods. A total of 100 sets of one-year-long traffic flow are generated for each updating and the traffic load effects are calculated using the influence lines in Figure 3.11. The estimated 100-year maximum traffic load effects after the extrapolation process are shown in Tables 3.2 to 3.5.

The results show that the traffic load effects decrease gradually and eventually reduced by 9-13%. This is because as the updating progresses, the traffic volume of trucks increases, but the heavy vehicle ratio and axle weight decrease more significantly. Although it is impossible to verify that the traffic load effects converge into certain values due to the lack of data measurement period, it is expected to converge if there is a large amount of data that represents constant traffic environment accumulated as shown in Section 3.4.1.

Through this example, when information and data of traffic environment on a particular bridge are limited, the accuracy of estimation of traffic load effects can be improved by the Bayesian inference framework with the proposed updating methodology and the generic probabilistic model of traffic loads in Chapter 2, which are used as the prior model. Also, Bayesian updating can be carried out reasonably by setting up hyper-parameters according to the belief of the prior model and the accuracy of the new observation for each variable.

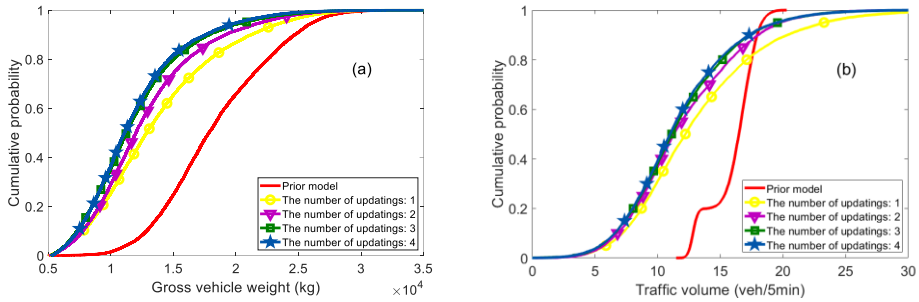

Figure 3.13 The CDFs of prior (original) and posterior (updated) probability distribution from Gibbs sampling: (a) Gross vehicle weight of vehicle type 5, (b) Traffic volume at 11 am in the car lane

Table 3.2 Estimated 100-year maximum traffic load effects of the 2nd Jindo Bridge (Axial force of a tower #102)

	Prior (0 updating)	May (1st updating)	June (2nd updating)	July (3rd updating)	August (4th updating)
Axial force (kN)	19,444.90	19,805.01	19,245.37	18,220.71	17,683.67
Rate of change (%)		+1.85	−1.03	−6.30	−9.06

Table 3.3 Estimated 100-year maximum traffic load effects of the 2nd Jindo Bridge (Moment of a tower #102)

	Prior (0 updating)	May (1st updating)	June (2nd updating)	July (3rd updating)	August (4th updating)
Moment (kN·m)	38,086.02	36,715.86	36,082.55	34,860.60	33,203.84
Rate of change (%)		−3.60	−5.26	−8.47	−12.82

Table 3.4 Estimated 100-year maximum traffic load effects of the 2nd Jindo Bridge (Moment of a girder #13)

	Prior (0 updating)	May (1st updating)	June (2nd updating)	July (3rd updating)	August (4th updating)
Moment (kN·m)	38,760.08	36,662.88	34,190.31	33,567.95	33,891.97
Rate of change (%)		−5.41	−11.79	−13.40	−12.56

Table 3.5 Estimated 100-year maximum traffic load effects of the 2nd Jindo Bridge (Tension of a cable #616)

	Prior (0 updating)	May (1st updating)	June (2nd updating)	July (3rd updating)	August (4th updating)
Tension (kN)	1,573.17	1,497.41	1,437.14	1,443.80	1,382.83
Rate of change (%)		−4.82	−8.65	−8.22	−12.10

3.5. Summary

This chapter proposed a Bayesian updating methodology for the probabilistic model of bridge traffic loads in Chapter 2. Three main Bayesian inference methods were employed by the proposed methodology: the Gaussian-inverse-gamma distribution for parameters following Gaussian distributions, the Bayesian linear regression for linear regression models, and the Gibbs sampling for the Gaussian mixture in the model. Additionally, the hyper-parameters of the prior model were set to take into account the relative degrees of belief in the prior models and the measurement accuracy of the new observations.

The proposed updating methodology was successfully demonstrated by

showing that the updated traffic load effects converge into the traffic load effects by new observations in both short- and long-span bridge cases. This example also confirmed that changing the degrees of belief of the prior model through adjustment of hyper-parameters varies the rate of convergence. It was also demonstrated that the proposed methodology can reflect the degrees of belief in the prior models during the updating process. Next, the developed methodology was applied to update the probabilistic model of bridge traffic loads using the assumed scenarios of traffic environment changes on the bridge and the measured in-service WIM data from the real bridge. The first bridge example showed that the traffic load effects are reduced by 10 to 20% if the perfect restriction of overweight vehicles is enforced on the bridge. In the second bridge example, the traffic scenario represents decreases in the traffic volume and the heavy vehicle ratio on the bridge due to the construction of new roads and bridges around. The 100-year maximum traffic load effects were estimated after each updating, which showed convergence after around 10 updatings. These two examples demonstrated quantitative impacts of changes in variables related to traffic environment on the traffic load effects on the bridge. The third example used the proposed updating methodology with the generic bridge traffic load model as the prior model to improve the accuracy of estimating the traffic load effects on a particular bridge whose actual data and information about the traffic environment alone are not sufficient for precise estimation of the traffic load effects. The traffic load effects were estimated by Bayesian updating using the data measured from May to August 2019 on the 2nd Jindo Bridge. The results showed that the proposed method can incorporate new observations into the probabilistic model for

bridge traffic loads to facilitate precise estimation of the site-specific traffic load effects.

The methodology proposed in this chapter was applied to updating examples using assumed traffic scenarios and in-service traffic data measured for a short period due to the lack of measured dataset. However, with long-term and continuous observations, it is expected that the Bayesian updating of a probabilistic model of traffic loads will enable us to accurately estimate the traffic load effects throughout the service life of the bridges while considering changes in the actual traffic environment of the bridge.

Chapter 4. New Design Live Load Model for Long-Span Bridges

4.1. Introduction

In Chapters 2 and 3, a comprehensive probabilistic model and updating methodology are developed for the accurate estimation of traffic loads on bridges over their service life using measurements at bridges in operation. This chapter focuses on the live load model in the bridge design code to accurately estimate the live load effects in the bridge design stage. As explained in Chapter 1, each bridge has a unique traffic environment. So, it is most desirable to estimate the live load by accurately considering the site-specific traffic environment of the bridge during the design stage. But, on the other hand, it can cost a lot of computation effort for engineers. Therefore, for convenient and practical calculation, many live load models in bridge design codes are simply defined for applicability to all bridges, i.e., regardless of the structural type and span length by assuming the worst traffic scenario such as the full stop situation which causes maximum live load effects.

Most design live load models consist of a combination of design truck load and lane load. Design truck load represents the critical heavy vehicle in each country or region which is loaded where it produces the maximum live load effect on the bridge. The design lane load is defined in terms of the uniformly distributed load (Eurocode LM1, AASHTO HL-93, KHBDC, and KHBDC-CB) for efficient and fast calculations of a long vehicle sequence load. In addition, for multi-lane bridges,

some design codes extend the lane load defined on the reference lane to the total loads on the multi-lane by means of the multiple presence factor (MPF). These factors are estimated by using the probability of simultaneous loading of heavy vehicles to take into account the different traffic situations of each lane.

As explained in Chapter 2, the dominant traffic flow which produces maximum live load effects depends on the span length of bridges. Hence, design live load models should be defined while considering this point. Currently, the most commonly used design live load models were basically developed for short- to medium-span bridges. On the other hand, many studies about live load models for long-span bridges have been still carried out using reliable traffic information from WIM technology and sensors because there are few design live load models applicable to long-span bridges (BS 5400 (BSI, 2006), ASCE recommendation (Buckland, 1981), KHBDC-CB).

Lutomirska (2009) estimated design lane load for long-span bridges and that of bias factor and coefficient of variation (C.O.V) using WIM data by assuming traffic jam scenarios to consider the effects of multiple trucks rather than one truck. Hwang et al. (2013) and Hwang and Kim (2015) proposed the live load model for long-span bridges and live load factors for reliability-based bridge evaluation using WIM data of South Korea and traffic congestion scenarios (full stop condition). The proposed model was adopted as a live load model for bridge design code in South Korea (KHBDC-CB). In recent years, statistical characteristics of live load effects have been investigated using WIM data for code calibration (Lee, 2014; Kim, 2015, Kim, 2018).

Many studies focus on MPFs calculation. Fu et al. (2013) estimated and recommended MPF values for truck loads using WIM data of the United States, and confirmed that the MPF values of existing bridge design codes are highly conservative. Vander Spuy et al. (2019) computed MPF for span length from 10 to 50 m using WIM data of South Africa and extreme value theory. The MPFs proposed in the previous two studies are applicable to short-span bridges only. On the other hand, Zhou et al. (2018) proposed a novel framework for MPF that can be applied to any bridge length and type using bivariate extreme value theory. Furthermore, as a further study, three methods for estimation of MPF were reviewed and compared with existing bridge design codes (Zhou et al., 2020).

However, despite various research efforts, the following limitations still exist for the design live load model for long-span bridges. Most design live load models of studies and codes are overestimated for conservatism based on simple traffic jam scenarios (full stop situation) to estimate precise maximum live load effects. In the case of multi-lane bridges, several studies confirmed that heavy trucks mainly use the outer lane while passenger cars use the inner lane through analysis of WIM data, and the lanes are classified into the slow lane (truck lane) and the fast lane (car lane) (O'Brien and Enright, 2011; Kim and Song, 2019). This phenomenon implies that the live load effect on each lane is significantly different. Eurocode LM1 considers this phenomenon by assigning different lane load for each lane, but KHBDC-CB still assigns the same lane load for all lanes regardless of the characteristics of the lane. Hence, it is necessary to define the design lane load to consider the disparity of lane load according to the location of the lane.

Thus, this chapter focuses on developing a new design live load model for long-span bridges in South Korea (over 200m span length) that can consider the diverse traffic environment of long-span bridges based on the extensive traffic data. A reasonable design lane load and multiple presence factors for long-span bridges are suggested by capturing real patterns of extreme traffic conditions. Then, a discussion is provided to combine the design live load model for short- to medium-span bridges with that for long-span bridges. The final design live load model that can cover short- to long-span bridges is proposed. In addition, statistical characteristics of live load and live load effects are investigated for code calibration.

4.2. Traffic environment investigation and classification about long-span bridges

The traffic environment of a bridge is diverse depending on the location of the bridge. To reflect the traffic environment of many long-span bridges, this study first investigates the traffic environment of long-span bridges in Korea and classifies them suitably based on the results of the investigation to maintain a convenient bridge design. This section describes the results of the traffic investigation and classification of the important two factors that influence the maximum live loads of long-span bridges: traffic congestion and the percentage of heavy vehicles (Kim and Song, 2019).

4.2.1 Heavy vehicle traffic environment

As shown in Figure 2.2, vehicle types 3 to 12 are classified as trucks and used

to measure ADTT (Average daily truck traffic), which is a general indicator of the traffic volume of trucks in traffic investigation. However, vehicle types 3 and 4 are small trucks and their average total weights are around 3 tons, which has a relatively small influence on the maximum live loads than the vehicle types 5 to 12 which are defined as heavy vehicles or heavy trucks in Chapter 2. Although heavy trucks are relatively more important among trucks, since ADTT is used as important as AADT (Annual average daily traffic) when designing roads and bridges in practical use, this study investigates the percentage of trucks among all vehicles and the percentage of heavy trucks (type 5 to 12) among trucks (type 3 to 12).

According to the yearbook of road, bridge and, tunnel statistics in 2020 (MOLIT, 2020b), Korea has a total of 35,902 bridges, of which 56 bridges are long-span bridges with a maximum span length of over 200 m. However, since most long-span bridges do not have the proportion of vehicle types data, the data measured from the surrounding roads are used instead. This study also suggests that it is not necessary to investigate the proportion of vehicle types by limiting only the data measured on long-span bridges because vehicles drive continuously on diverse roads and bridges like a network. Therefore, in order to use as much data as possible, this study refers to the annual traffic volume report (MOLIT, 2020a), which investigated the traffic information of 3,770 roads in Korea.

To investigate the percentage of trucks and heavy trucks on roads with frequent traffic congestion, the traffic data of roads whose AADT is more than 10,000 veh/day are used. The annual traffic volume report classifies 7 a.m. to 7 p.m as “daytime” and other hours as “night” and it shows that 75 to 80% of trucks pass during the

daytime which was also reported in the literature. For this reason, this study uses the proportion of vehicle type data measured from 7 a.m. to 7 p.m to investigate the percentage of trucks among all vehicles and the percentage of heavy trucks among trucks, and the result is shown in Figure 4.1.

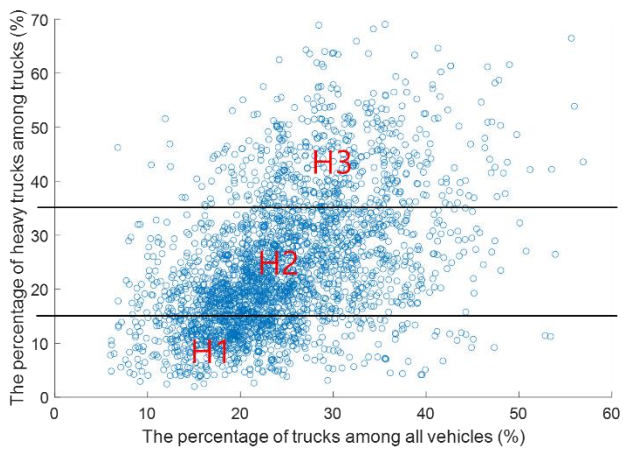

Figure 4.1 The classification of traffic environment in terms of the percentage of heavy trucks

It is shown in the figure that the percentage of trucks and the percentage of heavy trucks have a positive correlation, and both have values between 10 and 70%. This study classifies the heavy vehicle traffic environment as H1 (15% or less), H2 (15~35%), and H3 (35% or more) as shown in Figure 4.1, based on the percentage of heavy trucks among trucks that are more critical to the maximum live load between the two percentages. To consider the variability within the heavy vehicle traffic environment when simulating congested traffic flow, it is assumed that two variables of percentage for each category follow the Gaussian distribution whose parameters (mean and C.O.V) are provided in Table 4.1.

Table 4.1 Mean and C.O.V for three categories of heavy vehicle traffic environment

	The percentage of truck	The percentage of heavy truck
H1	Mean: 20%, C.O.V: 0.33	Mean: 10%, C.O.V: 0.27
H2	Mean: 25%, C.O.V: 0.30	Mean: 25%, C.O.V: 0.24
H3	Mean: 30%, C.O.V: 0.25	Mean: 45%, C.O.V: 0.16

4.2.2 Traffic congestion environment

Long-span bridges can accommodate a larger number of vehicles simultaneously than short-span bridges, so the number of existing vehicles on the bridge is a key factor for the maximum live load of the bridge. Thus, the dominant traffic flow for long-span bridges is congested traffic flow and many studies proposed the live load model for long-span bridges based on this dominant traffic flow (Buckland, 1981; Lutomirska, 2009; Hwang and Kim, 2015; Guo and Caprani, 2019). In particular, recent studies introduced microsimulation models that can consider the lane and speed change of vehicles for a precise simulation of congested traffic flow (Lipari, 2013; Caprani et al., 2016). The dissertation developed a WIM data-based bridge traffic load model using microsimulation models as well in Chapter 2. This study calculates the design lane load and MPFs for long-span bridges using simulation of congested traffic flow based on the developed probabilistic model for bridge traffic load. Traffic flow simulation and calculation methods for design live load models will be explained in Section 4.3, and before this, the following two factors related to traffic congestion are investigated in this section.

The first factor is how severely traffic congestion occurs when it occurs, i.e. average speed during traffic congestion, and the second factor is how often this

traffic congestion occurs, i.e. the occurrence frequency of traffic congestion (hours/year). Unlike the percentage of trucks investigated in Section 4.2.1, the traffic environment related to traffic congestion is a unique characteristic of the bridge, so the target bridge of the investigation is limited to 56 long-span bridges with a span length longer than 200 m. However, since the only data available in the yearbook of road, bridge and, tunnel statistics in the 2020 year is the daily traffic volume, traffic data of surrounding roads of the annual traffic volume report are used additionally. However, despite these investigation efforts, data such as speed and the occurrence frequency of traffic congestion still cannot be obtained. Therefore, the average speed during traffic congestion is indirectly estimated through the traffic volume using the volume delay function (VDF) as follows (Spiess, 1990):

$$t_i' = t_i^0 \times \left[1 + \alpha \left(\frac{V}{C}\right)^{\beta}\right] \tag{4.1}$$

where t_i^0 is the standard travel time under free traffic flow, t_i' is the travel time given the traffic volume, C denotes the capacity of the road, V denotes the traffic volume, and α and β are the model parameters. The KOTI database (KOTI, 2018) analyzes the traffic data of Korea and provides the speed range of free traffic flow, the capacity of the road, and parameters α and β of VDF for each type of road, region, and the number of lanes. Since *C* in Eq. (4.1) has a unit of hourly traffic volume, so the investigated daily traffic volume should be converted into hourly traffic volume. In Korea, the road design manual (MOLIT, 2012) recommends estimating the capacity of the road based on the design hourly volume (DHV). This volume is calculated by multiplying AADT by the design hour factor *K*. The average

speed during traffic congestion is estimated by calculating the V in Eq. (4.1) using K value 0.18 ~ 0.28 for 2-lane bridges and 0.12 to 0.17 for 4 or more-lane bridges because most long-span bridges are located around rural and tourist areas. Table 4.2 shows the average speed of 7 long-span bridges where traffic congestion occurs among 56 long-span bridges through the inference using VDF.

Table 4.2 Estimated average speed during traffic congestion of long-span bridges

Bridge	Average speed (km/h)
Mokpo Bridge	35~45
Gwangan Bridge	15~20
Yeongjong Bridge	45~55
Dolsan Bridge	25~30
Daedong-Hwamyeong Bridge	25~30
Samcheonpo Bridge	35~45
Seohae Grand Bridge	10~15

The result shows that traffic congestion rarely occurs on long-span bridges in Korea because of their location and purpose (rural area and tourism). These average speed values are merely estimated not directly measured, and data about the occurrence frequency of traffic congestion are still not available. Therefore, additional bridges on the Han river in Seoul where traffic congestion occurs frequently are investigated. The Seoul metropolitan government provides the average speed data for each month of bridges on the Han river. Accordingly, this study can obtain necessary information of the traffic environment about congested traffic flow from this dataset. The more severe congested traffic condition, i.e. the average speed is lower, causes larger live loads to be applied to the bridge (Caprani

et al., 2016). Therefore, to ensure the conservatism of the design code, this study assumes that traffic congestion with an average speed of less than 20km/h (homogeneous congestion state) occurs on long-span bridges. Over the three years from 2017 to 2019, the total amount of time for occurred traffic congestion which has an average speed of less than 20 km/h is investigated for the bridges on the Han river. The investigated total time is expressed as occurrence frequency based on 260 days on weekdays (one year) in Table 4.3.

Table 4.3 The occurrence frequency of traffic congestion (<20 km/h) for bridges on the Han river

Bridge	Occurrence frequency (hours/260day) South to north	Occurrence frequency (hours/260day) North to south
Hannam Bridge	38	63
Olympic Bridge	2	6
Seogang Bridge	24	57
Dongho Bridge	230	338
Dongjak Bridge	10	45
Banpo Bridge	5	1020
Cheongdam Bridge	25	1456
Yanghwa Bridge	11	25
Seongsan Bridge	27	7
Jamsil Bridge	3	22
Hangang Bridge	1077	376
Seongsu Bridge	378	610
Mapo Bridge	3	4
Wonhyo Bridge	5	6
Yeongdong Bridge	6	129
Cheonho Bridge	136	0
Gayang Bridge	5	319

After excluding bridges with unduly frequent traffic congestion such as Banpo, Cheongdam, Hangang, and Seongsu Bridge as outliers, the mean value is estimated as 58.5 hours/260 days. As a result, three categories for the traffic congestion environment are proposed in Table 4.4. 60 hours/260 days, close to the mean value, are determined to represent traffic environment C2. Category C3 assumes that severe traffic congestion occurs for 1 hour every day in commuting time. Category C1 assumes that traffic congestion occurs for about 10 hours for 260 days and represents a bridge having rare traffic congestion.

Table 4.4 Occurrence frequency of traffic congestion (<20 km/h) for three categories of traffic congestion environment

Category	Occurrence frequency of traffic congestion
C1	10 hours/260 days
C2	60 hours/260 days
C3	260 hours/260 days

4.3. Calculation method for multiple presence factor and design lane load

In order to calculate the lane load and MPFs, congested traffic flows are simulated using microsimulation models for nine traffic environment categories (3×3) proposed in Section 4.2. When simulating traffic flow, vehicle characteristic variables such as axle weight and axle distance for each vehicle type are generated from the probabilistic model developed in Chapter 2. This section explains how to calculate the lane load and multiple presence factor based on calculated live loads from the simulated congested traffic flow.

4.3.1 Characteristics lane and lane usage ratio

The traffic lanes in Korean long-span bridges are mainly two-way 2 to 10-lane (multi-lane). In the case of multi-lane bridges, the lane mainly used by drivers is different depending on the type of vehicle they drive. This phenomenon was already identified when developing the model for bridge traffic load in Chapter 2. To reflect this characteristic, three categories of lanes were proposed in the dissertation in terms of the total percentage of heavy vehicles in Section 2.4.3. This chapter also defines three characteristic lanes (car, middle, and truck lane) in terms of the lane location referring to the literature and general traffic information. In general, the car lane (inner lane) mostly carries passenger cars and buses, while the truck lane (outer lane) carries mostly heavy trucks and trailers. The middle lane is the lane where various vehicle types use mixed. This study allocates these characteristic lanes to each lane in a multi-lane bridge and the results for two-way 2 to 10-lane are shown in Figure 4.2.

In the case of two-way 4-lane, the inner lane is defined as the middle lane rather than the car lane which was defined in Section 2.4.3. The reason is that there are only two lanes (based on one-way), so when the maximum live load effect occurs on the bridge, it is likely that heavy trucks are located on both two lanes. On the other hand, in the case of two-way 6-lane, the probability that the truck is located on the most inner lane is very small when the maximum live load effect occurs because there are three lanes (based on one-way). This phenomenon can be also confirmed in the lane usage ratio defined below this section. It is noted that the locations of characteristics lanes for two-way 2 to 10-lane defined here are applicable to one-way 1 to 5-lane.

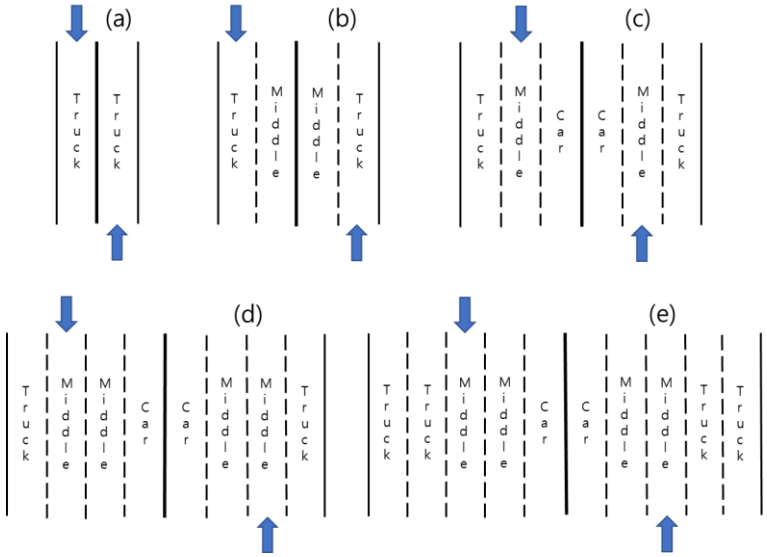

Figure 4.2 The location of characteristics lanes on two-way roads: (a) 2-lane, (b) 4-lane, (c) 6-lane, (d) 8-lane, and (e) 10-lane

Next, the proportion of vehicle types for each lane should be determined to adjust the parameters of the probabilistic model for bridge traffic load. However, because the percentage of vehicle types surveyed in Section 4.2 is based on roads (all lanes), not each lane, the proportion of vehicle types for each lane should be estimated using the lane usage ratio of vehicle types. The lane usage ratio means the probability that the driver will use each lane in a multi-lane road or bridge. In pavement engineering, a lane distribution factor of trucks (for truck lane or outer lane) is used to consider this ratio. AASHTO (1993) proposes a lane distribution factor of 0.8 to 1.0 for one-way 2-lane, and ARA (2004) suggests 0.9 for 2-lane, 0.6 for 3-lane, and 0.45 for 4-lane as lane distribution factor for the truck lane. Lu et al. (2009) analyzed the WIM data of California and showed that the mean values of lane distribution factor are 0.87, 0.67, and 0.59 for one-way 2, 3, and 4 -lane respectively.

In addition, the truck lane usage ratio of trucks of 0.9 (Vrouwenvelder and Waarts, 1993) and 0.93 (O'Brien and Enright, 2011) are used for one-way 2-lane (two-way 4-lane). A lane usage ratio of trucks of 0.75 for the truck lane, 0.25 for the middle lane, and 0 for the car lane are observed in the 3-lane road with high traffic volume (Fwa and Li, 1995). However, because the lane usage ratio calculated based on Korean traffic data does not exist, the lane usage ratio is directly calculated using the highway WIM data of the three sites used in Chapter 2. The lane usage ratio is calculated using the data measured during the daytime because this study assumes that traffic congestion occurs between 7 am and 7 pm.

The lane usage ratio is calculated for each vehicle type, and the results are shown in Figure 4.3 by grouping the types which have a similar ratio. In the case of types 3 and 4 which belong to the same small truck type, the lane usage ratios of them are different. On the other hand, types 5 to 12, which are classified as heavy trucks have similar lane usage ratios so the same value of lane usage ratio is used for them. At all three sites, the results confirm that trucks generally use the truck lane and passenger cars while buses use the car lane. The values of lane usage ratio are consistent with those reported in the literature above. This study defines the lane usage ratio of a total of 5 vehicle type groups (car, bus, small truck (type 3), small truck (type 4), and heavy truck) for two-way 4 to 10-lane by referring to the results from the WIM data and literature. The final lane usage ratios depending on the number of lanes are provided in Tables 4.5 to 4.8 for 4, 6, 8, and 10-lane cases.

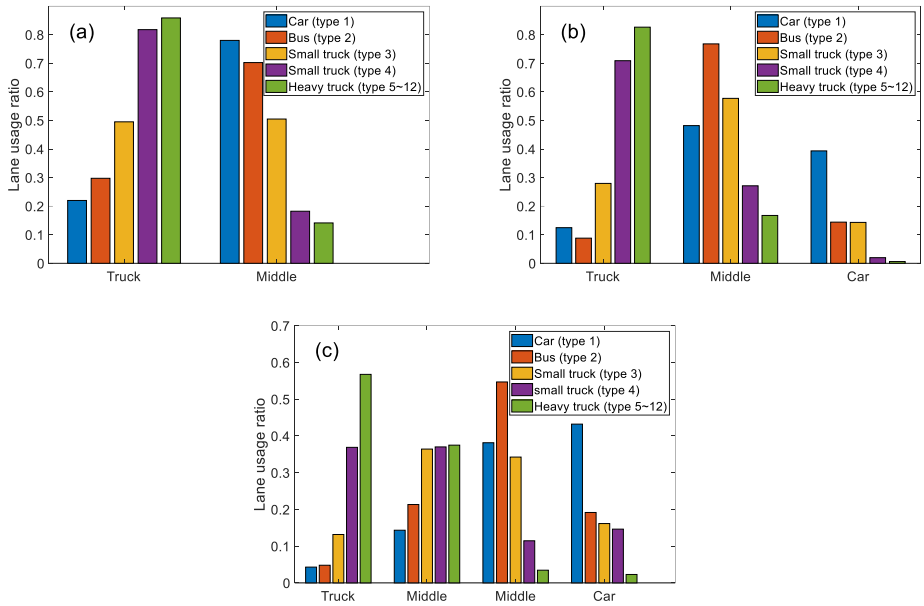

Figure 4.3 Calculated lane usage ratio of vehicle types: (a) 4-lane, two-way (Sunsan), (b) 6-lane, two-way (Gimcheon), (c) 8-lane, two-way (Waegwan)

Table 4.5 Lane usage ratio of vehicle types (two-way 4-lane or one-way 2-lane)

Vehicle type	Middle lane (lane 1)	Truck lane (lane 2)
Car (type 1)	0.8	0.2
Bus (type 2)	0.7	0.3
Small truck (type 3)	0.5	0.5
Small truck (type 4)	0.2	0.8
Heavy truck (type 5~12)	0.1	0.9

Table 4.6 Lane usage ratio of vehicle types (two-way 6-lane or one-way 3-lane)

Vehicle type	Car lane (lane 1)	Middle lane (lane 2)	Truck lane (lane 3)
Car (type 1)	0.40	0.50	0.1
Bus (type 2)	0.15	0.75	0.1
Small truck (type 3)	0.15	0.55	0.3
Small truck (type 4)	0.02	0.28	0.7
Heavy truck (type 5~12)	0	0.20	0.8

Table 4.7 Lane usage ratio of vehicle types (two-way 8-lane or one-way 4-lane)

Vehicle type	Car lane (lane 1)	Middle lane (lane 2)	Middle lane (lane 3)	Truck lane (lane 4)
Car (type 1)	0.45	0.35	0.15	0.05
Bus (type 2)	0.20	0.55	0.20	0.05
Small truck (type 3)	0.15	0.35	0.35	0.15
Small truck (type 4)	0.10	0.10	0.40	0.40
Heavy truck (type 5~12)	0	0.05	0.35	0.60

Table 4.8 Lane usage ratio of vehicle types (two-way 10-lane or one-way 5-lane)

Vehicle type	Car lane (lane 1)	Middle lane (lane 2)	Middle lane (lane 3)	Truck lane (lane 4)	Truck lane (lane 5)
Car (type 1)	0.45	0.35	0.15	0.03	0.02
Bus (type 2)	0.20	0.55	0.20	0.03	0.02
Small truck (type 3)	0.15	0.30	0.30	0.20	0.05
Small truck (type 4)	0.05	0.10	0.20	0.25	0.40
Heavy truck (type 5~12)	0	0.02	0.08	0.35	0.55

4.3.2 Method

To describe the live loads of a vehicle sequence that consists of several vehicles with headways, five live loading methods in use are summarized as shown in Figure 4.4 (Zhou et al., 2019). Load model (LM) 6~8 are axle weight loading, gross vehicle weight loading, and uniformly distributed loading considering the headway of individual vehicles respectively. LM 9 and LM 10 use distributed loading without headway which enables rapid calculations. LM 9 uses distributed lane load with various values along the span while LM 10 uses uniformly distributed lane load

(UDL) which reduces the fidelity further. Among these five methods, most of the international codes of practice define lane load by adopting LM 10, which can quickly calculate live loads with a slight sacrifice of accuracy (AASHTO HL-93, Eurocode LM1, KHBDC). UDL for single-lane bridges is calculated as follows:

$$\text{UDL} = \frac{Total\ loads\ on\ a\ bridge}{Lengh\ of\ a\ bridge} \tag{4.2}$$

The multiple presence factor (MPF) is a reduction factor introduced to consider the rare event that the large live load occurs on each lane simultaneously. In general, the MPF is defined as follows.

$$MPF = \frac{L_T}{N \times L_R} \tag{4.3}$$

where N is the number of lanes, L_T is the characteristic total live load on bridges, and L_R is the characteristic reference-lane live load, which is used for the design lane load. When using the MPFs calculated from Eq. (4.3), the same MPF value is used for all lanes to assign the equal reduced lane load value following the procedure used by KHBDC. According to Zhou et.al (2020), there are three methods of calculating MPF or the so-called multi-lane factor (MLF). The first method is the "multiple-presence truck weights approach" which was used to define the MLF of CAN/CSA-S6-00 and the Chinese bridge design code (MCT, 2015). The second method is the "multi-presence truck load effects approach" proposed by Nowak (1993). AASHTO HL-93 and KHBDC define MPF based on this method. Recently, Hwang et al. (2013) also calculated MPFs based on this method using WIM data in Korea. However, the truck traffic scenario considered in these two approaches is suitable for short-span bridges, but not for long-span bridges where various vehicle

types can exist mixed during traffic congestion. On the other hand, the recently proposed "coincident lane load effects approach" (Zhou et al., 2018) is a method that is applicable regardless of bridge length or bridge structure type. Thus, this study mainly employs this approach to calculate and propose MPF for each characteristic lane to consider the disparity of lane load according to the location of the lane.

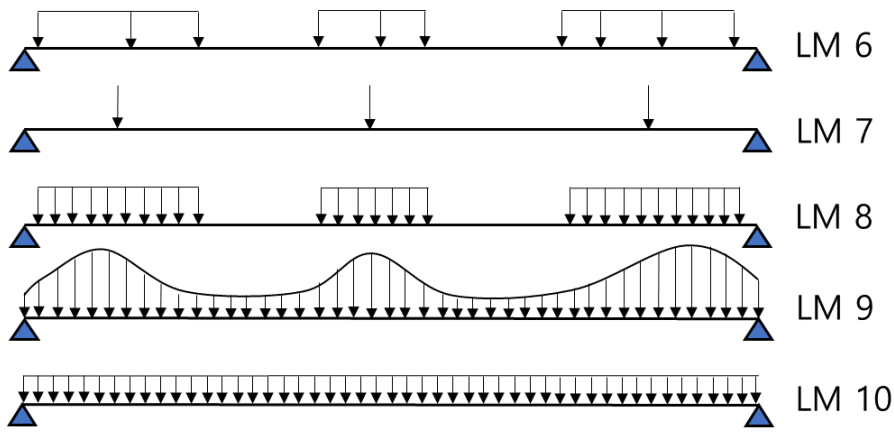

Figure 4.4 Methods for the loading of a vehicle sequence (adapted from Zhou et al. (2019))

Zhou et al. (2018) introduces the share factor similar to the lateral distribution factor in the bridge design code to consider the effect of the number of girders. However, the goal of this study is to calculate the lane load and develop MPF which can be applied regardless of the structural type of bridges. Hence, after excluding the share factor, the bridge total loads (BTL) is computed as follows:

$$BTL = \sum_{j=1}^{N} LTL_j \tag{4.4}$$

in which N is the number of lanes, and lane total loads (LTL_j) is the sum of the weights of vehicles on each lane j. Among LTL_j, the reference lane total loads ($RLTL$) is defined as follows.

$$RLTL = max\, LTL_j \tag{4.5}$$

$RLTL$ is used to calculate the design lane load. Samples of BTL, LTL_j, and $RLTL$ defined in Eqs. (4.4) and (4.5) can be obtained at every time step through traffic flow simulation. However, the samples to be required for the design code are the maximum values that occur during the return period or the service life of the bridge. It is noted that obtaining sufficient samples through direct traffic flow simulation to estimate the maximum live loads during the long service life of the bridge (more than 100 years) entails high computational cost.

To reduce the computational cost, the coincident lane load effects approach employs bootstrapping and extrapolation based on the bivariate extreme value theory. The maximum value samples for a short period of time, e.g. weekly maximum, are extrapolated to compute the correction coefficient γ and combination coefficient η which are components of MPF for the service life (Zhou et al., 2018). However, since the computation of BTL and LTL_j by bootstrapping and extrapolation can produce combinations of BTL and LTL_j that do not physically occur in practice, this study directly computes and analyzes many combinations of BTL and LTL_j that can occur in real traffic situations as a data-driven approach. Sufficient annual maximum samples which can occur in reality are calculated instead of computing directly many 100-year maximum samples considering the computation cost. Then, annual

maximum samples are analyzed to estimate MPF and lane load for 100-year service life.

First of all, BTL, LTL_j, and $RLTL$ are obtained every 0.25 seconds through congested traffic flow simulations for 100 years after setting the parameters of the bridge traffic load model to represent each of the 9 ($=3 \times 3$) defined traffic environments in Section 4.2. In case of severe traffic congestion, congestion occurs in all parts of the bridge, so it is reasonable to apply lane loads on the structurally continuous length of the bridge, instead of applying to the unfavorable area only, which ignores the area that can relieve the maximum live loads. However, further studies must be conducted to investigate whether this loading method guarantees the maximum load, depending on the shape of the influence line (e.g., the wide beneficial area which produces adverse live load effects against maximum live load effects exists in the influence line). In this study, to ensure conservatism and maintain compatibility with the current bridge design code, the span length is used as a reference length for lane load and MPF. The live loads are calculated for a total of 11 span lengths 200, 300, 400, 600, 800, 1000, 1200, 1400, 1600, 1800, and 2000 m. Based on the BTL value, a total of 100 annual maximum BTL and its component LTL_j samples are obtained while a total of 100 annual maximum $RLTL$ samples based on the $RLTL$ value are also obtained. To define the design lane load, the annual maximum $RLTL$ samples of the reference lane can be modeled by the following GEV distribution based on the extreme value theory using Eq. (2.8). The maximum $RLTL$ which is the so-called characteristic $RLTL$ ($CRLTL$) during a

service life of 100 years defined in KHBDC-CB is extrapolated through the GEV distribution and the concept of return period using Eqs. (2.9) and (2.10). Estimated $CRLTL$ for a total of 11 span lengths are converted to UDL using Eq. (4.2) and UDL are used to define the design lane load in Section 4.4.2

The multiple presence factor is defined by correction coefficient γ and combination coefficient η proposed by Zhou et al. (2018) in this study. If the design lane load is defined by using $RLTL$ which is the maximum live load on the reference lane, an event that the maximum live load occurs on the reference lane does not guarantee an event that the maximum live load occurs on the entire multi-lane bridge at the same time. It implies that the lane load should be reduced when estimating the maximum live load effects for multi-lane bridges. To consider this, the correction coefficient γ that reduces the live load is introduced as follows using the annual maximum sample of BTL and $RLTL$.

$$\gamma = \frac{\max LTL_j \; of \; annual \; maximum \; BTL}{annual \; maximum \; RLTL} \tag{4.6}$$

where $\max LTL_j \; of \; annual \; maximum \; BTL$ means the maximum value among LTL_j which are components of the annual maximum BTL obtained among calculated live load samples during each one-year interval.

Next, the combination coefficient η for each characteristic lane (*cl*), which represents the ratio of each lane's contribution to the maximum total live loads on the entire bridge, is calculated as follows using the maximum value of LTL_j in the same *cl* to ensure conservatism:

$$\eta_{cl} = \frac{\max_{j \in cl} LTL_j \; of \; annual \; maixmum \; BTL}{\max LTL_j \; of \; annual \; maximum \; BTL} \tag{4.7}$$

Finally, for each characteristic lane, the MPF is defined as follows:

$$MPF_{cl} = \gamma \times \eta_{cl} \tag{4.8}$$

A total of 100 samples of γ and η are obtained using the annual maximum sample of BTL and $RLTL$ through congested traffic flow simulation for 100 years and analyzed in the next section to propose a rational design lane load model and multiple presence factor.

4.4. Proposed multiple presence factor and design lane load

4.4.1 Multiple presence factor

To propose a new MPF, this section analyzes the samples of coefficients γ and η calculated based on the annual maximum live loads. These samples naturally have variability so the mean and 95% confidence interval are used under the assumption that the samples follow Gaussian distribution to clearly show the results. Figures 4.5 to 4.9 show the γ and η calculated for two-way, 2 to 10-lane at the most common traffic environment: heavy vehicle traffic environment H2, traffic congestion environment C2.

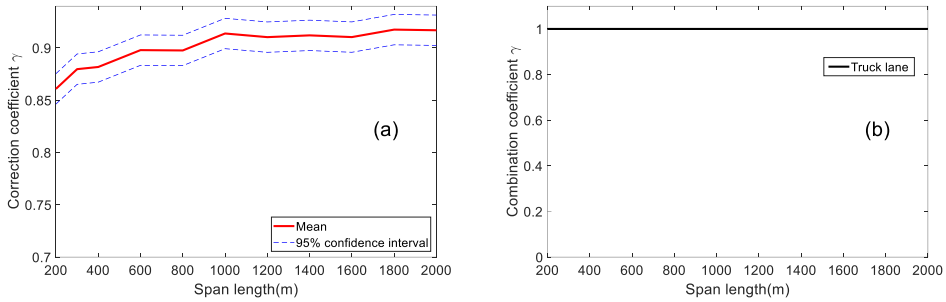

Figure 4.5 Mean and 95% confidence interval of (a) correction coefficient γ, and (b) combination coefficient η for two-way 2-lane

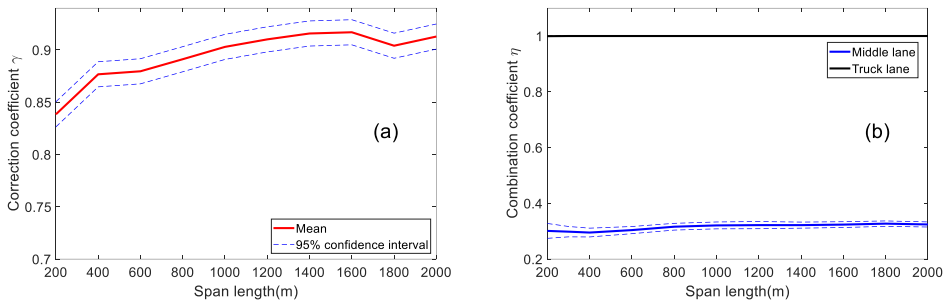

Figure 4.6 Mean and 95% confidence interval of (a) correction coefficient γ, and (b) combination coefficient η for two-way 4-lane

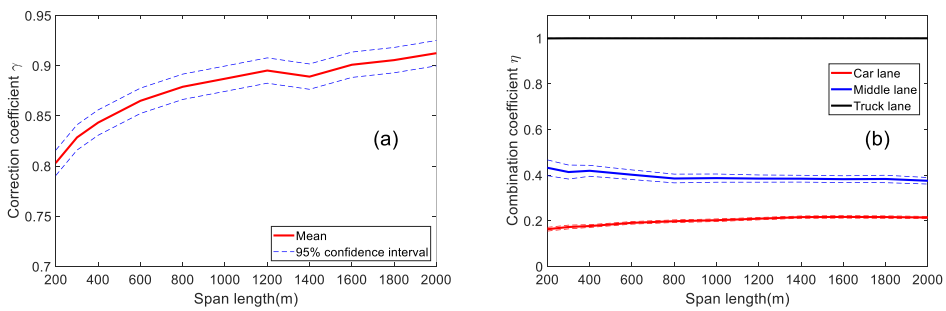

Figure 4.7 Mean and 95% confidence interval of (a) correction coefficient γ, and (b) combination coefficient η for two-way 6-lane

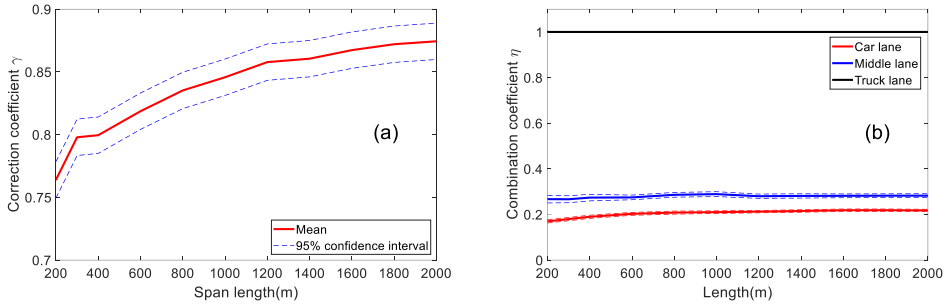

Figure 4.8 Mean and 95% confidence interval of (a) correction coefficient γ, and (b) combination coefficient η for two-way 8-lane

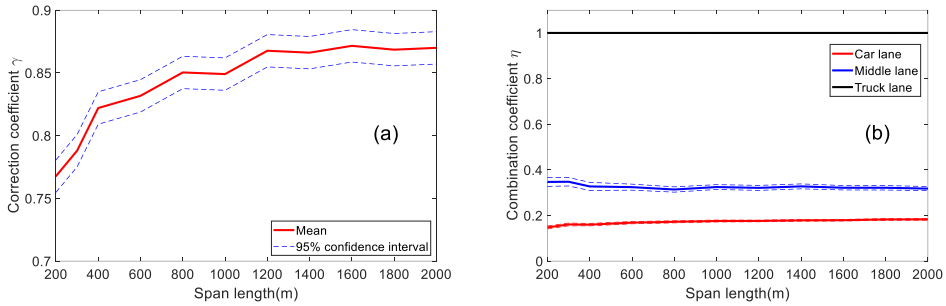

Figure 4.9 Mean and 95% confidence interval of (a) correction coefficient γ, and (b) combination coefficient η for two-way 10-lane

In the case of 6-lane, the coefficient γ has values around 0.8 to 0.9, and it tends to grow when the span length increases. The coefficient η of the truck lane has little variability in samples and its values are calculated as 1 over all span length cases. This means that when the maximum live load occurs on the entire bridge, the lane that has the maximum value at that time is always the truck lane. The middle lane has η values of 0.4 to 0.5, and the car lane has η values of about 0.2. It is noted that the other numbers of lane cases also show similar results.

Next, to determine the MPF values for the bridge design code, four main analyses of samples are conducted using the samples. The first one is to check

whether the occurrence frequency of traffic congestion affects the MPF. The samples of γ and η in each category of the traffic congestion environment C1, C2, and C3 are compared. For example, Figure 4.10 shows the comparison at the two-way 6-lane and the heavy vehicle traffic environment H2. Hereafter, only the means of γ and η samples are plotted in the figures to make the comparison more clear.

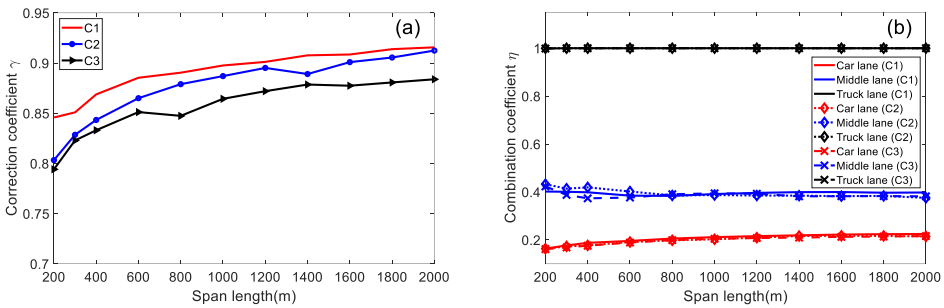

Figure 4.10 Comparison of (a) correction coefficient γ, and (b) combination coefficient η depending on the traffic congestion environment

The coefficient η has similar values regardless of the traffic congestion environment for all three characteristic lanes, while the coefficient γ has smaller values when the traffic congestion occurs more frequently. This is because a more frequent traffic congestion environment requires longer traffic simulation. As a result, the more various live load scenarios are generated and the probability of the following event increases: Even though when the maximum live load occurs on the truck lane, the maximum live load does not occur on the entire bridge at the same time because the live loads on other lanes are likely to be small. There is a slight difference in γ values, but not a significant one, so it can be confirmed that the MPF is not significantly influenced by the occurrence frequency of traffic congestion.

In the second analysis, this study checks whether the percentages of trucks and heavy trucks affect the multiple presence factor. Samples of γ and η at the heavy vehicle traffic environments H1, H2, and H3 are compared. For example, Figure 4.11 shows the comparison at the traffic congestion environment C2 and two-way 6-lane.

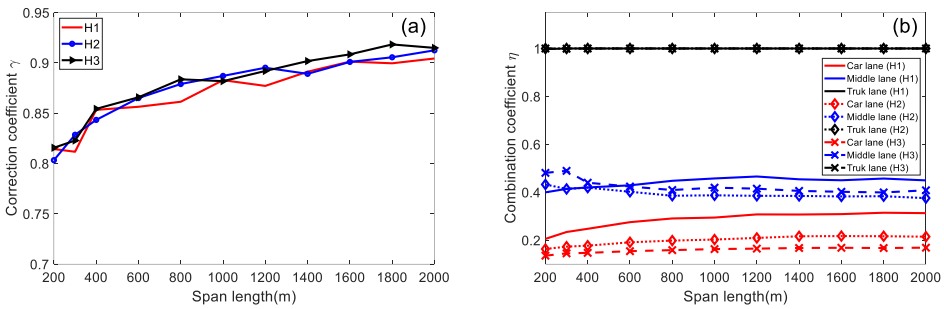

Figure 4.11 Comparison of (a) correction coefficient γ, and (b) combination coefficient η depending on the heavy vehicle traffic environment

The result shows that the coefficient γ has similar values regardless of the heavy vehicles traffic environment, whereas the coefficient η varies depending on the heavy vehicles traffic environment for the middle and car lane. In particular, the higher the percentage of trucks and heavy trucks is, the lower the coefficient η value becomes for the car lane. This is because, as the traffic volume of trucks and heavy trucks increases, the relatively large live loads occur more frequently on the truck lane than on the middle and car lane. From this analysis, this study confirms that the MPF is more affected by the heavy vehicle traffic environment than by the traffic congestion environment.

The third analysis checks whether there is a significant difference in the two coefficients depending on the BTL value. The samples of the two coefficients γ and

η currently used in the analysis are calculated based on the annual maximum live loads, not the 100-year (service life) maximum live loads which are originally required for the code. Samples of γ and η based on the 100-year maximum BTL and $RLTL$ will have a larger BTL value than those based on annual maximum BTL and $RLTL$, so this study checks whether the coefficients change as the BTL value increases. Among the calculated 100 samples of γ and η, 30 samples which are the top 30% based on the BTL value, are extracted and compared with all 100 samples. Figure 4.12 shows the comparison at the heavy vehicle traffic environment H2 and the traffic congestion environment C2. It is confirmed that even if the BTL value increase, the two coefficients do not change significantly. Thus, it would be acceptable to define MPF for the design code based on annual maximum live loads instead of 100-year maximum live loads.

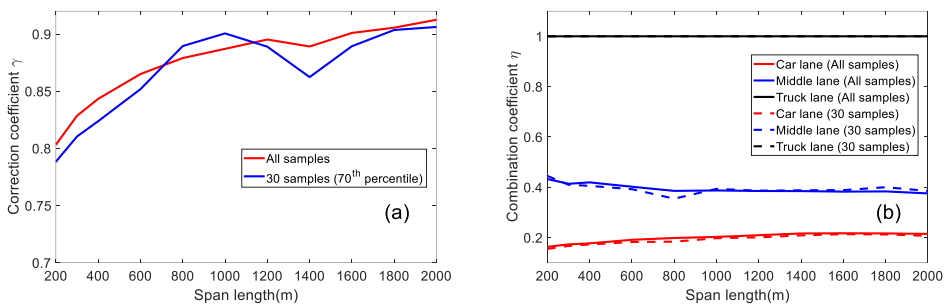

Figure 4.12 Comparison of (a) correction coefficient γ, and (b) combination coefficient η between all samples and 30 samples (70^{th} percentile)

Nevertheless, to check whether it would be valid to define MPF for the code based on annual maximum live loads, this study simulates longer congested traffic flow (10000 years) to directly obtain MPF based on the 100-year maximum live

loads which are originally appropriate for the code. Considering the computational cost, 100 samples of γ and η based on the 100-year maximum live loads are calculated for two-way 6-lane at the traffic environments H1C1, H2C1, and H3C1, instead of calculating samples of γ and η at the all categories of the traffic environment. Then, the samples based on the 100-year maximum live loads are compared with the samples based on the annual maximum live loads. Figures 4.13, 4.14, and 4.15 show the comparison results at the traffic environment H1C1, H2C1, and H3C1.

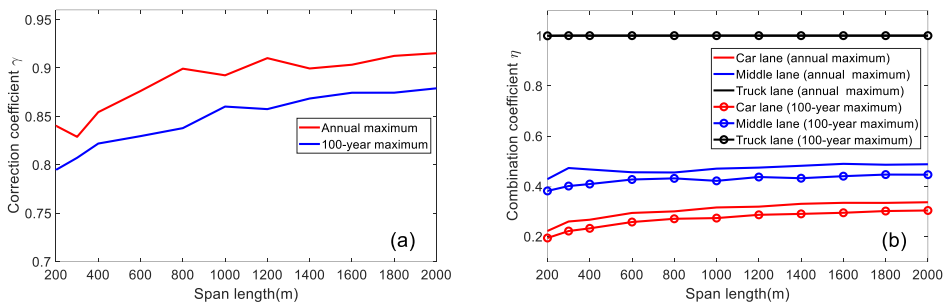

Figure 4.13 Comparison of (a) correction coefficient γ, and (b) combination coefficient η based on the annual maximum and the 100-year maximum live loads at the traffic environment H1C1

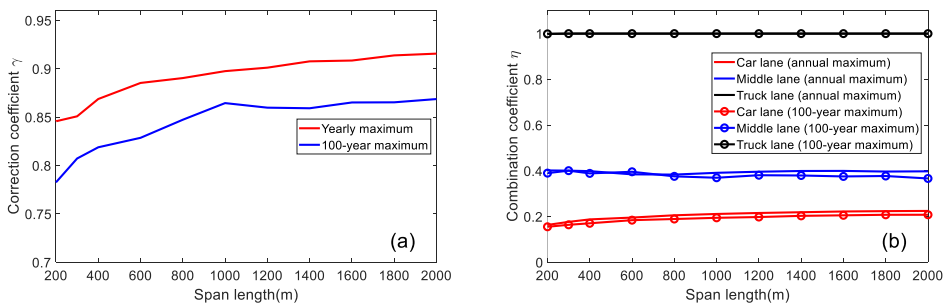

Figure 4.14 Comparison of (a) correction coefficient γ, and (b) combination coefficient η based on the annual maximum and the 100-year maximum live loads at the traffic environment H2C1

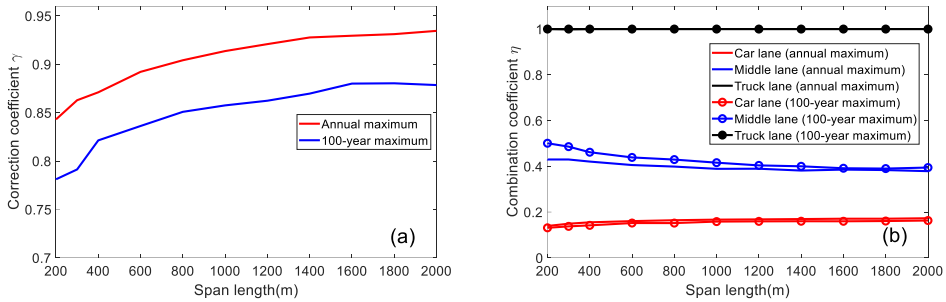

Figure 4.15 Comparison of (a) correction coefficient γ, and (b) combination coefficient η based on the annual maximum and the 100-year maximum live loads at the traffic environment H3C1

It is shown that the coefficient η has similar values regardless of the span during which maximum live load values are extracted at all three heavy vehicle traffic environments, whereas the coefficient γ has smaller values based on the 100-year maximum live loads than those based on the annual maximum live loads at the H1C1, H2C1, and H3C1. Extracting the maximum value over a longer time span is more relevant to the traffic congestion environment than to the heavy vehicle traffic environment. This is because the percentage of heavy vehicles does not change depending on the span during which the maximum value is extracted. On the other hand, more various traffic scenarios are simulated to obtain the 100-year maximum live load than to obtain the annual maximum live load, which corresponds to the fact that traffic congestion occurs more frequently. Thus, the coefficient η value, which is more affected by the heavy vehicle traffic environment than the traffic congestion environment (refer to the second analysis), is similar regardless of the span during which maximum values are extracted. On the other hand, samples of the coefficient γ based on 100-year maximum live loads are smaller than those based on the annual

maximum live loads because of the reason explained in the first analysis. In conclusion, some difference exists in γ samples according to the span during which maximum live load values are extracted, but since the coefficient γ of the annual maximum samples is larger (more conservative) than that of 100-year maximum samples, this study uses the annual maximum samples instead of 100-year maximum samples to take advantage of low computational cost for calculation of MPFs.

The coefficients γ and η for each *cl* calculated from annual maximum live loads are summarized in Tables 4.9, 4.10, and 4.11 according to the heavy vehicle traffic environment category, not the traffic congestion environment. Because the MPF is more sensitive to the heavy vehicle traffic environment than the traffic congestion environment.

The coefficient γ is almost constant regardless of the heavy vehicle traffic environment, as previously explained, but decreases as the number of lanes increases. This is because even if the maximum live load occurs on the truck lane, the small live loads can occur more frequently on the other lanes due to the existence of more lanes. This implies that maximum live load less occurs on the entire bridge even if the maximum live load occurs on the truck lane. The coefficient η varies slightly depending on the number of lanes but does not show a constant tendency, and the coefficient η_{middle} increases as the percentage of heavy vehicles increases, while the coefficient η_{car} decreases. The representative values of γ and η are selected conservatively, and using these values and Eq. (4.8), the MPF values for traffic environment H1, H2, and H3 are obtained as shown in Table 4.12. Lastly, this study proposes final MPF values of 0.9, 0.45, and 0.25 for truck, middle, and car lanes,

respectively regardless of the heavy vehicle traffic environment to maintain a convenient bridge design. Because the MPF values do not differ significantly depending on the heavy vehicle traffic environment.

Table 4.9 Results of the coefficients of multiple presence factor at the traffic environment H1

Number of lanes	γ	η_{truck}	η_{middle}	η_{car}
2	0.85~0.92	1		
4	0.80~0.92	1	0.35~0.44	
6	0.82~0.90	1	0.35~0.4	0.20~0.30
8	0.77~0.88	1	0.30~0.37	0.23~0.30
10	0.75~0.86	1	0.32~0.35	0.18~0.24
Representative value	0.9	1	0.45	0.3

Table 4.10 Results of the coefficients of multiple presence factor at the traffic environment H2

Number of lanes	γ	η_{truck}	η_{middle}	η_{car}
2	0.86~0.91	1		
4	0.80~0.92	1	0.3~0.35	
6	0.80~0.91	1	0.4~0.43	0.18~0.20
8	0.76~0.86	1	0.26~0.30	0.16~0.21
10	0.77~0.87	1	0.32~0.37	0.16~0.18
Representative value	0.9	1	0.45	0.2

Table 4.11 Results of the coefficients of multiple presence factor at the traffic environment H3

Number of lanes	γ	η_{truck}	η_{middle}	η_{car}
2	0.85~0.92	1		
4	0.80~0.92	1	0.28~0.35	
6	0.80~0.91	1	0.42~0.50	0.13~0.16
8	0.78~0.88	1	0.27~0.30	0.14~0.18
10	0.77~0.87	1	0.35~0.42	0.12~0.16
Representative value	0.9	1	0.5	0.2

Table 4.12 Results of multiple presence factor for characteristic lanes

	MPF_{truck}	MPF_{middle}	MPF_{car}
H1	0.9	0.41	0.27
H2	0.9	0.41	0.18
H3	0.9	0.45	0.18
Proposed	0.9	0.45	0.25

4.4.2 Lane load

According to the KHBDC-CB, the live load is defined as the sum of 75% of the design truck load and the lane load. So, the lane load should be defined using $CRLTL$ excluding the load effects of 75% design truck load, and then the loads (kN) are converted into UDL (kN/m) using Eq. (4.2). To this end, Kim (2018) calculated the design lane load using the following equation, assuming that the live load effect of the design truck load is uniformly distributed over the span length especially in the case of the long-span bridge.

$$\omega = UDL - 0.75 \times \left(1.5 \times \frac{510}{L}\right) \tag{4.9}$$

where ω is the final uniformly distributed load used to define the design lane load and L is span length. A reasonable way to convert the concentrated load (design truck load) into the uniformly distributed load is that the magnitude of the design truck divided by L is multiplied by 2.0 in the case of the moment at the mid-span of a simple beam. However, the simple beam assumption is not valid for long-span bridges, and to ensure conservatism, 1.5 is alternatively used in Eq. (4.9). This study uses this equation to compute ω for the 11 span lengths and two-way 2 to 10-lane. It is desirable to propose the design lane loads for all the number of lanes and traffic

environments for accurate estimation of the live load of the bridge, but it would be impractical for engineers when designing bridges. Therefore, this study proposes the new design lane load model whose form is similar to that of the current design code as follows by introducing additional coefficients considering the effect of the traffic congestion environment and the number of lanes.

$$Lane\ load = \nu \times \lambda_1 \times 13.2 \times \left(\frac{200}{L}\right)^{\lambda_2} \quad (4.10)$$

where ν is a coefficient for the traffic congestion environment, and λ_1 and λ_2 are coefficients for the number of lanes. The constant value 13.2 in Eq. (4.10) is determined as ω at the 4-lane bridge with a span length of 200m. λ_1 and λ_2 are calculated using nonlinear least-squares fitting in MATLAB®, while *v* is determined by dividing the ω at the traffic environments C1 and C3 into ω at the C2. Tables 4.13 and 4.14 are coefficients in the design lane load model for heavy vehicle traffic environment H2.

Table 4.13 Coefficient ν for design lane load at the traffic environment H2

Traffic congestion environment	C1	C2	C3
ν	0.95	1.0	1.05

Table 4.14 Coefficient λ_1 and λ_2 for design lane load at the traffic environment H2

Number of lanes	2	4	6	8	10
λ_1	0.75	1.0	1.1	1.2	1.28
λ_2	0.24	0.18	0.18	0.16	0.13

In the same way, at the heavy vehicle traffic environment H1, the design lane load model equation is as follows, and Tables 4.15 and 4.16 show the coefficients in the design lane load model.

$$Lane\ load = v\lambda_1 \times 9.5 \times \left(\frac{200}{L}\right)^{\lambda_2} \tag{4.11}$$

Table 4.15 Coefficient v for design lane load at the traffic environment H1

Traffic congestion environment	C1	C2	C3
v	0.96	1.0	1.06

Table 4.16 Coefficient λ_1 and λ_2 for design lane load at the traffic environment H1

Number of lanes	2	4	6	8	10
λ_1	0.7	1.0	1.1	1.2	1.5
λ_2	0.24	0.22	0.20	0.17	0.16

In the heavy vehicle traffic environment H3, the design lane load model equation is given as follows, and Tables 4.17 and 4.18 show the coefficients in the design lane load model.

$$Lane\ load = v\lambda_1 \times 16.2 \times \left(\frac{200}{L}\right)^{\lambda_2} \tag{4.12}$$

Table 4.17 Coefficient v for design lane load at the traffic environment H3

Traffic congestion environment	C1	C2	C3
v	0.93	1.0	1.05

Table 4.18 Coefficient λ_1 and λ_2 for design lane load at the traffic environment H3

Number of lanes	2	4	6	8	10
λ_1	0.8	1.0	1.05	1.13	1.18
λ_2	0.20	0.16	0.14	0.13	0.10

As the number of lanes increases, the distinction between the truck lane and the car lane becomes clear. Therefore, when traffic congestion occurs, there are no more passenger cars and buses which are relatively light vehicles on the truck lane. Therefore, it is not surprising that the design land loads increase when the number of lanes increases because the design lane load is defined based on the maximum loads on the reference lane (mostly truck lane). Finally, Figure 4.16 shows the uniformly distributed load ω (dotted line) and the proposed design lane load model at the traffic environment H2 through the fitting process. It is confirmed that the new design lane load model successfully represents ω.

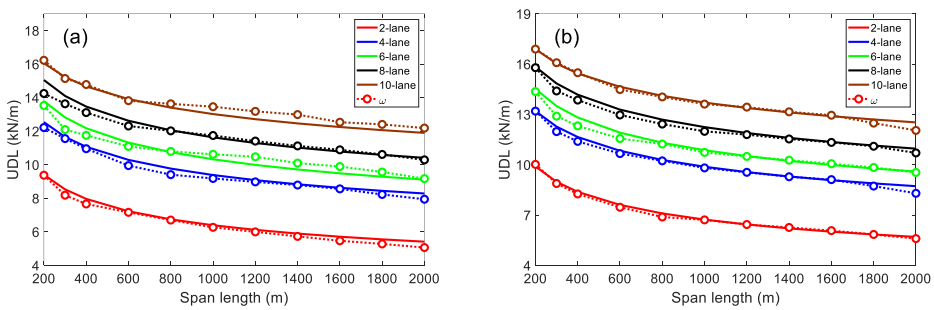

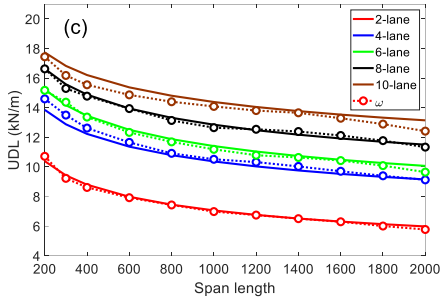

Figure 4.16 Proposed design lane load model: (a) Traffic environment H2C1, (b) Traffic environment H2C2, and (c) Traffic environment H2C3

4.5. Comparison with bridge design codes

4.5.1 Multiple presence factor and lane load model

The design live load model, which was proposed in Section 4.4 for long-span bridges, is compared with the existing design codes and related studies. In the case of the lane load model, this is compared with studies and the design code of South Korea (KHBDC-CB) because lane loads are highly influenced by the regional characteristics of heavy vehicles. On the other hand, the MPF is affected by more universal factors such as the occurrence probability of the maximum live load and the lane usage ratio on multi-lanes, so it can be compared with the MPF of design codes and studies of other countries.

Figure 4.17 shows a comparison of the design lane load model. It is noted that the proposed lane load model for two-way 4-lane (one-way 2-lane) is similar to the lane load model of the current design code and other studies in South Korea, and the lane load model of more than 6 lanes has larger values than existing studies. This is because existing studies use traffic scenarios on one-way 1 to 3-lane and define the

lane load by dividing the maximum live load on the bridge by the number of lanes (average value) whereas this study uses the maximum load on the reference lane.

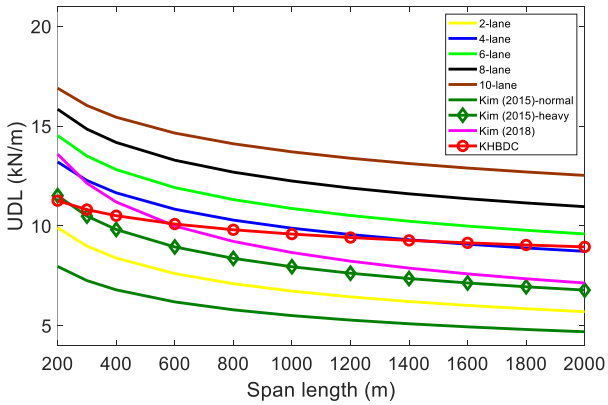

Figure 4.17 Comparison of the design lane load model

Table 4.19 shows a comparison of the MPF of this study and design codes (one-way lanes). These MPF values are normalized to the single-lane MLF for equivalent comparison using Eq. (4.3). It is confirmed that the proposed MPF has smaller values than other design codes and has similar values to Eurocode LM1. This is because, unlike other codes, Eurocode LM 1 and this study basically use the same approach to define the different live load values depending on the location of the lane. Lane number 1 in Eurocode LM 1 as shown in Table 1.5 can be considered as the truck lane defined in section 4.3.1. Lane numbers 2 and 3 represent the middle lane and car lane respectively. Thus, in the case of the number of lanes are 1 to 3, MPF values of this study and Eurocode are similar because the same characteristics lanes are used. However, in the case of the number of lanes are 4 to 5, MPF values of this study are higher than Eurocode LM 1. This is because, in this study, the middle and truck lane which have high MPFs are added while, in Eurocode LM 1, the other lanes

in Table 1.5 which have low live load values are added. In addition, the result shows that when designing a multi-lane long-span bridge using current MPFs of KHBDC-CB, the live loads of the bridge can be overestimated due to the high MPF values of KHBDC-CB.

Unlike other design codes, the proposed MPF value in this study increases in one-way 5-lane (two-way 10-lane) because the truck lane is added at the 5-lane as shown in Figure 4.2, i.e., it means that MPF_{truck} 0.9 is added. However, there are not many long-span bridges that have one-way 4 or 5-lane and data on traffic patterns during congestion and how often traffic congestion occurs on one-way 4 or 5-lane. Therefore, it is necessary to further investigate whether severe traffic congestion occurs on bridges with many lanes in reality and if it takes place, traffic patterns should be captured, e.g., how many heavy vehicles exist on the outer lanes.

It might be natural that existing design live load models are more conservative than the proposed design live load model. Because existing design live load models use fixed value so they should be inherently conservative to cover diverse traffic environments whereas the design live load model proposed in this chapter can vary depending on the traffic environment classification. In addition, it is difficult to predict the exact traffic environment in the design stage of bridges, so it is worth considering using the proposed design live load model for evaluating the condition of bridges in operation if sufficient traffic information and data are available to determine accurate traffic environment of bridges.

Table 4.19 Comparison of the multiple presence factor

Design code	Number of lanes				
	1	2	3	4	5
This study	1(0.9)[a]	0.675	0.533	0.513	0.59
KHBDC	1	0.9	0.80	0.70	0.65
AASHTO	1	0.833	0.708	0.542	0.542
ASCE-1981	1	0.85	0.70	0.63	0.58
Eurocode-LM1	1	0.64	0.52	0.46	0.42
Kim (2018)	1	0.85	0.80	0.75	0.75

[a] one-way 1-lane for 1.0 and two-way 2-lane for 0.9

4.5.2 Estimated live load effects using influence lines

Finally, live load effects are estimated using the influence lines of long-span bridges in South Korea and the proposed design live load model. Then, these estimated load effects are compared with those from the current code for long-span bridges (KHBDC-CB). The Incheon Grand Bridge and the 2nd Jindo Bridge, which are explained in Chapter 3, are used as example bridges. Figure 4.18 shows the influence line used for the comparison.

KHBDC-CB estimates live loads as follows. 75% of the design truck load is located where it produces the maximum load effect and the lane load is only loaded on the unfavorable part of the influence line. The live load effects are estimated for two-way 2 to 10-lane and expressed as the ratio divided by the calculated load effects from the code (Tables 4.20 to 4.23). As another live loading method, the design lane load is loaded on the entire influence line that is a physically suitable method for congested traffic flow.

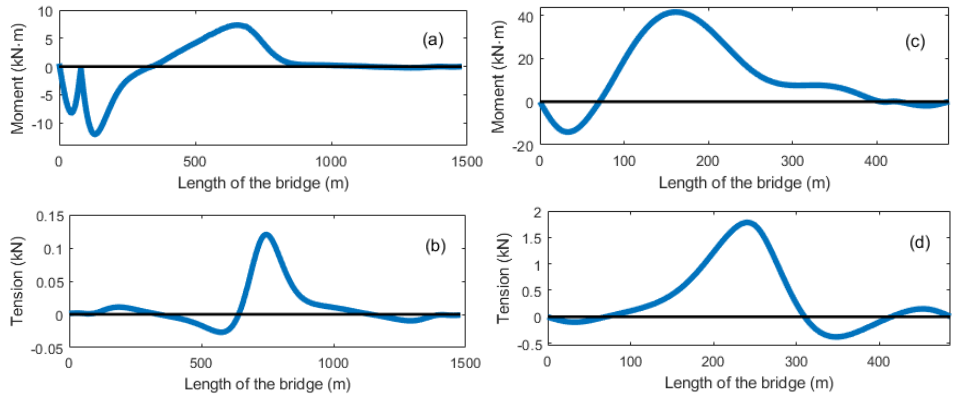

Figure 4.18 Influence lines of bridge members: (a) moment of a girder #79 (Incheon Grand Bridge), (b) tension of a cable #52 (Incheon Grand Bridge), (c) moment of a tower #102 (the 2nd Jindo Bridge) and, (d) tension of a cable #616 (the 2nd Jindo bridge)

Table 4.20 Comparison of live load effect using moment of a girder #79 (Incheon Grand Bridge)

Number of lanes	H2C2 (effective)	H2C2 (full)	H1C1 (effective)	H3C3 (effective)
2	0.68	0.19	0.50	0.85
4	0.78	0.19	0.57	0.98
6	0.76	0.18	0.55	0.95
8	0.92	0.21	0.66	1.16
10	1.26	0.28	0.90	1.59

Table 4.21 Comparison of live load effect using tension of a cable #52 (Incheon Grand Bridge)

Number of lanes	H2C2 (effective)	H2C2 (full)	H1C1 (effective)	H3C3 (effective)
2	0.70	0.56	0.53	0.85
4	0.78	0.61	0.58	0.96
6	0.75	0.58	0.56	0.93
8	0.91	0.70	0.67	1.13
10	1.23	0.95	0.90	1.54

Table 4.22 Comparison of live load effect using moment of a tower #102 (the 2nd Jindo Bridge)

Number of lanes	H2C2 (effective)	H2C2 (full)	H1C1 (effective)	H3C3 (effective)
2	0.70	0.64	0.52	0.81
4	0.78	0.71	0.56	0.92
6	0.75	0.68	0.55	0.90
8	0.90	0.82	0.66	1.11
10	1.22	1.11	0.99	1.69

Table 4.23 Comparison of live load effect using tension of a cable #616 (the 2nd Jindo Bridge)

Number of lanes	H2C2 (effective)	H2C2 (full)	H1C1 (effective)	H3C3 (effective)
2	0.72	0.64	0.55	0.81
4	0.78	0.69	0.58	0.90
6	0.74	0.66	0.56	0.89
8	0.89	0.78	0.67	1.08
10	1.20	1.05	0.99	1.63

In Tables 4.20 to 4.23, the “effective” means that the lane load is only loaded on the unfavorable part of the influence line, while the “full” means that the lane load is loaded on the entire part of the influence line. When the number of lanes increases, the live load effects from the proposed model increase because the MPF value becomes similar to that of KHBDC-CB. In particular, the live load effects of 10-lane increase significantly compared to those of 8-lane because, as previously explained, the truck lane is added. The results also show that the live load effect of the proposed model at the traffic environment H3C3 is similar to that of KHBDC-CB. This means that the current bridge design code is defined conservatively because this traffic environment represents a bridge that has frequent severe traffic

congestion and a high proportion of heavy vehicles.

Next, this study analyzes the estimated live load effects depending on the live loading method. In the case of Tables 4.21, 4.22, and 4.23 which do not have wide beneficial parts of the influence line, the full live loading method does not reduce significantly live load effects than the effective live loading method, whereas the live load effects of the full loading method reduce significantly in the case of Table 4.20 which has wide beneficial parts that can highly relieve live load effects. This indicates that severe traffic congestion (average speed is very low) is not always a traffic scenario that causes the maximum live load effect especially for the influence line which has wide beneficial parts. In this regard, it is necessary to perform further research about how to apply the design lane load on the influence lines of various bridge members, such as reducing the live loads on the beneficial part of the influence line by loading free traffic flow on the beneficial part, not congested traffic flow (Guo and Caprani, 2019).

4.6. Unified design live load model for short- to long-span bridges

This section discusses how to expand the proposed design live load model for long-span bridges to short- and medium-spans, in order to propose the design, live load model that covers all span lengths. Next, the final unified model for short- to long-span bridges is proposed with explanations on how to determine traffic environment categories and the live loading method.

4.6.1 Multiple presence factor and lane load model for short- and medium-span bridges

The multiple presence factor is discussed first. For long-span bridges, maximum live loads vary significantly depending on the characteristics of the lane (car, middle, and, truck lane) as described in Section 4.3.1. Especially, in the car and middle lane, maximum UDL can be reduced by many light vehicles on lanes even if a few heavy vehicles exist. On the other hand, the shorter the span length, the more critical the total weights of one or two heavy vehicles are to maximum live loads because maximum UDL cannot be relieved by many light vehicles. This implies that the characteristics lanes become indistinguishable anymore when estimating maximum live loads of short-span bridges

Therefore, the MPF proposed in this chapter cannot be applied to short- and medium-span bridges because the proposed MPFs are calculated considering the characteristics of lanes. Unlike the MPFs for long-span bridges, the MPFs for short and medium-span bridges have been sufficiently studied based on the serial and side-by-side heavy truck probability and the proposed MPFs that can cover up to a span length of 200 m (Hwang, 2008) are adopted for KHBDC. In this dissertation, the existing MPFs of KHBDC is already reasonably defined, so suggest using the MPFs of KHBDC for short- and medium-span bridges whose span lengths are shorter than 200 m and using the MPFs newly proposed for long-span bridges in this chapter for bridges whose span length are over 200 m.

Next, the design lane load model is discussed. The existing lane load model of KHBDC and KHBDC-CB in Table 1.1 is defined as a constant uniformly distributed

load value of 12.7 kN/m for span length shorter than 60 m while for longer than span length of 60 m, uniformly distributed load values which decrease according to the span length is used. It is natural to use decreasing load values according to the span length for a span length shorter than 60 m, but a constant load value was used to define a convenient design code (Hwang and Kim, 2015). To maintain the same form of the existing lane load model, this study also uses a uniformly distributed load value for span length shorter than 200 m, and uniformly distributed load values that decrease along the span length are used for span length longer than 200 m. The reason for using 200 m as the standard is that the newly proposed lane load model for long-span bridges is defined from 200 m, and the effect of errors occurring in a fitting process for span length shorter than 200 m to the estimation of maximum live loads is insignificant. This is because the lane load accounts for less than 40% of maximum live loads for shorter than span length of 200m (Hwang and Kim, 2015).

Constant uniformly distributed load values for shorter than 200m are defined as lane load values except for $(200/L)^{\lambda_2}$ in Eq. (4.10), (4.11), and, (4.12) to ensure continuity over the span length of the design lane load model. To calculate the error that occurs when using these constant load values, the *RLTL* of Eq. (4.5) are additionally calculated for the span length of 40, 60, 80, 100, and 150 m, and then uniformly distributed load ω values are calculated using Eq. (4.9). It is noted that the conservative 1.5 value in Eq. (4.9) is not used for shorter than span length of 200m. Instead, a reasonable 2.0 value is used under the simple beam assumption. This is because the simple beam assumption explained in section 4.4.2 is more valid for shorter than span length of 200 m, and the proportion of design truck load in the

maximum live load effect increases by more than 60%.

The errors are calculated for all traffic environments and the number of lanes cases and as one of the examples, Figure 4.19 illustrates errors occurring at the span length shorter than 200 m between ω and the lane load model. Table 4.24 shows the calculated average errors between ω and lane load model at the shorter span length of 200 m of all traffic environment cases. Although slight errors occur, the constant uniformly distributed load values proposed above are used as the lane load model for short- and medium-span bridges since the results are conservative.

Table 4.24 Average errors between ω and lane load model for shorter than span length of 200 m

Number of lanes	2	4	6	8	10
Average error	1.04%	-0.30%	1.08%	2.23%	5.74%

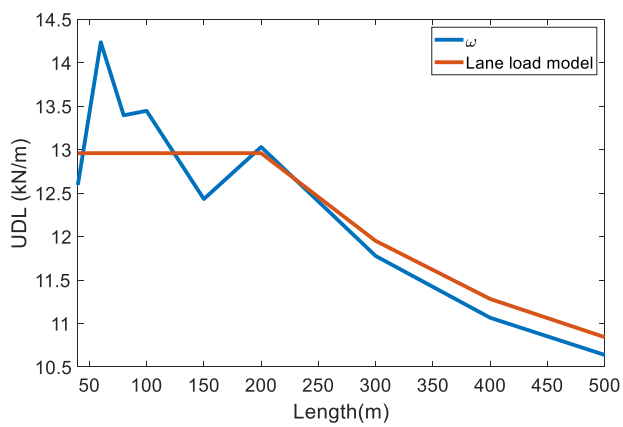

Figure 4.19 Comparison between ω and the proposed design lane load model for two-way 2-lane and traffic environment H3C2

4.6.2 Final design live load model

Including the live load model for short- and medium-span bridges described in the above section, the final design live load model is proposed in this section. First, the lane load is defined as follows:

$$Lane\ load = \begin{cases} \nu\lambda_1 \times \tau, & L \leq 200\ m \\ \nu\lambda_1 \times \tau \times \left(\frac{200}{L}\right)^{\lambda_2}, & L > 200\ m \end{cases} \quad (4.13)$$

where L is span length, ν is a coefficient for the traffic congestion environment, λ_1 and λ_2 are coefficients for the number of lanes, and τ is a constant value coefficient. These coefficients for each heavy vehicle traffic environment are provided in Section 4.4.2. Table 4.25, 4.26, 4.27, and 4.28 provide the coefficients clearly again.

Table 4.25 Coefficient ν for the proposed design lane load model

Traffic congestion environment / Heavy vehicle traffic environment	C1	C2	C3
H1	0.95	1.0	1.05
H2	0.96	1.0	1.06
H3	0.93	1.0	1.05

Table 4.26 Coefficient λ_1 for the proposed design lane load model

Number of lanes / Heavy vehicle traffic environment	2	4	6	8	10
H1	0.70	1.0	1.10	1.20	1.50
H2	0.75	1.0	1.10	1.20	1.28
H3	0.80	1.0	1.05	1.13	1.18

Table 4.27 Coefficient λ_2 for the proposed design lane load model

Number of lanes / Heavy vehicle traffic environment	2	4	6	8	10
H1	0.24	0.22	0.20	0.17	0.16
H2	0.24	0.18	0.18	0.16	0.13
H3	0.20	0.16	0.14	0.13	0.10

Table 4.28 Coefficient τ for the proposed design lane load model

Heavy vehicle traffic environment	H1	H2	H3
τ	9.5	13.2	16.2

The multiple presence factors for long-span bridges (longer than span length of 200 m) are provided in Table 4.29 and for short- and medium-span bridges (shorter than span length of 200 m) are provided in Table 4.30. The design truck load model of KHBDC as shown in Figure 1.1 is recommended to use as the design truck load model.

Table 4.29 Multiple presence factors for long-span bridges

Characteristic lane	Truck lane	Middle lane	Car lane
MPF	0.9	0.45	0.25

Table 4.30 Multiple presence factors for short- and medium-span bridges

Number of loaded lanes	1	2	3	4	5≤
MPF	1.0	0.9	0.8	0.7	0.95

Next, this study presents guidelines for engineers to determine the categories of the traffic environment. For heavy vehicle traffic environment, the ranges of the percentage of heavy trucks among trucks for each category are determined by referring to the mean and C.O.V in Table 4.1. However, it might be difficult to obtain an exact percentage of heavy trucks among trucks in the design stage, so this study additionally provides the ranges of the ratio of trucks among all vehicles by referring to Figure 4.1. Table 4.31 shows the ranges of two ratios for each category of the heavy vehicle traffic environment.

Table 4.31 The ranges of two percentages for each category of heavy vehicle traffic environment

Category	H1	H2	H3
Percentage of heavy trucks among trucks	<15%	15~35%	35%<
Percentage of trucks among all vehicles	<20%	20~30%	30%<

For traffic congestion environment, Table 4.4 shows the occurrence frequency of traffic congestion for three categories of traffic congestion environment under the assumption that the average congested speed is lower than 20 km/h. However, predicting the exact congested speed is almost impossible in the design stage. Instead, traffic and congestion data around the bridge can be obtained through the government or local government agencies. According to the road design manual (MOLIT, 2012), features of traffic congestion generally vary depending on the location of a bridge. Therefore, based on these data and information, the approximate occurrence frequency of traffic congestion can be estimated.

Based on the average speed of 30 km/h, which typically determines whether congestion occurs, the mean occurrence frequency of traffic congestion is proposed for each category of traffic congestion environment as shown in Table 4.32. C3 represents the bridge where traffic congestion occurs regularly almost everyday. This kind of bridge normally locates in huge cities with large traffic volume. C2 represents the bridge on which traffic congestion occurs regularly on specific days. For example, bridges located near tourist areas suffer congestion on Friday or weekends. C1 represents the bridge on which traffic congestion occurs irregularly. This study proposes the traffic congestion environment classification based on diverse traffic data through investigations of wide areas. Nevertheless, it still requires more data and studies to define the traffic congestion environment more quantitatively and strictly.

Table 4.32 The mean occurrence frequency of traffic congestion for each category of heavy vehicle traffic environment

Category	C1	C2	C3
Mean occurrence frequency	<52 hours /260 days	52~208 hours /260 days	208 hours< /260 days

Finally, this study explains how to apply the previously proposed design live load model onto the influence line to calculate the live load effect. Among diverse shapes of influence lines, sharp shapes that show large values in narrow areas such as Figure 4.18(a) and 4.18(b) are quite common. Therefore, which vehicle is located in this area has a significant effect on the live load effect of bridges regardless of short-span or long-span bridges. In particular, if heavy trucks are located in this area,

the live load effect increases significantly, so it is important how and which trucks are to be located in this area. However, an accurate estimation of the weight of overweight vehicles and the location of heavy trucks in multi-lanes through probabilistic methods is limited, as there are lots of uncertainties arising from various overweight vehicles, truck platoons, and unpredictable traffic situations such as an accident.

Therefore, this study suggests applying different lane load values for each characteristic lane using the proposed design lane load model in this chapter, whereas loading the same design truck load defined KHBDC on the most unfavorable position for all lanes to ensure conservatism of design codes. Furthermore, to obtain the final live load effect, the same way of KHBDC which selects the larger values between calculated live load effects by 1) design truck load, and 2) the sum of 75% design truck load and lane load is used.

4.7. Statistical characteristics of live loads and live load effects

This section investigates the statistical characteristics of live loads and live load effects for the calibrations of load and resistance factors in KHBDC and KHBCD-CB. In recent years, three studies have been conducted to identify the statistical model, bias factor, and C.O.V of the live load effect in South Korea (Lee, 2014; Kim, 2015; Kim, 2018). However, these studies have limitations because they calculated live load effects based on the assumed simple traffic scenarios that cannot consider various traffic environments of bridges and speed and lane change of vehicles during

traffic congestion.

Therefore, this study simulates congested traffic flow using the developed WIM data-based probabilistic model for traffic loads in Chapter 2 for each traffic environment and two-way 2 to 10-lane defined in Chapter 4. A total of 16 span lengths of 40 to 2000 m used in Chapter 4 are used for the calculation of live loads. To describe statistical characteristics of live loads and live load effects, three components are important as follows: 1) probability distribution type, 2) bias factor, and 3) coefficient of variation. Bias factor and coefficient of variation (C.O.V) of variable X are defined as follows:

$$\lambda_X = \frac{\mu_X}{X_0} \tag{4.14}$$

$$\delta_X = \frac{\sigma_X}{\mu_X} \tag{4.15}$$

where λ_X and δ_X denotes bias factor and C.O.V of X respectively. $\mu_X, \sigma_X,$ and X_0 are mean, standard deviation, and nominal value of X respectively. These three components are investigated in this section.

4.7.1 Statistical characteristics of live loads

First, to obtain the statistical characteristics of live loads, this study defines the design life as 100 years which is the target design life for general cable-supported bridges in KHBDC-CB. Next, to determine the nominal value, this study obtains the probability distribution of maximum live loads that can occur over 100 years which is appropriate for ultimate limit state design. The maximum live load distribution is commonly modeled as a GEV distribution, as described in section 2.6.1.1. Therefore,

GEV distribution is used as the probability distribution of maximum live loads in the dissertation. It should be noted that the calculated live load samples in Section 4.3 are annual maximum samples, not 100-year (design life) maximum samples. So, the 100-year maximum distribution is calculated through the extrapolation process described in Section 2.6.1.1 with GEV distribution. Figure 4.20 shows one of the results of extrapolation to obtain CDF of 100-year maximum total loads on a bridge.

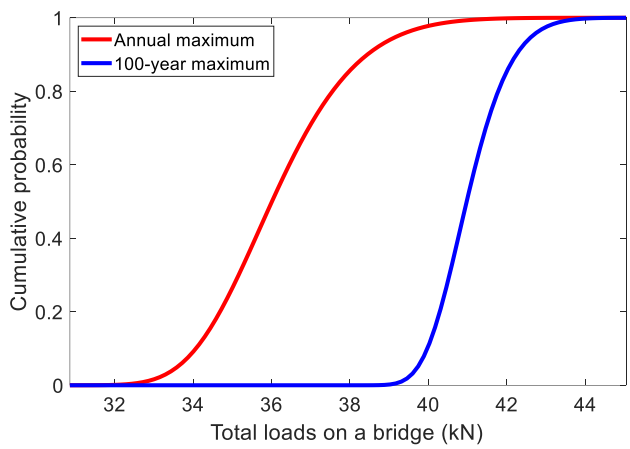

Figure 4.20 CDF of the 100-year maximum total loads on a bridge through the extrapolation

After obtaining the 100-year maximum live load distribution, among several values that can be extracted from these probability distributions, this study uses the 100-year return period value which is explained in Section 2.6.1.1 as the nominal value. Based on this, bias factors and C.O.V are calculated for each number of lanes and the traffic environment, and the results are shown in Figures 4.21, 4.22, 4.23, 4.24, and 4.25 by mean, maximum, and minimum values.

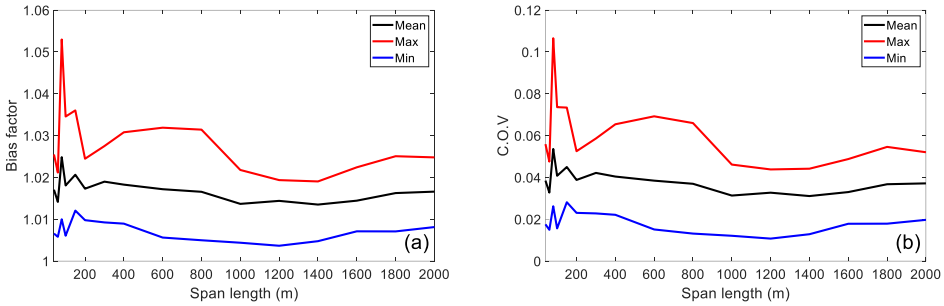

Figure 4.21 (a) Bias factors, and (b) C.O.V of 100-year maximum live loads for two-way 2-lane

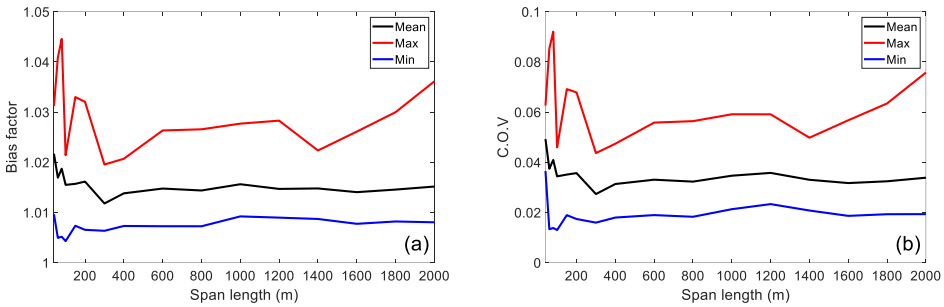

Figure 4.22 (a) Bias factors, and (b) C.O.V of 100-year maximum live loads for two-way 4-lane

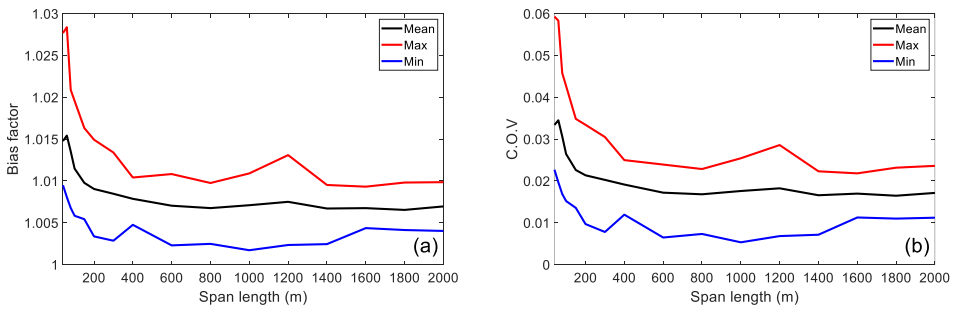

Figure 4.23 (a) Bias factors, and (b) C.O.V of 100-year maximum live loads for two-way 6-lane

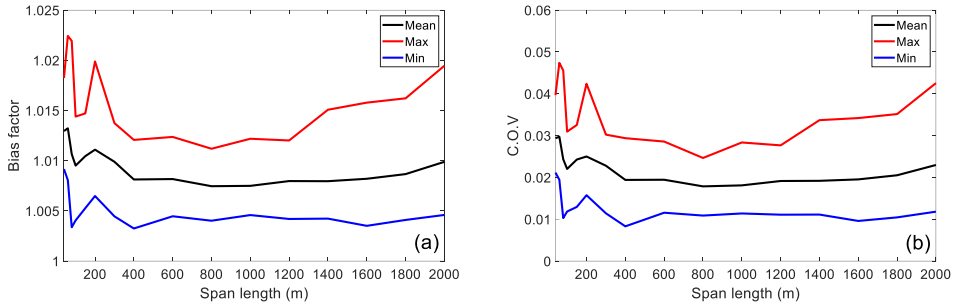

Figure 4.24 (a) Bias factors, and (b) C.O.V of 100-year maximum live loads for two-way 8-lane

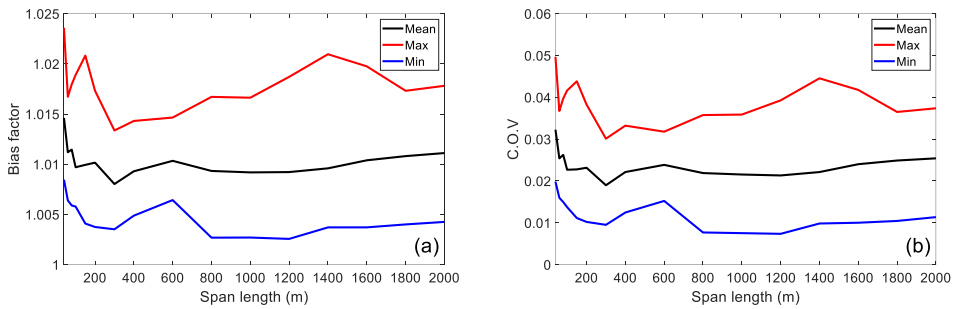

Figure 4.25 (a) Bias factors, and (b) C.O.V of 100-year maximum live loads for two-way -lane

The results show that when the number of lanes increases and the span length increases, the bias factor and C.O.V tend to decrease. This is because the disparity of lane load according to the location of the lane has been pronounced. Figure 4.26 shows the histogram of calculated a total of 720 (5 number of lanes cases × 9 traffic environment categories × 16 span length cases) bias factors and C.O.V. Due to the limitation of the number of samples during the extrapolation process, the values of bias factor and C.O.V larger than 1.04 and 0.08 are identified as outliers intuitively. Excluding them, the bias factor has values between 1.0 and 1.04 while C.O.V has

values between 0.01 and 0.08.

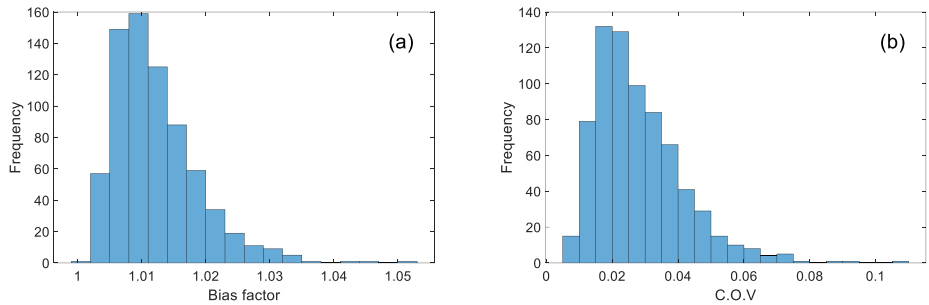

Figure 4.26 Histogram of calculated (a) Bias factors, and (b) C.O.V of 100-year maximum live loads

4.7.2 Statistical characteristics of live loads

Live load effects (moment, tension, shear force, and axial force) vary depending on the shape of the influence line of bridge members. Therefore, it is desirable to estimate the statistical characteristics of live load effects using diverse influence lines but entails high computational cost. So, this study follows the method in the previous study for efficient calculation (Kim, 2018).

Ellingwood et al. (1980) describes the uncertainty of load effect on structural members by three variables as follows:

$$Q_i = B_i \times C_i \times q_i \tag{4.18}$$

where Q_i is the load effect caused by the structural load q_i, the influence factor C_i, and the modeling parameter B_i. In the perspective of bridge live load, Q_i means random variable of the live load effect, B_i represents the uncertainty caused by idealizing the actual traffic load as a live load model in the design code, C_i represents the uncertainty arising from the structural analysis to calculate the traffic

load effect, and q_i means the traffic load (axle weight, total weight of the vehicle) acting on the bridge. The GEV distributions of 100-year maximum q_i are already obtained above section. For C_i and B_i, Nowak (1999) used 1.0 as bias factor for both factors and 0.12 and 0.06 as C.O.V for C_i and B_i, respectively under the assumption that C_i and B_i follow the Gaussian distribution. Hence, Q_i samples can be obtained by MCS with statistical models of $B_i, C_i,$ and q_i. These samples are used to determine the distribution type, bias factor, and C.O.V of the live load effects.

The probability distribution type of the live load effect Q_i is determined by the K-S test with a significance level of 0.05. Candidate probability distributions for the K-S test are Gaussian, lognormal, gamma, and Gumbel distribution, and a total of 6 sample sizes are used from 10^1 to 10^6. Samples of Q_i are generated by MCS and parameters of each candidate distribution are estimated by maximum likelihood estimation. After that, the K-S test is performed. From 10^3 sample sizes, Gaussian and Gumbel distributions are all rejected. In the case of 10^6 sample sizes, all candidate distributions are rejected for all cases of traffic environment categories and span lengths. Therefore, this study analyzes focusing on the results of the K-S test with 10^4 and 10^5 sample sizes for lognormal and gamma distributions. A total of 144 K-S tests are performed for each two-way 2 to 10-lane. This study computes the acceptance rate for each probability distribution and the results are shown in Tables 4.33 and 4.34. It is confirmed that the acceptance rate for the gamma distribution is higher than that of the lognormal distribution, so this study concludes that the live

load effect follows the gamma distribution.

Table 4.33 K-S test results for live load effects (lognormal distribution)

Number of lanes / Sample size	2	4	6	8	10
10^4	7%	4%	1%	0%	1%
10^5	0%	0%	0%	0%	0%

Table 4.34 K-S test results for live load effects (gamma distribution)

Number of lanes / Sample size	2	4	6	8	10
10^4	86%	87%	73%	78%	74%
10^5	4%	6%	5%	0%	0%

Next, bias factor and C.O.V are obtained from the parameters of gamma distribution estimated by maximum likelihood estimation. Tables 4.35 and 4.36 show the mean, minimum, and maximum values of the bias factor and C.O.V, depending on the number of lanes. The bias factor has a value between 1.0 and 1.05 and the coefficient of variation has a value between 0.13 and 0.17. Lastly, statistical characteristics of the live load effect investigated in this study and previous studies are summarized in Table 4.37.

Table 4.35 Estimated bias factors for the live load effect

Number of lanes	2	4	6	8	10
Mean	1.02	1.02	1.01	1.01	1.01
Min	1.00	1.00	1.00	1.00	1.00
Max	1.05	1.04	1.03	1.02	1.02

Table 4.36 Estimated coefficient of variation for the live load effect

Number of lanes	2	4	6	8	10
Mean	0.14	0.14	0.14	0.14	0.14
Min	0.13	0.13	0.13	0.13	0.13
Max	0.17	0.16	0.15	0.16	0.14

Table 4.37 Summary of the statistical characteristic of live load effects

	Probability distribution	Bias factor	Coefficient of variation
This study	Gamma	1.00~1.05	0.13~0.17
Lee (2014)	Lognormal	1.00	0.20
Kim (2015)	Gumbel	0.8~1.2	0.16
Kim (2018)	Gamma	1.00	0.17

Furthermore, bias factors are calculated using a ratio of return period to design life (RRD) which is the concept proposed in Lee (2019) to identify the effects of return period on maximum live load effects. Since the design life is defined as 100 years and the nominal value is defined as the return period value in this dissertation, the bias factor depending on the RRD of maximum live load effect is calculated as follows:

$$\lambda_{LL} = \frac{mean\ value\ of\ 100-year\ maximum\ live\ load\ effect}{return\ period\ value\ of\ live\ load\ effect} \quad (4.16)$$

The return period is expressed by

$$Return\ period = RRD \times Design\ life \quad (4.17)$$

A total of 144 bias factors (9 categories for traffic environment × 16 span lengths) are computed for each number of lanes case. The extreme results according to tail behavior are provided since all of these results cannot be shown on the graph. The return period value of live load effects naturally depends on the tail behavior of the gamma distribution of the maximum live load effects. The bias factor decreases more steeply with RRD in heavy-tailed cases while the bias factor decreases more gradually with RRD in light-tailed cases. Figure 4.27 shows the most heavy-tailed case, the most light-tailed case, and the mean of bias factors.

It is confirmed that when the RRD is around 1.7, the bias factor is closer to 1 which means that the 200-year return period values are similar to the 100-year maximum mean live load effects. Even with the heaviest tail, the bias factor is greater than 0.9 when the RRD is 20. This means that the increase of the 2000-year return period values of live load effects is 10% less than that of the 100-year mean values of maximum live load effects. Also, bias factors are almost similar regardless of tail behavior especially at more than 6 lanes whose C.O.V of q_i is small. This is because the same C.O.V of C_i and B_i which has a larger value than that of q_i are used for each traffic environment classification and number of lanes cases. In other words, C.O.V.s of C_i and B_i determine the tail behavior of the gamma distribution for live load effects. These results imply that there is a limit to the increase in live loads even though RRD increases significantly, which also conforms to actual traffic conditions.

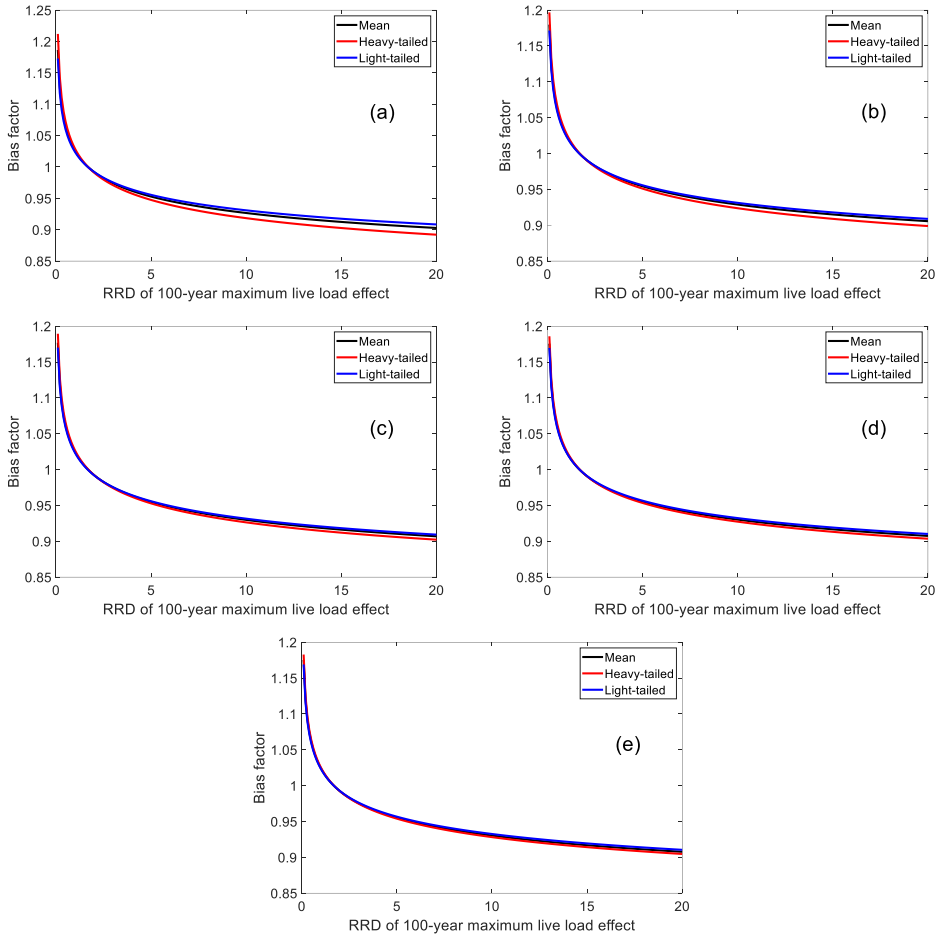

Figure 4.27 Bias factors according to RRD of 100-year maximum live load effect: (a) two-way 2-lane, (b) two-way 4-lane, (c) two-way 6-lane, (d) two-way 8-lane, and (e) two-way 10-lane

4.8. Summary

This chapter proposed a new live load model that reflects the diverse traffic environments of long-span bridges in South Korea. The traffic environments of long-span bridges in Korea were investigated, upon which this study defined the classification of traffic environment depending on two important factors. The first

traffic environment is the occurrence frequency of traffic congestion. Three categories were defined using traffic survey data of long-span bridges in Korea and bridges on the Han river where traffic congestion occurs frequently. The second traffic environment was also classified into three categories based on the percentage of trucks and heavy trucks among trucks. For multi-lane bridges, the positions of the car, middle, and truck lane are defined for two-way 2 to 10-lane to consider the characteristics of the lanes.

In order to calculate the live load on bridges, congested traffic flows were simulated for each nine categories of the traffic environment. Next, from the calculated live loads, the annual maximum total loads on the bridge and the annual maximum load on the reference lane were obtained. The maximum 100-year load on the reference lane was calculated through extrapolation of the annual maximum load samples on the reference lane. Design lane load model was defined as a similar form of the current code through a fitting process. For the multiple presence factor, the correction coefficient and the combination coefficient were calculated using the annual maximum samples and the final MPF values were proposed for each characteristic lane by analysis of annual maximum samples. The newly proposed design lane load model and MPF were compared with the existing design codes and related studies. Additionally, the live load effects were estimated using the influence line of the actual long-span bridge and compared with those from the current bridge design code of Korea. The comparison results showed that the live load model of the current design code is somewhat conservative and further study about the live loading method is needed. Furthermore, the final design live load model that can

covers short- to long-span bridges was proposed and statistical characteristics of live loads and load effects for code calibration were investigated. The proposed design live load model is expected to enable us to estimate the live load effects more precisely by reflecting the expected traffic environment of the bridge in the design stage.

Chapter 5. Time-Dependent Reliability Evaluation and Updating for PSC Box Girder Bridges Considering Traffic Environment and Strength Degradation

5.1. Introduction

In the last decade, many countries have adopted reliability-based Limit State Design (LSD) and Load and Resistance Factor Design (LRFD) in their bridge design codes. These design approaches enable us to achieve the target level of reliability by using the estimated nominal values and the factors of the two main components (load and strength) which are defined based on the uncertainties in each component. However, it should be noted that the load and strength keep varying over the service life of a bridge. This dissertation focused on estimating precise traffic loads on bridges over the service life. In this chapter, not only traffic loads but also the accurate estimation of strength considering strength degradation are studied in this chapter to evaluate the bridge reliability during the service life.

Strength degradation is caused by various environmental factors such as corrosion, crack, and damage. Among these many factors, this chapter focuses on the strength degradation caused by corrosion of strands as one of the examples of the strength degradation phenomenon. The reason why the dissertation focuses on strength degradation due to corrosion of strands is because of an event to be explained next. In 2016, external tendons failed in one of the Jeongneungcheon overpass prestressed concrete (PSC) box girder bridges in Seoul, South Korea, which

raised a significant alarm to the structural engineering community. Many investigations and studies have been conducted regarding this event. According to the investigation results, the corrosion of strands in external tendons was the main cause of the failure (SMFMC, 2017). It is widely known that the corrosion phenomenon in strands is a major cause of the reduction in the load-carrying capacity and serviceability of PSC girder bridges (Nakamura and Suzumura, 2013; Sajedi et al., 2017). Similar incidents occurred in many areas of the world, including France, UK, the United States, and Japan (FIB, 2006; SMFMC, 2017; Yoo et al., 2018). Therefore, it is essential to monitor and consider the strength degradation due to corrosion of strands in estimating the strength during the service life of a PSC girder bridge.

In order to calculate the strength and evaluate the reliability of PSC girder bridges with consideration of corroded strands, many studies have been carried out. Darmawan and Stewart (2007) performed a time-dependent reliability analysis of PSC girder bridges using the spatial maximum pit depth model developed by experimental results of pitting corrosion and extreme value theory. Strengths are evaluated under the assumption that corroded strands behave as a perfectly brittle parallel system and corrosion effects are considered by reducing the sectional area. Nguyen et al. (2013) studied the reliability-based optimal design of PSC box girder bridges considering pitting corrosion by models of corrosion initiation and propagation (Val and Melchers, 1997; Thoft-Christensen, 1998). Moment capacity is evaluated by reducing the sectional area of tendons where sufficient amount of wire failures due to the stress redistribution phenomenon. Guo et al. (2016) evaluated

the reliability of a PSC box girder bridge over the service life through the phased incremental static analysis using advanced composite degenerated shell element modeling. However, corrosion is considered in a relatively simple manner by reducing yield stress proportional to sectional loss area. Tu et al. (2019) evaluated time-dependent reliability and redundancy of corroded PSC girder bridges at material, component, and system levels. Corrosion of tendons is considered by the constitutive model of corroded prestressed tendons and a simplified and efficient FE methodology, grillage model, is used for system resistance analysis. Pillai et al. (2014) evaluated the time-variant flexural reliability of post-tensioned bridges by using the time-variant moment capacity model considering void, damage, and environmental conditions associated with the tendons.

In the perspective of traffic loads, Kim et al. (2016) assessed the reliability of the highway PSC girder bridge considering a few categories of traffic load models and corrosive environments. Guo et al. (2011) assessed the reliability index of deteriorating PSC box girder bridges by considering increasing vehicle loads over the service life and uniform and pitting corrosion under concrete carbonation and chloride attack. In addition, many other studies have been carried out to calculate the strength and reliability of general and RC bridges through probabilistic modeling and analysis of other deterioration processes, corrosion of reinforcement bars, and load history (Enright and Frangopol, 1998; Stewart, 2010; Ma et al., 2015; Li et al., 2015; Sajedi et al., 2017; Wang et al., 2017).

Despite these research efforts, there are remaining limitations in evaluating time-dependent reliability during the service life of the PSC box girder bridge. First,

when calculating the strength with consideration of strand corrosion, an accurate material model for corroded strands such as a stress-strain model using maximum pit depth and section loss area has not been introduced yet. Alternatively, many studies just simply reduced the section area by the amount of the section loss from corrosion and lowered the yield strength of a wire proportionally to consider the effect of corrosion. Second, many studies have been conducted for precise estimation of the strength of PSC girder bridge members through many experiments and advanced structural analysis models. However, time-dependent reliability assessment of bridges using such complex structural analysis models and experiments generally entails high computational cost. For efficient evaluation of the reliability which is comparable with the target level of reliability in current design codes, it is necessary to calculate the strength based on the same method defined in codes. The third limitation is that most of the previous studies have not considered the characteristics and changes of the traffic environment during the service life of bridges although they are critical components of the time-dependent reliability evaluation. Finally, few studies have evaluated and updated reliability practically by taking into account the data and inspection results measured in structure safety inspections.

Thus, this study proposes a new framework for comprehensive evaluation and updating of time-dependent reliability of PSC box girder bridges in operation by incorporating information regarding the traffic environment and corroded strands of bridges. The framework uses probabilistic models and methods to calculate the flexural strength degradation and traffic load effects during the service life of bridges

based on (1) corrosion-related data collected from the current practice of structure safety inspection, and (2) the traffic environment data obtained through WIM systems and traffic investigation.

5.2. Modelling corrosion of strands in PSC box girder bridges

5.2.1 Initiation and propagation of corrosion

The main cause of corrosion of steel strands and reinforcement bars is the chemical reaction between iron ions, water, and oxygen. Various environmental factors of corrosion can be divided into external and internal factors. External factors include the quality of concrete and rebar, admixtures, water fertilization, grout quality, and voids whereas relative humidity, temperature, carbonation, chloride content, pH, etc. are considered major internal factors (Ahmad, 2003). Because factors associated with the corrosive environment are uncertain, and their quantitative effects and interrelationship have not been clearly revealed, an accurate simulation of corrosion of strands is still challenging. Many previous studies described the corrosion of strands in two main phases: corrosion initiation and corrosion propagation (Enright and Frangopol, 1998; Ma et al. 2015; Guo et al. 2016).

In the corrosion initiation phase, it is assumed that corrosion is initiated by the diffusion of chloride into the surface of strands. If the chloride concentration at the surface of the wire increases and exceeds the threshold, the corrosion reaction is activated. When the chloride concentration at the surface is assumed to be a constant value, the corrosion initiation time can be described as (Thoft-Christensen, 1998)

$$T_i = \frac{C^2}{4D_c}\left[erf^{-1}\left(\frac{C_0 - C_{cr}}{C_{cr}}\right)\right]^{-2} \quad (5.1)$$

where T_i is the corrosion initiation time, D_c is the chloride diffusion coefficient, C is the concrete cover thickness, C_{cr} is the threshold of chloride concentration, C_0 is the constant chloride concentration at the surface, and $erf()$ denotes the error function.

Next, in the corrosion propagation phase, the maximum pit depth, which indicates how much the corrosion has propagated, can be calculated by the following model (Val and Melchers, 1997):

$$p(t) = 0.0116(t - T_i)i_{corr}R_{pen} \quad (5.2)$$

where $p(t)$ is the maximum pit depth at time t; i_{corr} is the corrosion current density; and R_{pen} represents the penetration ratio, i.e. the ratio between the maximum to the average penetration. The model in Eq. (5.2) was developed to describe the corrosion of reinforcement bars. On the other hand, the corrosion of strands, which is made of high-quality steel through a more strict manufacturing process, tends to propagate more slowly. In this case, the coefficient of 0.0116 in Eq. (5.2) is replaced by 0.0035 (Li et al. 2011; Guo et al. 2016).

Although this study can simulate the existence and progress of the corrosion in strands of a PSC box girder at the desired time using Eqs. (5.1) and (5.2). The simulation results are inevitably uncertain due to the uncertainties or lack of measurement and spatial variability of the parameters. It is also noted that the threshold C_{cr} is affected by pH, carbonation depth, temperature, and the presence of

void while i_{corr} is affected by humidity, water-cement ratio, and a chloride content (Song and Saraswathy, 2007; Virmani and Ghasemi, 2012). Therefore, the values of these parameters such as C_{cr} and i_{corr} should be determined based on various factors of the corrosive environment. However, because there exist no well-established methods or equations to describe the relationship between the parameters in Eqs. (5.1) and (5.2) and the corrosive environment (pH, temperature, humidity, water-cement ratio, etc), it is reasonable to model the parameters as random variables. For efficient modeling and analysis, instead of assigning the random variables to each strand, this study defines corrosive environment categories, to each of which the random variables are introduced. In Sections 5.2.2 and 5.4.1, probability distributions and their parameters are selected to describe these random variables appropriately based on data and categories from related literature and guidelines of the current practice of structure safety inspection.

5.2.2 Categories of corrosive environment of strands

In general, each tendon of a post-tensioned concrete box girder has several strands located inside the duct as illustrated in Figure 5.1(a) while the inside of the duct is filled with grout to prevent corrosion of the steel strands. Each strand is mainly composed of 7 to 9 wires as shown in Figure 5.1(b). In a tendon, the most important component regarding corrosion is the grout, which fixes strands in the duct and blocks penetration of water and chloride. However, voids are often generated in the grout due to the low quality of grout material, effects of the construction method, etc.

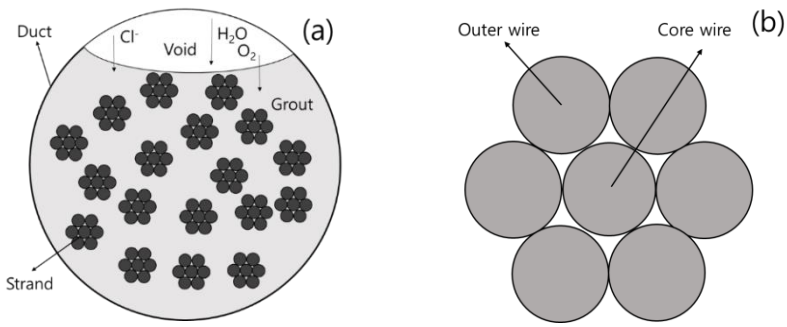

Figure 5.1 Cross sections of (a) external tendon; and (b) seven-wire strand

A void in the grout allows corrosion-promoting substances such as moisture, oxygen, and chloride to contact the strands, which may induce corrosion in the area. In fact, according to the samples of corroded strands obtained from the actual bridge (SMFMC, 2017), most of the corrosion was found in the strands exposed to the void. Therefore, in many countries, the presence of voids in the grouts is checked during safety inspections of PSC girder bridges. In addition, carbonation depth, water-cement ratio, and chloride content are often measured to investigate the corrosive environment. According to the FHWA report (Lee and Zielske, 2014), the farther the strand is located away from the void or the lower the water-cement ratio and chloride content are, the safer it is against corrosion. Thus, it is reasonable to classify the corrosive environment in terms of the distance between the strand and the void inside the duct. It is also noted that the guideline on annual safety inspection in South Korea (KISTEC, 2019) classifies the corrosive environment in terms of the existence of void and the carbonation depth. Accordingly, this study classifies the corrosive environment of strands into the four categories as described in Table 5.1. Figure 5.2

illustrates the layers of strands matching the categories A, B, C, and D in Table 5.1.

Table 5.1 Four categories of corrosive environment of strands

Category	Definition	Level of Corrosion Risk
A	No void, Carbonation depth > 30 mm	Very low
B	No void, 10 mm < Carbonation depth ≤ 30 mm	Low
C	Void, 0 mm < Carbonation depth ≤ 10 mm	Intermediate
D	Void, Exposed strands, Carbonation depth ≤ 0 mm	High

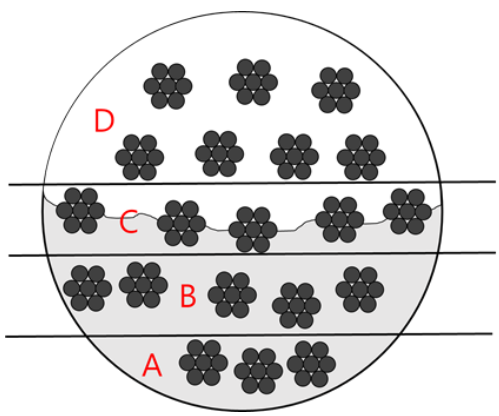

Figure 5.2 Strands matching four categories of corrosive environment in Table 5.1

Furthermore, the threshold of chloride concentration, C_{cr} in Eq. (5.1), which is the criterion regarding the occurrence of corrosion, should be determined differently for each category of the corrosive environment. To determine C_{cr}, several studies were carried out using experimental corrosion data from laboratories and corrosion samples from actual PSC girder bridges. Virmani and Ghasemi (2012) reviewed these studies to identify common characteristics of corroded steel strands as follows:

(1) the bleeding water accumulates during the grouting process, (2) corrosion initiates where the void exists in the grout, (3) carbonated local area exists, (4) high relative humidity and moisture accelerate corrosion propagation, and (5) once corrosion initiates, corrosion can propagate rapidly because of high chloride concentration, presence of moisture, water, and high humidity. However, there is no well-established formula for the threshold of chloride concentration that can analytically consider the effects of the environment, e.g. pH, temperature, humidity, moisture, even though these variables highly affect corrosion. Therefore, it is inevitable that the reference values for C_{cr} suggested by many researchers have significant variability.

To address the variability, in this study, C_{cr} is modeled as a random variable following a uniform distribution that employs the range values suggested in the literature and the guidelines of the current practice of structure safety inspection in South Korea. Currently, the values of C_{cr} from the guidelines are expressed as the total chloride content mass per unit volume (kg/cm^3). On the other hand, Glass and Buenfield (1997) suggested that the best way to express the chloride threshold value is by using the chloride content percentage of the weight of cement. Accordingly, this study divides the total chloride content mass into 1,300 kg/cm^3 (mass per unit volume of cement) to determine the values of C_{cr} with a unit of percent of the weight of cement. The maximum threshold value in category A, the safest category against corrosion, is determined as 1.5% of the weight of cement, which represents the best field conditions with high-quality grout containing no void or moisture

(Virmani and Ghasemi, 2012). Table 5.2 shows the ranges of the chloride concentration thresholds introduced for the four categories.

Lastly, the corrosion current density i_{corr} in Eq. (5.2), related to the corrosion propagation rate, also depends on the corrosive environment. The value of i_{corr} can be measured by the linear polarization resistance (LPR) technique and the criteria of the corrosion current density are often presented for four conditions of the corrosive environment: negligible, low, moderate, and high (Song and Saraswathy, 2007; Lee and Zielske, 2014). Based on the criteria, this study determines the range of corrosion current density i_{corr} for the four categories as shown in Table 5.2

Table 5.2 The ranges of C_{cr} and i_{corr} for each category of corrosive environment

Category	Threshold of chloride concentration (% of weight of cement)	Corrosion current density ($\mu A/cm^2$)
A	0.4 ~ 1.5	0.01 ~ 0.1
B	0.19 ~ 0.4	0.1 ~ 0.5
C	0.1 ~ 0.19	0.5 ~ 1.0
D	0.023 ~ 0.1	1.0 ~ 2.0

5.2.3 Material model of corroded strands

To reflect the actual behavior of corroded strands of PSC box girder bridges, this study employs the stress-strain material model by Jeon et al. (2019). The model was developed based on corrosion inspection and tensile strength tests of a total of 16 seven-wire strands samples taken from the Jeongneungcheon overpass bridge which experienced the failures of external tendons. The original (not corroded) seven-wire strand has a nominal cross-sectional area of 138.7 mm^2, and a nominal

diameter of 15.2 mm, while the nominal radii of outer wires and core wire are 2.6 mm and 2.5 mm, respectively. This is one of the most widely used strand types of PSC box girder bridges in Korea. The material model covers three corrosion types defined in terms of the corrosion shape of the wire. The section loss in each wire is calculated using the maximum pit depth and radius of the wire (more details available in Jeon et al. (2019)). The stress-strain relationship was described by a bi-linear model whose parameters are defined as follows based on the regression analysis:

$$f_{u,c} = a\eta + b \tag{5.3}$$

$$f_{y,c} = 0.85 f_{u,c} \tag{5.4}$$

$$\varepsilon_{u,c} = \begin{cases} c\eta^2 + d\eta + e & for\ d_p < 0.5 \\ f\eta^g & for\ d_p \geq 0.5 \end{cases} \tag{5.5}$$

where $f_{u,c}$ and $\varepsilon_{u,c}$ are the ultimate stress and strain of a corroded strand, respectively; $f_{y,c}$ is the yield stress; d_p is the maximum pit depth; η denotes the section loss ratio; and *a, b, c, d, e, f*, and *g* are the model coefficients described in Table 5.3.

Table 5.3 Coefficients of the material model of corroded strands (Jeon et al., 2019)

	a	*b*	*c*	*d*	*e*	*f*	*g*
Type 1	–1,991.8	1,748.0	–5.96	–1.30	0.0754	0.0025	–0.621
Type 2	–1,995.6	1,801.6	–1.00	–0.69	0.0754	0.0045	–0.305
Type 3	–2,302.7	1,752.7	9.54	–1.77	0.0754	0.0045	–0.298

5.3. Estimation of traffic load effects and flexural strength

5.3.1 Cross-sections of the example bridge (Hwayang-Jobal Bridge)

To demonstrate the time-dependent reliability analysis based on the estimation of traffic load effects and flexural strength, the Hwayang-Jobal Bridge is selected as the example bridge. This cable-stayed bridge connecting Yeosu and Goheung in South Korea has two lanes and a total length of 854 m and a main span of 500 m. The type of a stiffened girder of this bridge is post-tensioned concrete (PSC) box girder with external and internal tendons, each of which consists of 22 steel strands and a duct. A finite element model was constructed based on the structural calculation document of the bridge to estimate traffic load effects (moment of a girder) and the flexural strength of each cross-section. The cross-sections with the lowest level of reliability with regards to the positive moment and the negative moment are selected respectively. Figure 5.3 shows the constructed finite element model and the locations of selected cross-sections (#207 element for the positive moment, and #161 element for the negative moment). Figures 5.4(a) and 5.4(b) show the selected cross-sections for the positive and negative moments. The positive moment cross-section has two external tendons while the negative moment cross-section has four internal tendons. The next section presents how the traffic load effects and the flexural strength are estimated for these cross-sections.

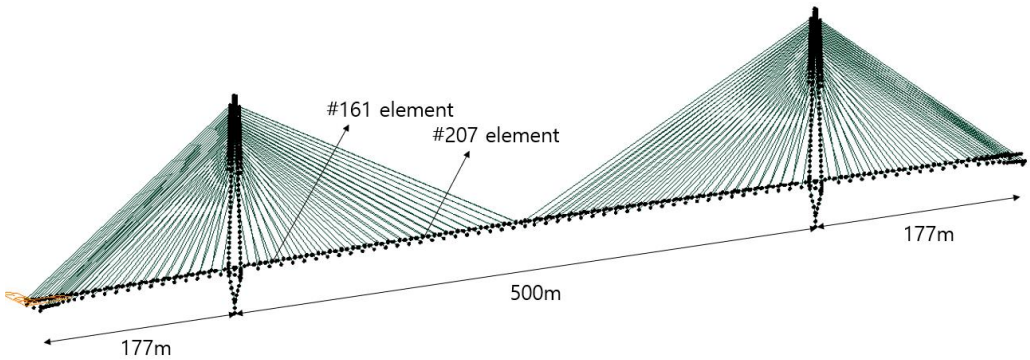

Figure 5.3 FE model of Hwayang-Jobal Bridge and selected elements for time-dependent reliability assessment

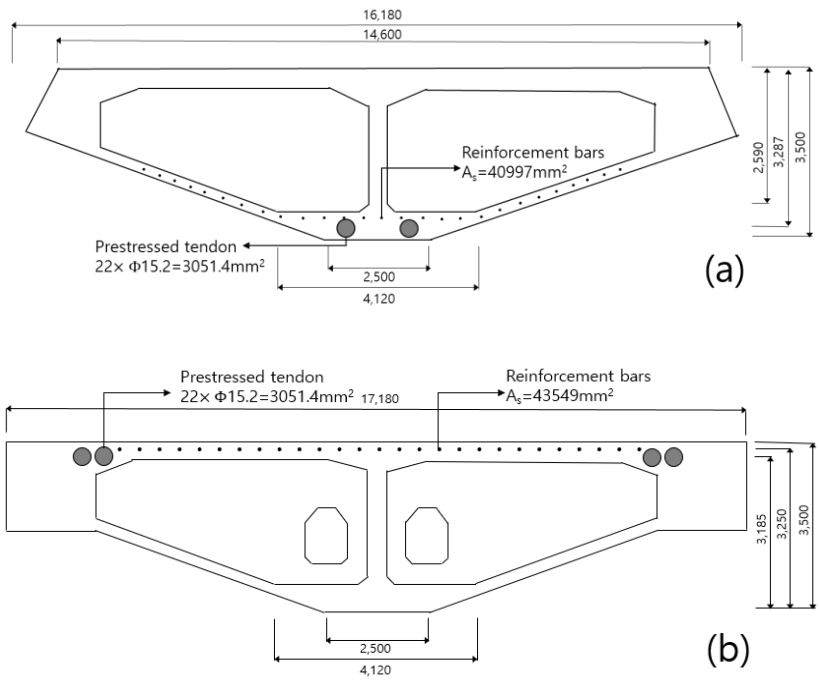

Figure 5.4 Girder cross-sections which have the lowest level of reliability in terms of (a) positive moment, and (b) negative moment

5.3.2 Calculation of traffic load effects using traffic environment information

To estimate the traffic load effects based on the actual traffic environment of Hwayang-Jobal Bridge, the probabilistic model of bridge traffic loads developed in

Chapter 2 and the Bayesian updating methodology in Chapter 3 are used. First, appropriate values are set for the parameters of the probabilistic models for traffic load based on the traffic investigation and WIM data of the example bridge and surroundings. Next, the artificial WIM data are generated to simulate traffic flows for the desired period. Then, the traffic load effects are computed using the influence lines of the structural members of interest. Lastly, the probabilistic distribution of the maximum traffic load effects during the service life of a bridge or the return period of a load level is obtained through the extrapolation process.

To estimate the traffic load effects of the selected cross-sections, the bending moment influence lines for the two cross-sections are first obtained as shown in Figure 5.5, and the traffic environment of the Hwayang-Jobal Bridge is investigated. However, the data related to the traffic environment accumulated over a long period are not available because of the short operation period of the bridge. So, this study uses the traffic information of roads, which was obtained from the regular traffic investigation on the area around the example bridge, to approximate the actual traffic environment. Since the example bridge has a long span (a total length of 854 m), the maximum traffic load effect occurs under a congested traffic flow, i.e., where many vehicles exist on the bridge. Hence, the average speed under traffic congestion and the occurrence frequency of traffic congestion are needed when simulating the traffic flow. The percentage of heavy vehicles such as large trucks and trailers, which is an important variable affecting the maximum traffic load effect, is also needed. To this end, this study infers the traffic environment of the example bridge based on its location. Because the bridge is located around many islands and tourist attractions,

it is assumed that, on weekends, the traffic volume increases significantly, the ratio of heavy vehicles is low, and the ratio of the passenger car is high. Actually, the traffic volume measured during a weekend was 10,944 veh/day, which exceeded the design traffic volume of 7,142 veh/day. Using the measurement of traffic volume, the average speed under traffic congestion is estimated indirectly through the volume delay function (VDF) in Eq. (4.1).

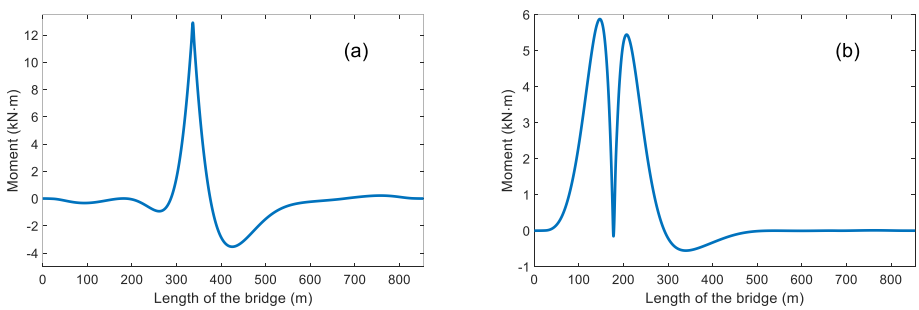

Figure 5.5 Influence lines of the selected cross-sections: (a) positive moment of a girder #207, and (b) negative moment of a girder #161

As a result, the average speed under congestion is estimated as 25~30 km/h, and it is assumed that this level of congested traffic flow occurs for 2 hours per weekend (104 hours/year). The ratio of heavy vehicles is assumed to be 3% based on the traffic data from the surrounding of the bridge (MOLIT, 2020a). To consider the impact load, the 25% impact load factor, which is specified in the KHBDC, is used in the study.

Based on the assumed parameters of the traffic environment, 100 samples of the annual maximum traffic load effect are calculated from the 100 simulated traffic flows for one year. The 100-year maximum traffic load effects (corresponding to the

estimated traffic load effect from the design code) are then calculated using extrapolation as shown in Table 5.4. The traffic load effects estimated from the initial traffic environment are smaller than those from the design code because the ratio of heavy vehicles is relatively low and severe traffic congestion does not occur frequently under the initial traffic environment.

Table 5.4 Estimated traffic load effects considering traffic environment of Hwayang-Jobal Bridge

	Positive moment (kN· m)	Negative moment (kN· m)
Design code	18,323.4	16,946.1
Initial traffic environment	12,446.2	13,494.5
Changed traffic environment (100 years)	19,219.1	22,542.7

Furthermore, the change in the traffic environment during the service life of the bridge is incorporated in this study through the following virtual scenario. It is assumed that, due to the industrialization of cities and the construction of many factories around Hwayang-Jobal Bridge in the future, the demand for the volume of cargo transportation continues to increase, resulting in a growth of the ratio of heavy vehicles, and severe traffic congestion occurs more frequently on weekdays than on weekends. To reflect this change of traffic environment, it is assumed that the ratio of heavy vehicles and the frequency of congested traffic flow increase linearly, and the average congested speed decreases. Accordingly, after 100 years, the ratio of heavy vehicles is assumed to reach 35% based on the data from other roads

experiencing many heavy vehicles in Korea. It is also assumed that traffic congestion occurs for one hour on each weekday (260 hours/year) and the average congested speed decreases to 5~10 km/h. Based on these assumptions, the traffic load effects for the changed traffic environment after 100 years are estimated as shown in Table 5.4. It is noted that both estimated traffic load effects (positive and negative moment) from the changed traffic environment increase and exceed those from the design code. The negative moment increases more significantly than the positive moment because of the shape of the influence line as shown in Figure 5.5. The influence line of the positive moment has wide beneficial parts (causing adverse traffic load effect against maximum traffic load effect). On the other hand, the influence line of the negative moment has relatively small beneficial parts.

5.3.3 Calculation of flexural strength considering corroded strands

For efficient evaluation of reliability, which is comparable with that in the design code, this study calculates the flexural strength in the same way as the code. An iterative method to satisfy the force equilibrium and the strain compatibility condition specified in the current Korean highway bridge design code (MOLIT, 2016b) is employed. Additionally, the material model for corroded strands described in Section 5.2.3 is introduced when calculating the flexural strength of the girder with strand corrosion considered. The other material models used in the study are as follows. For concrete and reinforcement bars, the parabolic-rectangular model and the elastic-perfectly plastic model provided in the design code (MOLIT, 2016b) are used, respectively. A seven-wire corrosion-free strand, in which each of the six outer

wires has a radius of 2.6 mm and the core wire has a radius of 2.5 mm, has a nominal cross-sectional area of 138.7 mm^2, and a nominal diameter of 15.2 mm. The strand is represented by, the bi-linear model with the material properties in Table 5.5 (Jeon et al., 2019) is employed.

Before computing the flexural strength, the effect of axial force should be considered in the case of cable-stayed bridges. However, according to the actual structural calculation document made for the example bridge, engineers judged that the design criterion for axial strength is automatically satisfied even if the cross-section is designed by considering only the flexural strength. Accordingly, this study also calculates flexural strengths without considering the action of axial force to calculate the reliability which is comparable to the reliability estimated from the design stage and for efficient computation of reliability. However, in the future, it is necessary to quantitatively analyze the effect of the axial force on the flexural strength through such as P-M interaction diagram for a more accurate reliability evaluation.

Table 5.5 Parameters of the bi-linear material model of seven-wire strand

Elastic modulus (Mpa)	Yield strength (Mpa)	Yield strain	Ultimate strength (Mpa)	Ultimate strain
195,000	1,628	0.0083	1,865	0.075

According to the design code, when starting the calculation of flexural strength with the iterative method, the maximum strain of the compression part of the concrete is assumed as the ultimate compressive strain of concrete, i.e., around 0.003,

to induce ductile failure. Next, assume the depth of the neutral axis and then the strain of the reinforcement bars and strands are obtained by

$$\varepsilon_s = \left(\frac{d_s - x}{x}\right)\varepsilon_{cu} \tag{5.6}$$

$$\varepsilon_{ps} = \left(\frac{d_{ps} - x}{x}\right)\varepsilon_{cu} + \frac{\sigma_{eff}}{E_{ps}} \tag{5.7}$$

where ε_s and ε_{ps} are the strains of reinforced bars and strands respectively; ε_{cu} is the ultimate compressive strain of concrete; d_s and d_{ps} are the distances from the top of the concrete compression part to the centroid of the rebars and the strands, respectively; x denotes the depth of neutral axis; σ_{eff} represents the effective prestress; and E_{ps} is the elastic modulus of the strand. In the case of PSC bridges, unlike general reinforced concrete bridges, prestressing force is applied in advance, so a term containing σ_{eff} is included in Eq. (5.7). The loss of the prestressing force occurs instantaneously and gradually over time due to the elastic deformation of concrete, the relaxation of the strand, the anchorage slip, etc. Therefore, the loss of prestressing force should be considered.

This study considers the ratio as follows:

$$R_{dis} = \frac{d_{ps} - x}{x} \tag{5.8}$$

which is defined as the distance between the neutral axis and the top surface of the concrete under compression to the distance between the neutral axis and the centroid of the PS strands. For PSC box girder bridges, this ratio is usually high because the width of the compression part is relatively wide as shown in Figure 5.4 (Youn, 2013).

When the ratio is larger than 4 in a flexural member, the initial strain caused by the effective prestress (the second term including σ_{eff} in Eq. (5.7)) is much smaller than that caused by ultimate loads (the first term including ε_{cu} in Eq. (5.7)). Thus, the effects of the loss of prestressing force on the flexural strength of the PSC box girder are negligible (Youn, 2013). The ratio in Eq. (5.8) for the selected cross-sections of the girder of the example bridge is also greater than 4. Therefore, for efficient estimation of flexural strength, it is assumed that the prestressing force is reduced by 30 % instead of accurately calculating the prestressing force loss. Besides, since x is significantly small due to the wide width of the compression part, the failure of the strand sometimes occurs before the maximum strain of the compression part of the concrete reaches ε_{cu}. This case violates the assumption in the design code introduced to induce ductile failure, and thus may lead to a convergence problem when calculating the flexural strength. This issue is addressed by gradually reducing the assumed maximum strain of the compression part of concrete when a convergence problem occurs.

Once corrosion occurs in steel strands, the corroded wires no longer behave linearly. Therefore, σ_{eff}/E_{ps} in Eq. (5.7) cannot represent the strain caused by the effective prestressing force. In this case, ε_{ps} should be calculated differently by calculating the initial strain $\varepsilon_{ps,eff}(\sigma_{eff})$ caused by the prestressing force from corroded strands, i.e.

$$\varepsilon_{ps} = \left(\frac{d_{ps} - x}{x}\right)\varepsilon_{cu} + \varepsilon_{ps,eff}(\sigma_{eff}) \tag{5.9}$$

To obtain $\varepsilon_{ps,eff}(\sigma_{eff})$ by considering the nonlinear behavior of the corroded wire,

this study uses an assumption that the strain is proportional to the distance from the neutral axis even if corrosion occurs (Jeon et al., 2019). Then, the initial strain $\varepsilon_{ps,eff}(\sigma_{eff})$ is calculated iteratively through the stress redistribution among seven wires while maintaining the prestressing force of the strand. Next, using the strains of strands calculated by Eq. (5.9), the tensile forces of the strands are calculated using the material model of corroded strands. The tensile force of the reinforcing bar and the compression force of concrete are also calculated based on the estimated strain and the corresponding material models. Finally, this study checks whether the force equilibrium condition is satisfied through the calculated tensile force and compression force and if so, the iteration is terminated to determine the flexural strength. Additionally, given that corrosion mainly occurs in outer wires, it is conservatively assumed that corrosion occurred in six outer wires excluding the core wire among the seven-wire strand. Figure 5.6 is the flow chart describing the iterative method to calculate the flexural strength.

Using Eqs. (5.1) and (5.2), and the iterative method described above, the flexural strength of the girder during the service life is calculated as follows. First, each strand is assigned to one of the categories of corrosive environment in Table 5.1. Next, the corrosion initiation time for the strands in the same category is calculated using Eq. (5.1). Then, the strands with and without corrosion are distinguished using the calculated corrosion initiation time and the relevant parameters for each strand. For the strand without corrosion, a material model for strands without corrosion is used. For the strands with corrosion, the maximum pit depth for the strands in the same category is calculated using Eq. (5.2), and the depth

is used to obtain the section loss ratio of wires in the strand (More details in Jeon et al. 2019). Subsequently, the material model of corroded strands in the section "Material model of corroded strands" is determined through the section loss ratio. Finally, the flexural strength is calculated by the iterative method based on the material models defined for strands. For example, Figure 5.7 shows the result of calculated flexural strength over 100 years for the cross-section of the negative moment using certain fixed values for random variables. Among 22 strands in each tendon, 5, 5, 6, and 6 strands are classified into categories A, B, C, and D respectively. Strands in categories A and B do not experience corrosion while corrosion initiates at the strands in category D in the 18^{th} year and total failure occurs in the 33^{rd} year. Strands in category C suffer corrosion from the 54^{th} year and totally failed in the 81^{st} year.

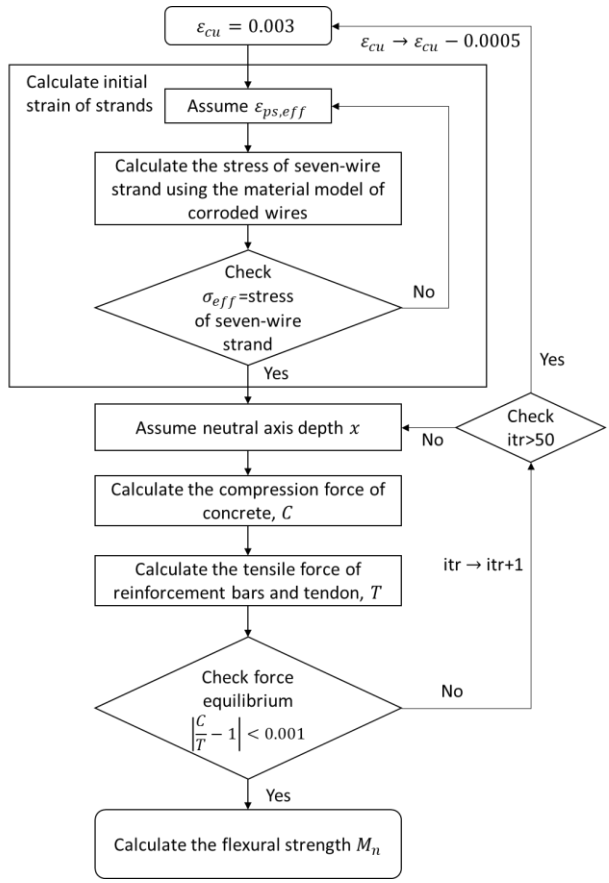

Figure 5.6 Flow chart of the iterative method proposed to calculate the flexural strength

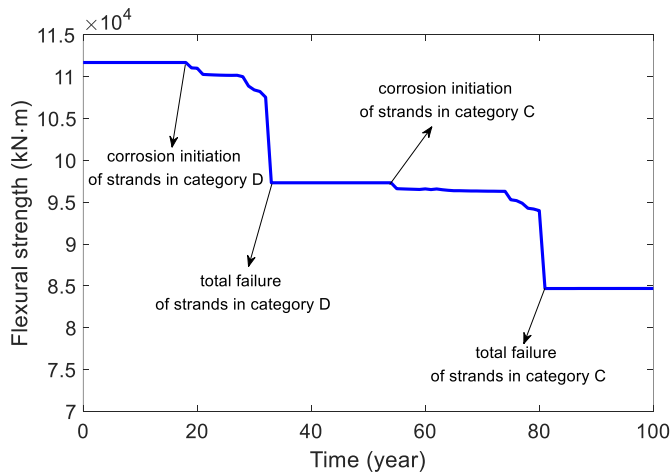

Figure 5.7 Example history of calculated flexural strength over the service life

5.4. Time-dependent reliability evaluation

5.4.1 Limit state function and random variables

This section describes the limit state function and random variables used in the time-dependent reliability evaluation of the example bridge over its service life. The KHBDC and KHBDC-CB define ultimate, serviceability, fatigue, and extreme event limit states. Among them, the ultimate limit state 1 (ULS 1), which is a basic load combination that mainly considers the traffic flow (without wind load), is selected for the time-dependent reliability assessment in this study. The limit state function of ULS 1 is given as

$$g(\boldsymbol{X}, DC, DW, PS, t) = R(\boldsymbol{X}, t) - D(DC, DW) - PS - LL(\boldsymbol{X}, t) \quad (5.10)$$

where $R(\boldsymbol{X}, t)$ is the flexural strength of the girder; and D is the bending moment determined by the dead load of structural members and non-structural attachments (denoted by DC), and the dead load of wearing surfaces and utilities (denoted by DW). PS is the bending moment from the prestressing force applied by the cables and tendons; and $LL(\boldsymbol{X}, t)$ is the bending moment from the traffic loads. It might seem inappropriate to use traffic load effects estimated by influence lines from a linear structural analysis because the behavior of the bridge is usually in a nonlinear range when exceeding the ultimate limit state (ULS). However, it is noted that existing design codes and many previous studies employ such an approach as an approximation because nonlinear structural analysis may require exceedingly high computational cost, especially when a sampling method is used for reliability calculations. Therefore, this study adopts the approximate method for efficiency,

while leaving its impact on accuracy as a future research topic.

To perform reliability analysis, statistical properties of the random variables, which represent the uncertainties in material properties, corrosive environment, and loads in the limit state function, are investigated through the literature. As a result, the statistical properties of the 22 random variables are summarized as shown in Table 5.6. This study mainly refers to the statistical properties related to loads and strengths recently investigated in Lee (2019) for code calibration of KHBDC.

The nominal and mean values for material properties such as concrete strength and ultimate strength of strands are determined from the structural calculation document. The statistical properties of corrosion-related variables used in Eqs. (5.1) and (5.2) are determined based on the literature and guidelines of the current practice of structure safety inspection. As for the random variable C_{cr}, a bounded range is assigned to C_{cr} representing each of the four categories of corrosive environment in Table 5.2. In addition, C_{cr} has large variabilities because it is significantly affected by many factors such as pH, temperature, humidity (Virmani and Ghasemi, 2012) while there exist no well-established methods or equations to consider these factors. Thus, uniform distribution is used to describe C_{cr} in this study instead of normal or lognormal distributions which were generally used in previous studies. The parameters of uniform distribution for C_{cr} and i_{corr} are determined by their feasible ranges for each category of the corrosive environment described in Table 5.2. The random variable *sla* represents the uncertainty in estimating the sectional loss area through the maximum pit depth (Lee et al., 2020). The professional factor *prf* is a coefficient describing the uncertainty from the difference between the

strength analysis model and the actual strengths of structural members (Ellingwood et al., 1980). This study adopts the statistical properties of *prf* suggested by Nowak and Szerszen (2003). The nominal values of *D* and *PS* are estimated based on the structural calculation document and their statistical properties are determined based on the literature.

The uncertainty in the traffic load effect can be considered through Eq. (4.18) which is explained in Section 4.7. Since the traffic load effect is calculated by direct simulation of the traffic flow with the influence line in this study, q_i can be described as a random variable following the generalized extreme value (GEV) distribution based on the extreme value theory. B_i is not included as a random variable because a live load model of the design code is not used in this study when estimating the traffic load effects. The influence factor C_i (Nowak, 1999) is selected as a random variable as shown in Table 5.6.

Table 5.6 Statistical properties of the random variables

Variable	Property	Parameter	Distribution	Reference
f_{ck}	Concrete strength	Nominal: 45 Mpa, Bias: 1.158, C.O.V: 0.095	Lognormal	Kim (2018)
f_{pu}	Ultimate strength of prestressed wire	Mean: 1,865 Mpa, C.O.V: 0.02	Normal	Lee et al. (2020)
f_y	Yield strength of reinforcement bar	Nominal: 400 Mpa, Bias: 1.15, C.O.V: 0.08	Lognormal	Kim (2018)
E_s	Elastic modulus	Nominal: 200,000 Mpa, Bias: 1.0, C.O.V: 0.06	Lognormal	Lee (2019)
C	Concrete cover	Mean: 21mm, C.O.V: 0.05	Normal	Nguyen et al. (2013)

D_c	Diffusion coefficient	Mean: 0.631cm^2/year, C.O.V: 0.2	Lognormal	Val and Trapper (2008)
$C_{cr,A}$	Chloride concentration threshold (A)	[0.4, 1.5] % of cement weight	Uniform	KISTEC (2019), Virmani and Ghasemi (2012)
$C_{cr,B}$	Chloride concentration threshold (B)	[0.19, 0.4] % of cement weight of cement	Uniform	KISTEC (2019), Virmani and Ghasemi (2012)
$C_{cr,C}$	Chloride concentration threshold (C)	[0.1, 0.19] % of cement weight	Uniform	KISTEC (2019), Virmani and Ghasemi (2012)
$C_{cr,D}$	Chloride concentration threshold (D)	[0.023 ,0.1] % of cement weight	Uniform	KISTEC (2019), Virmani and Ghasemi (2012)
$i_{corr,A}$	Corrosion current density (A)	[0.01, 0.1] $\mu A/cm^2$	Uniform	KISTEC (2019), Song and Saraswathy (2007)
$i_{corr,B}$	Corrosion current density (B)	[0.1, 0.5] $\mu A/cm^2$	Uniform	KISTEC (2019), Song and Saraswathy (2007)
$i_{corr,C}$	Corrosion current density (C)	[0.5, 1.0] $\mu A/cm^2$	Uniform	KISTEC (2019), Song and Saraswathy (2007)
$i_{corr,D}$	Corrosion current density (D)	[1.0, 2.0] $\mu A/cm^2$	Uniform	KISTEC (2019), Song and Saraswathy (2007)
R_{pen}	Penetration ratio	[4, 6]	Uniform	El-Maaddawy and Soudki (2007)
sla	Sectional loss area	Bias: 1.0, C.O.V: 0.05	Lognormal	Lee et al. (2020)

prf	Professional factor for strength	Mean: 1.0, C.O.V: 0.06	Lognormal	Nowak and Szerszen (2003)
DC	Dead load of structural members	Bias: 1.03, C.O.V: 0.08	Normal	Nowak (1999)
DW	Dead load (2^{nd})	Bias: 1.00, C.O.V: 0.25	Normal	Nowak (1999)
PS	Prestress force	Bias: 1.0, C.O.V: 0.06	Normal	Nowak (1999)
LL	Live load	Estimated parameters	GEV	Kim and Song (2019)
C_i	Influence factor for live load	Mean: 1.0, C.O.V: 0.06	Normal	Nowak (1999)

5.4.2 Computation of time-dependent reliability

Time-dependent reliability evaluation aims to evaluate the reliability of an engineering system over its service life. Many researchers have studied how to efficiently calculate time-dependent reliability and have applied various methods to actual structures (Andrieu-Renaud et al., 2004; Li and Ellingwood, 2015; Wang et al., 2017; Straub et al., 2020). According to Gong and Frangopol (2019), reliability methods that cover external loadings and the deteriorating process can be classified into three categories: the Poisson process load method (Yang et al., 2017), the extreme value-based method (Wang and Wang, 2012), and the FORM-based outcrossing rate method (Andrieu-Renaud et al., 2004). Among these categories, the extreme value-based method is employed because in the case of ULS1, the strength and the load process can be modeled independently and various loads can be grouped into time-invariant loads and time-variant loads which can be approximated by maximum loads. Further details of the computation process are provided below in

this section. In addition, for convenient and efficient computation, the service life is often discretized to a series of time intervals. The time-variant reliability problem is then transformed into a time-invariant reliability problem which can be solved through a system reliability method for the series system event (Melchers, 1999). This approach is adopted for time-dependent reliability analysis in this study.

Let us consider a limit state function defined by two groups of random variables describing strengths and loads, respectively, e.g. ULS 1. In this case, the limit state function can be described as (Straub et al., 2020)

$$g(\boldsymbol{X}_R, \boldsymbol{Q}(t), t) = R(\mathbf{X}_R, t) - S(\boldsymbol{Q}(t)) \tag{5.11}$$

where $R(\boldsymbol{X}_R, t)$ is the structural strength affected by the corrosion process, $\boldsymbol{X}_R$ is the vector of random variables related to the strength and corrosion, and $S(\boldsymbol{Q}(t))$ is the load effect determined by the combination of the loads, i.e. $\boldsymbol{Q}(t) = \{D(t), PS(t), LL(t)\}$ in Eq. (5.11). The service life is discretized into a series of time intervals indexed by $j = 1, \ldots, m$. The j-th interval corresponds to the time duration $\tau \in (t_{j-1}, t_j]$. The probability of the interval failure event F_j^* is formulated as

$$\begin{aligned} Pr(F_j^*) &= Pr\left(\min_{t_{j-1} < \tau \le t_j} g(\boldsymbol{X}_R, \boldsymbol{Q}(\tau), \tau) < 0\right) \\ &\approx Pr\left(R(\boldsymbol{X}_R, t_j) < \max_{t_{j-1} < \tau \le t_j} S(\boldsymbol{Q}(\tau))\right) \end{aligned} \tag{5.12}$$

where $\boldsymbol{Q}(\tau)$ is the time-varying load vector during the time interval j, and the time-varying strength during the time interval j is approximated by the strength at the end point, i.e. $R(\boldsymbol{X}_R, t_j)$. It is noted that the approximation made in Eq. (5.12) holds when the service life is discretized into a large number of intervals. To reduce the computational cost, a further approximation is made as follows by replacing the load

vector $\boldsymbol{Q}(\tau)$ by the maximum loads over the interval, $\boldsymbol{Q}_{max,j}$ through an extreme value analysis:

$$Pr\left(F_j^*\right) \approx Pr\left(R(\boldsymbol{X}_R, t_j) < S(\boldsymbol{Q}_{max,j})\right) \tag{5.13}$$

As a result, the failure probability during a given interval can be computed by time-invariant reliability analysis. It is noted that, in the case of ULS 1, the temporal variability of the traffic load is significantly larger than those in the other loads. Therefore, the load vector $\boldsymbol{Q}$ can be split into the time-variant load $Q_{tv} = LL,$ and the group of time-invariant loads $\boldsymbol{Q}_{ti} = [D(DC, DW), PS]$. As a result, the interval failure probability can be efficiently evaluated as (Straub et al., 2020):

$$\begin{aligned} Pr\left(F_j^*\right) &\approx Pr\left(g\left(\boldsymbol{X}_R, \boldsymbol{Q}_{ti}, LL_{max,j}, t_j\right) < 0\right) \\ &= Pr\left(R(\boldsymbol{X}_R, t_j) < S(\boldsymbol{Q}_{ti}, LL_{max,j})\right) \end{aligned} \tag{5.14}$$

where $LL_{max,j}$ denotes the maximum live load during the time interval *j*. Without losing general applicability, this study adopts subset simulation (Au and Beck, 2001) to obtain interval failure probability in Eq. (5.14) because the method facilitates efficient calculation of the probability of a rare event in a high dimensional problem. In this study, to calculate interval failure probability through subset simulation, $N = 2000$ samples and conditional probability $p_0 = 0.1$ are used for each intermediate subset. The adaptive conditional sampling method is used as the MCMC sampling method to obtain samples of each subset. For more details of the used sampling method, the reader is referred to Papaioannou et al. (2015).

Next, the failure of the structure up to the time t_i (or up to the endpoint of the interval *i*) can be described by the union of the interval failures, i.e.

$$Pr[F(t_i)] = Pr(F_1^* \cup F_2^* \cup \cdots \cup F_i^*) \tag{5.15}$$

In order to efficiently evaluate the series system failure probability $\Pr[F(t_i)]$, upper and lower bounds using uni-component probabilities can be computed as (Boole, 1854)

$$\max_{j\in[1,\dots i]} Pr(F_j^*) \le Pr[F(t_i)] \le \min\left(1, \sum_{j=1}^{i} \Pr(F_j^*)\right) \tag{5.16}$$

In addition, the following narrower bound, based on the assumption that interval failure events are independent of each other, is often used (Schneider et al., 2017):

$$\max_{j\in[1,\dots i]} Pr(F_j^*) \le Pr[F(t_i)] \le 1 - \prod_{j=1}^{i} \left[1 - Pr(F_j^*)\right] \tag{5.17}$$

However, these bounds are often too wide to be useful. For narrower bounds, the information regarding the statistical dependence between the interval failure events needs to be incorporated (Song and Der Kiureghian, 2003).

Among a variety of system reliability methods (Song et al. 2021) that were developed to compute the series system failure probability, this study adopts the approach by Straub et al. (2020) in which the first-order reliability method (FORM) approximation is estimated by a sampling method. This approach was developed to cover the same kind of problems as ULS1, which is used as the limit state in this study. In addition, this approach can update the time-dependent reliability using inspection and monitoring data and can reduce the computational cost. In this method, $Pr[F(t_i)]$ is evaluated by the FORM approximation (Hohenbichler and Rackwitz, 1982), i.e.

$$Pr[F(t_i)] = Pr(F_1^* \cup F_2^* \cup \cdots \cup F_i^*) \approx 1 - \Phi_n(\mathbf{b}; \boldsymbol{\rho}) \tag{5.18}$$

where $\Phi_n(\mathbf{b};\boldsymbol{\rho})$ is the multivariate standard normal cumulative distribution function (CDF) at vector $\mathbf{b} = [\beta_1;\beta_2;\cdots;\beta_i]$ which is the set of the reliability indices for the interval failure events $F_j^*, j = 1, \ldots, i$. The elements of the correlation coefficient matrix $\boldsymbol{\rho}$ are obtained by

$$\rho_{jk} = \alpha_j \alpha_k^{\mathrm{T}} \tag{5.19}$$

where ρ_{jk} means the correlation coefficient between the failures of the interval *j* and *k*, α_j and α_k are the negative normalized gradient vectors (Der Kiureghian, 2005) from FORM analysis of the corresponding intervals. Straub et al. (2020) proposed to estimate them using a sampling-based method, i.e.

$$\alpha_j \approx \frac{\sum_{l=1}^{s_{tot}} \mathbf{u}_{F,j}^{(l)}}{\left\| \sum_{l=1}^{s_{tot}} \mathbf{u}_{F,j}^{(l)} \right\|} \tag{5.20}$$

where $\mathbf{u}_{F,j}^{(l)}, l = 1, \ldots, s_{tot}$ is the *l*-th sample of standard normal vector in the failure domain, and s_{tot} is the total number of the samples. Refer to Straub et al. (2020) for more details.

Furthermore, it is noted that the uncertainties in the random variables related to corrosion and traffic environment are naturally large due to many uncertain factors in the surroundings. Therefore, it is desirable to update the reliability based on data and information gained during the service life of the bridge. Introducing an event $Z(t_z)$ representing the data measured up to the time t_z, the failure probability $Pr[F(t_i)]$ can be updated to the conditional probability

$$Pr[F(t_i)|Z(t_z)] = Pr[F_1^* \cup F_2^* \cup \cdots \cup F_i^*|Z(t_z)] \tag{5.21}$$

The data measurement at the time t_z implies that the structure must have survived

up to the time t_z. Therefore, the failure probability $Pr[F(t_i)]$ for $t_i > t_z$ should be updated accordingly as (Straub et al., 2020):

$$Pr\left[F(t_i)|Z(t_z) \cap \overline{F(t_z)}\right] = \frac{Pr\left[F(t_i) \cap \overline{F(t_z)}|Z(t_z)\right]}{Pr\left[\overline{F(t_z)}|Z(t_z)\right]} = \frac{Pr[F(t_i)|Z(t_z)] - Pr[F(t_z)|Z(t_z)]}{1 - Pr[F(t_z)|Z(t_z)]} \tag{5.22}$$

Both conditional probabilities $Pr[F(t_i)|Z(t_z)]$ and $Pr[F(t_z)|Z(t_z)]$ are calculated by Eq. (5.21) after changing the distribution parameters of the measured variables accordingly.

5.5. Numerical examples

5.5.1 Time-dependent reliability prediction considering traffic environment and corrosion of strands

In the first numerical example, the time-dependent reliability of the PSC box girder of the Hwang-Jobal bridge is evaluated by applying the proposed framework. To investigate the influences of the traffic load and corrosion on time-dependent reliability, three cases are investigated: (1) considering changes in traffic load only, (2) considering corrosion of the strand only, and (3) considering both. Besides, using the four categories of corrosive environment for the strand defined in Table 5.1, the 22 strands existing in each tendon are classified into A, B, C, and D categories. The time-dependent reliability over the 100-year service life is evaluated for three scenarios of corrosion environment defined in terms of the number of strands belonging to the four categories: (1) vulnerable to the corrosion (A: 0, B: 0, C: 11, D: 11), (2) moderate (A: 5, B: 5, C: 6, D: 6), and (3) robust (A: 11, B: 11, C: 0, D:

0). It is assumed that the cross-sectional areas of reinforcement bars decrease by 0.5% per year from the 20th year due to corrosion, and C_0 is set as 0.15% of the cement weight.

To calculate the probability of the interval failure F_j^*, this study discretizes the service life of the bridge (100 years) into 5-year-long intervals. For each interval, subset simulation is performed using the assumed conditions regarding corrosive environment and traffic, and the random variables summarized in Table 5.6. Next, $Pr[F(t_i)]$ is computed using the FORM approximation along with sampling to compute the correlation coefficients, as described in Section 4.2. However, if the interval failure probability is lower than about 10^{-12} (reliability index is greater than around 7), the CDF of the multivariate standard normal distribution in Eq. (5.18) cannot be precisely evaluated even if a state-of-the-art algorithm (Botev, 2017) is used. In this case, the upper and lower bounds on $Pr[F(t_i)]$ are evaluated by Eq. (5.16) instead and then converted to the corresponding reliability index. Since the bound widths of time-dependent reliability in the example are highly narrow, for a clear presentation, the lower bound of reliability index is shown as the result of time-dependent reliability analysis in Figures 5.8 and 5.9.

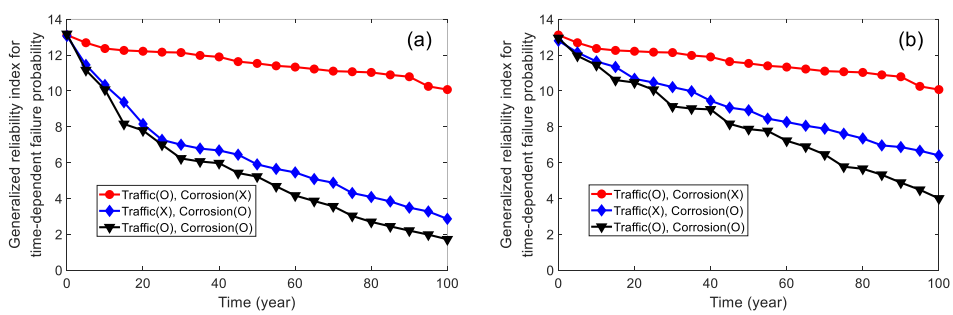

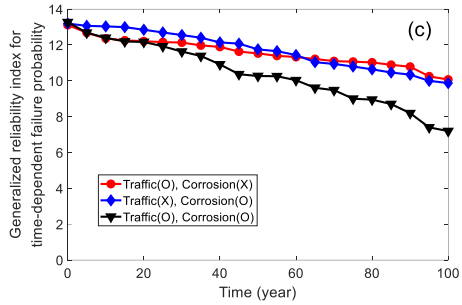

Figure 5.8 The result of time-dependent reliability evaluation of the PSC box girder (positive moment) for three conditions: (a) vulnerable to the corrosion, (b) moderate, and (c) robust

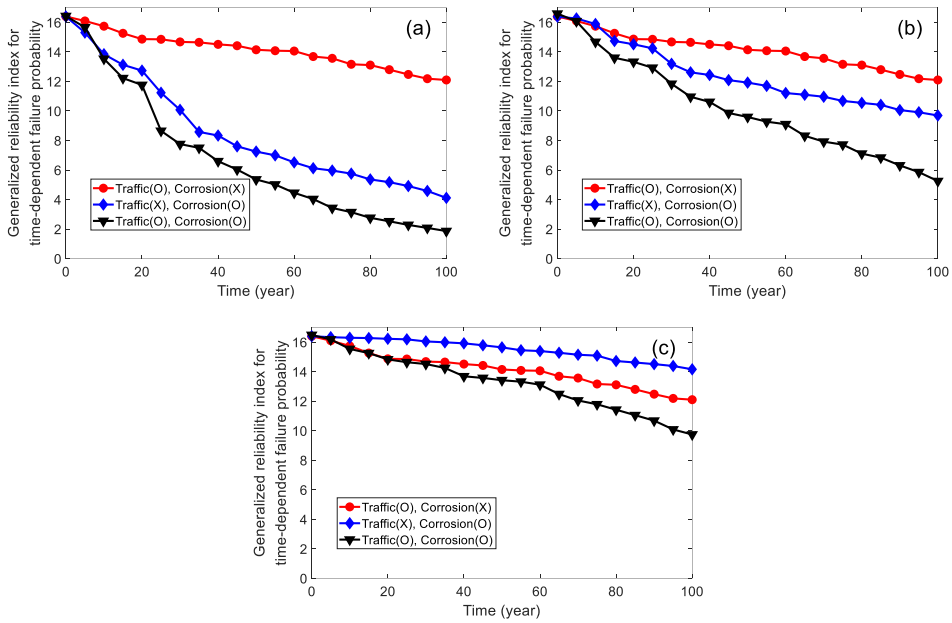

Figure 5.9 The result of time-dependent reliability evaluation of the PSC box girder (negative moment) for three conditions: (a) vulnerable to the corrosion, (b) moderate, and (c) robust

Before analyzing the results, it is noted that the evaluated reliability index is significantly higher than the general range of bridge reliability index around 3~4. This is because 1) the evaluated time-dependent reliability at a certain time point t_i

in this study is derived from the failure probability over the period $[0, t_i]$ not the whole service life t_s $[0, t_s]$. Therefore, the evaluated time-dependent reliability in the early time can be higher than the general bridge reliability index because of the short time duration. To clarify the meaning of the evaluated time-dependent reliability, it is expressed as "Generalized reliability index for time-dependent failure probability" in the dissertation; 2) this study uses the actual information of the bridge specified in the structural calculation document which might be the results of conservative bridge design. In practice, the factored strength is quite higher than factored loads for ULS1 in the structural calculation document of the example bridge; 3) As a result of accurate estimation of traffic load effects and flexural strengths, C.O.V of variables related to traffic loads and flexural strengths used in the examples are significantly smaller than that of traffic loads and strength used in bridge design codes; and 4) the example bridge is a cable-stayed bridge with PSC box girder, which has a higher level of redundancy than a general PSC box girder bridge. Furthermore, the reliability is evaluated for just ultimate limit state 1, in this study, so if the reliability is evaluated by considering other limit states, a lower reliability index can be derived.

The results show that, when the structure is vulnerable to corrosion, the effect of corrosion of the strand on reliability is much greater than that of traffic loads in both cross-sections of the positive and negative moment. For the second case in which the corrosive environment is moderate, corrosion of strands still has a greater effect than traffic loads in both cross-sections. However, in the third case (robust to the corrosion), the effects of corrosion and traffic loads on the reliability of the cross-

section of the positive moment become similar while traffic loads have a greater effect on the reliability than corrosion in the cross-section of the negative moment. This result implies that the effect of the traffic load on the reliability in the cross-section of the negative moment is greater than in the cross-section of the positive moment. The traffic load effects increase more over time in the cross-section of the negative moment than in the cross-section of the positive moment due to the difference in the shape of influence lines as explained in Section 5.3.2.

5.5.2 Updating effects of inspection data on time-dependent reliability prediction

To investigate updating effects of the measured data and information regarding the random strengths and loads on the time-dependent reliability, the predictions in Section 5.5.1 are updated by data and information that could be obtained through the current practice of structure safety inspection concerning the corrosion of the strands in the PSC box girder bridge. The structure safety inspection guidelines of KISTEC (2019) in South Korea cover various tests regarding concrete compressive strength, chloride content, and acoustic emission to check the existence of voids in the grout, carbonation depth test, and corrosion current density. As a general procedure of inspections regarding corrosion in PSC box girder bridges, an acoustic emission test can be performed first to check the presence of the void, which is the main cause of tendon corrosion. If the void is identified, the chloride content and carbonation depth test can be conducted as the next step. These tests can update the initiation time of corrosion, but cannot directly detect the occurrence of corrosion. Therefore, if there is a strong belief that corrosion has occurred, the inside of the tendon can be directly

examined through an endoscope (SMFMC, 2017), and the maximum pit depth, corrosion type, and corrosion current density can be measured additionally. However, it is noted that measuring the maximum pit depth and corrosion type of strands can be difficult especially for internal tendons.

Before updating the time-dependent reliability using inspection data over the service life (Section 5.5.3), updating the effects of measured data from each type of the aforementioned inspections on the reliability are investigated in advance. It is assumed that the data are measured in the 20th year. The time-dependent reliability after the 20th year is then updated using Eqs. (5.21) and (5.22) based on the measured data. As variables related to the corrosion initiation, the effects of the measured concrete cover thickness and chloride content on reliability are analyzed. In the meantime, as variables related to corrosion propagation, the effects of the maximum pit depth, corrosion current density, and corrosion type on reliability are also analyzed. As explained in Section 5.1, if the interval failure probability is extremely low, Eqs. (5.21) and (5.22) cannot be accurately evaluated. Therefore, the time-dependent reliability is conservatively updated in terms of the following upper bound:

$$\begin{aligned} Pr\left[F(t_i)|Z(t_z) \cap \overline{F(t_z)}\right] &= \frac{Pr[F(t_i)|Z(t_z)] - Pr[F(t_z)|Z(t_z)]}{1 - Pr[F(t_z)|Z(t_z)]} \\ &\leq \frac{\sum_{j=1}^{i} Pr(F_j^*|Z(t_z)) - \max\limits_{j\in[1,\dots z]} Pr\left(F_j^*|Z(t_z)\right)}{1 - \sum_{j=1}^{z} Pr(F_j^*|Z(t_z))} \end{aligned} \quad (5.23)$$

Figure 5.10 shows the time-dependent reliability updated based on the measured data of concrete cover thickness and chloride concentration at the surface. The results in Figure 5.10 confirm that the thinner the concrete cover thickness is and the higher the chloride concentration at the surface is, the earlier the corrosion

initiates. This, in turn, causes the updated reliability index to decrease after the 20th year. However, the reliability updated using the measured data of concrete cover thickness becomes similar to the original one in the long term (after the 70th year) whereas the chloride concentration at the surface has a large effect on the reliability in the long term. The reason why the updated reliability differs greatly at the 100th year (end of service life) depending on the chloride concentration at the surface is that the number of corroded strands is determined by the chloride content.

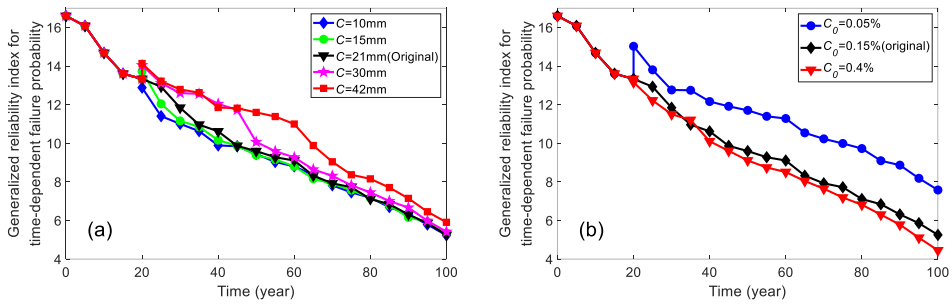

Figure 5.10 The time-dependent reliability updated based on the measured data of the variables associated with corrosion initiation: (a) concrete cover thickness, and (b) chloride concentration at the surface

On the other hand, Figure 5.11 shows the time-dependent reliability updated based on the measured data of maximum pit depth, corrosion current density, and corrosion type. Figure 5.11(a) shows that the change of reliability caused by the measurements of the maximum pit depth is quite large in the 20th year, i.e. the year when the data are measured. This is because the ultimate strain and strength of corroded strands are determined by the section loss area estimated using the maximum pit depth. However, regardless of the measurement of the maximum pit depth, 20 to 30 years after the inspection, the reliability of all three cases becomes

similar to the original reliability. This is because once corrosion initiates, it proceeds rapidly, which makes most corroded strands in categories C and D totally fail for all three cases. Figure 5.11(b) shows that when the measured data of corrosion current density have the value of lower bound for each category defined in Table 5.2, the updated reliability becomes larger than the original reliability owing to the slow propagation of corrosion. However, after a certain period passes, since most of the strands classified into vulnerable corrosive environments experience complete failures, the updated reliability becomes similar to the original reliability. As for the corrosion type, it is seen that the updated reliability of corrosion type 2 decreases the most because corrosion type 2 has the largest losses of section area when each corrosion type has the same maximum pit depth.

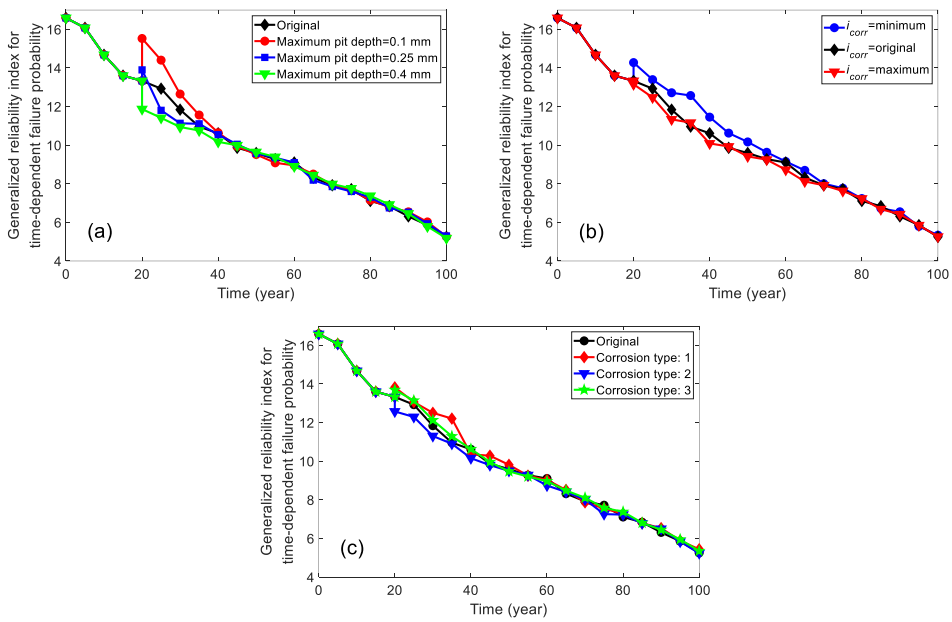

Figure 5.11 The time-dependent reliability updated based on the measured data of the variables associated with corrosion propagation: (a) maximum pit depth, (b) corrosion current density, and (c) corrosion type

5.5.3 Maintenance based on time-dependent reliability updating

This section shows how the time-dependent reliability for the two cross-sections are updated using measured data and traffic scenarios and can be used for the purpose of taking maintenance actions to assure the target level of reliability.

5.5.3.1 Updating the time-dependent reliability

The updating effects by measured data from the environment vulnerable to corrosion indicate that corrosion can propagate rapidly within 20 to 30 years and may lead to the complete failure of the corroded strand (Section 5.5.2). It was also reported in the literature that corrosion can propagate rapidly when the corrosive environment, e.g. the existence of voids, moisture penetration through air vents, low pH, high humidity, and high chloride content, is formed (Song and Saraswathy, 2007; Virmani and Ghasemi, 2012). Therefore, in the following updating example, it is assumed that the bridge is under a corrosive environment in which corrosion progresses rapidly for a short period (from the 30^{th} to the 60^{th} year). In addition, assumed measured data are introduced to describe the scenario of corrosion propagation and change of traffic environment. Every 6 years (30^{th}, 36^{th}, 42^{nd}, 48^{th}, and 54^{th} year), a total of 5 inspections and monitoring are performed and the time-dependent reliability is updated using the measurements. Furthermore, this study checks whether the updated reliability satisfies the target level of reliability in the KHBDC-CB.

The target reliability index in this code is 3.72 for the defined service life of 100 years. However, the period over which the time-dependent reliability is evaluated in

the examples depends on the time point of assessment, t_i, not 100 years. Therefore, it is necessary to obtain the equivalent target generalized reliability index for the period t_i corresponding to 3.72 (p_f=1×10^{-4}) for 100 years to check whether the updated reliability satisfies the target level of reliability. To this end, the mean annual failure probability $p_{f,a}$ corresponding to the reliability index of 3.72 for 100 years is first calculated by solving the following equation under the assumption that the failure events for one-year intervals have the same probability and are independent of each other:

$$1 - \left(1 - p_{f,a}\right)^{100} = 1 \times 10^{-4} \tag{5.24}$$

As a result, the annual failure probability $p_{f,a}$ corresponding to the reliability index of 3.72 for 100 years is 1×10^{-6} ($\beta = 4.75$). Then, the corresponding target generalized reliability index for time-dependent failure probability $\beta_{g,t}$ for the period $[0, t_i]$ is calculated by

$$\beta_{g,t} = -\Phi^{-1}(1 - \left(1 - p_{f,a}\right)^{t_i}) \tag{5.25}$$

The target generalized reliability index calculated by Eq. (5.25) is used in the examples to check whether the updated reliability satisfies the target level of reliability defined in the KHBDC-CB. It is noted that the target generalized reliability index calculated here is just an example to obtain the reliability corresponding to the target reliability index of design codes. It is necessary to determine the target reliability level in terms of bridge evaluations, not bridge designs, considering many factors such as inspection and maintenance periods, residual life, and risk attitude of bridge owners.

The following traffic scenario is considered in this example. Due to the urban development and industrialization of cities around the bridge from the 30th to 48th year, the ratio of heavy vehicles increases linearly from 10% to 35%. The frequency of congested traffic flow increases linearly from 120 hours/year to 260 hours/year while the average congested speed decreases from 30 km/h to 10 km/h. It is assumed that the changed parameters of the traffic environment are maintained until the 60th year. Next, For the cross-section of the negative moment, the measured data and information from the inspection conducted every six-year are created as follows. At the first inspection (30th year), the acoustic emission test confirms that there is no void in the grout, and the chloride content increases from 0.15% to 0.4%. At the second inspection (36th year), it is confirmed that there are voids in the grout, and the corrosive environment of the strands is classified by examining the inside of the tendon using an endoscope. The 22 strands belong to the four categories as A:2, B:2, C:7, and D:11. However, corrosion of strands has not been found yet. At the third monitoring (42nd year), as a result of examining the inside of the tendon using an endoscope, corrosion of strands is found and the corrosion has progressed rapidly, so the maximum pit depth of the categories C and D are measured as 0.12 mm and 0.25 mm respectively. In addition, the corrosion current densities for categories C and D are measured as maximum values 1 $\mu A/cm^2$ and 2 $\mu A/cm^2$ respectively. At the fourth monitoring (48th year), the maximum pit depth of category C increases to 0.2 mm, the maximum pit depth of category D increases to 0.4 mm, and most of the corroded wires are classified to have corrosion type 2. At the final monitoring (54th year), the measured corrosion current density decreases to the minimum values

0.5 $\mu A/cm^2$ and 1 $\mu A/cm^2$ for categories C and D, respectively.

The results of the updating by Eqs. (5.21) and (5.23) based on the measured data explained above are shown in Figure 5.12. The reliability index decreases in the 30th year because the chloride content increased. In the 36th year, although the corrosive environment deteriorates, the reliability index increases because the corrosion is not observed. In the next inspection (42nd year), the reliability index decreases drastically because corrosion proceeds rapidly. In the 48th year, the reliability decreases because of the observed corrosion type 2. In the final 54th year, the reliability slightly increases owing to the decreased measurement of corrosion current density. After the 50th year, it is confirmed that the updated time-dependent reliability becomes lower than the target generalized reliability index.

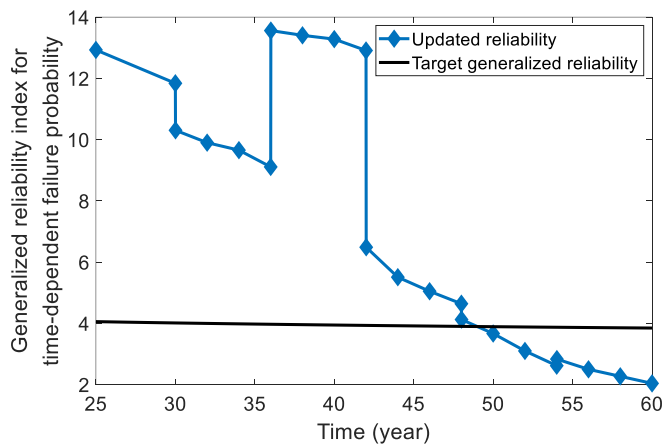

Figure 5.12 History of updating of time-dependent reliability for the cross-section of the negative moment using inspection data

In the example of updating reliability of cross-section of the positive moment, the same traffic and corrosion condition, and measured data are used as the negative

moment section explained above, except for the measured data in the 36th year. The measurement data in the 36th year are changed as follows to consider another scenario. In the second inspection (36th year), it is assumed that the acoustic emission test confirms the existence of voids in the grout, and the examination of the inside of the tendons by an endoscope classifies the corrosive environment of the strands. Among the two tendons, one tendon is under a dangerous corrosive environment (A: 0, B: 0, C: 4, D: 18), and the other tendon's corrosive environment is relatively safe (A: 4, B: 4, C: 10, D: 4). Corrosion of strands has not been found yet in either tendon. Figure 5.11 shows the result of updating the time-dependent reliability for the cross-section of the positive moment. The result is similar to the updated reliability of the cross-section of the negative moment in Figure 5.12 because similar measured data and the same initial corrosive and traffic environment are used. The updated reliability after the 50th year also becomes lower than the target generalized reliability index for the cross-section of the positive moment.

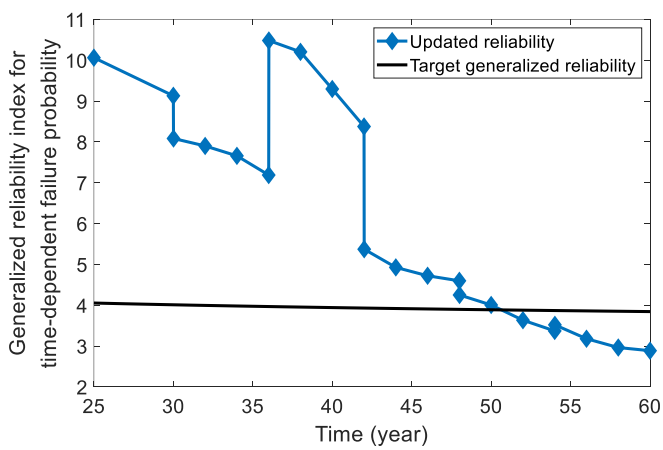

Figure 5.13 History of updating of time-dependent reliability for the cross-section of the positive moment using inspection data

5.5.3.2 Maintenance actions to secure target reliability

To assure the safety of the example bridge, this section establishes several maintenance strategies, and the reliability after implementing maintenance actions is re-evaluated. When repair and maintenance actions are taken on a structure to secure target reliability, the state of the structure after a repair and maintenance action can be considered statistically independent of the state before the repair action. Therefore, when calculating the reliability after the maintenance action, the reliability of the structure can be computed without consideration of the failure events before the maintenance action (Straub et al., 2020).

The first maintenance strategy this study considers for the cross-section of the negative moment is to refill the grout and eliminate voids in the ducts in the 48^{th} year to prevent further propagation of corrosion in the strands. The second strategy is to control the traffic environment by restricting the overweight vehicles (over 40 tons) and reduce the traffic volume of the bridge through the construction of additional roads in the surroundings, thereby returning the ratio of heavy vehicles, the frequency of congestion, and the congested speed to those under the initial condition (30^{th} year). The third strategy is to implement both the first and second strategies in the 48^{th} year to deal with corrosive and traffic environments simultaneously. Finally, the fourth strategy is to implement both strategies in the 42^{nd} year, earlier than the third strategy. Figure 5.14 shows the results of updating time-dependent reliability after implementing the maintenance strategies. Although both the first and second strategies make reliability decrease more slowly than the case of no maintenance decisions, i.e. the result in Figure 5.12, their reliabilities are still under the target

generalized reliability index. On the other hand, when the third strategy which can improve corrosive and traffic environment simultaneously is implemented, the generalized reliability index can be maintained at a higher level than 4. When the fourth strategy that implements the maintenance action earlier is adopted, the generalized reliability index can be maintained at a level higher than 6.

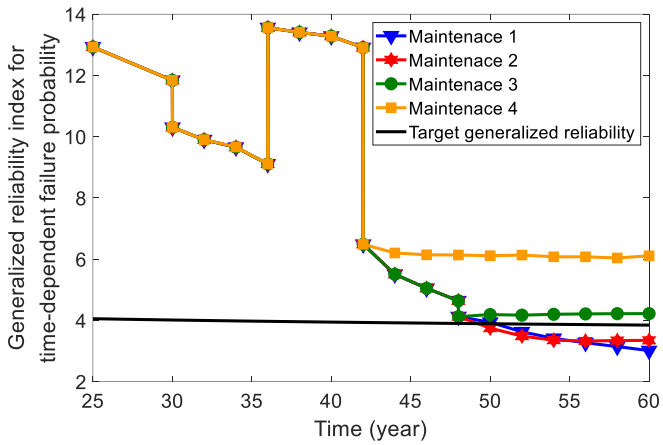

Figure 5.14 History of updating of time-dependent reliability for the cross-section of the negative moment after maintenance actions

Next, for the cross-section of the positive moment, other maintenance strategies are established. The first maintenance strategy is to replace the tendon whose corrosive environment is more vulnerable (A: 0, B: 0, C: 4, D: 18) with a new one. The second strategy for the cross-section of the positive moment is the same as the second strategy for the cross-section of the negative moment, i.e. to control the traffic environment by restricting the overweight vehicles (over 40 tons) and reducing the traffic volume of the bridge through the construction of roads surroundings, thereby returning the ratio of heavy vehicles, the frequency of congestion, and the congested

speed to those at the initial state (30th year). The third strategy is to implement both the first and second strategies in the 48th year to improve corrosive and traffic environments simultaneously. Figure 5.15 shows the results of updating time-dependent reliability after implementing the maintenance strategies. It is shown that after implementing both the first and second strategies the updated reliability exceeds the target generalized reliability index, unlike the example for the negative moment. In particular, the reliability significantly increases when the severely corroded tendon (first strategy) is replaced. Nevertheless, the reliability decreases continuously over time because corrosion of strands in another tendon keeps progressing. To handle this, the first and second strategies are executed together to improve the corrosive and traffic environment in the third strategy. As a result, the generalized reliability index can be maintained at a level higher than 7 during the service life by implementing the third strategy.

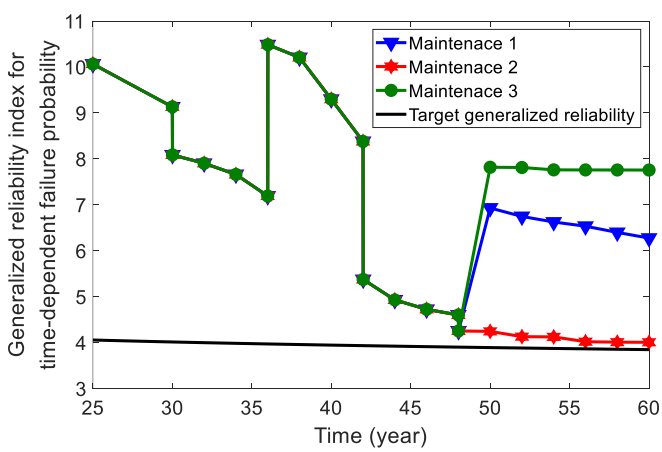

Figure 5.15 History of updating of time-dependent reliability for the cross-section of the positive moment after maintenance actions

The numerical examples demonstrate that the developed framework can successfully update the time-dependent reliability using the measured data and information regarding the corrosive environment and the traffic. The period in which the target level of reliability is not achieved can be predicted by the updated time-dependent reliability. Based on the results of this prediction, the decision-maker can establish an effective maintenance strategy and predict the outcomes. It should be also noted that, while most of the maintenance strategies in the related literature have focused on improving the condition of the structure, traffic environment control can be also an effective option to improve time-dependent reliability over the service life of the bridge.

5.6. Summary

This chapter developed a framework for time-dependent reliability evaluation and updating for PSC box girder bridges over their service life based on the information of the traffic environment of the bridge and strength degradation due to corrosion of prestressing strands. The corrosion of the strand was modeled while considering the uncertainty in a variety of random variables associated with the corrosion. It was proposed to describe the corrosive environment for the strands in terms of four categories based on the literature and the current structure inspection guideline of South Korea. In addition, an iterative algorithm introducing a recently proposed stress-strain model of corroded wire was proposed for the calculation of the flexural strength. The proposed framework was demonstrated and tested by an

actual cable-stayed bridge with PSC box girders, Hwayang-Jobal Bridge in South Korea. The traffic load effects of the cross-sections (positive and negative moments) were estimated based on the traffic information around the bridge and the assumed scenarios regarding the change of traffic environment. The flexural strength of the girder was calculated by the iterative method considering strength degradation due to corrosion. The ultimate limit state 1 was selected as the limit state of interest, and the statistical properties of a total of 22 random variables were determined based on a literature study. To efficiently evaluate the time-dependent reliability, this study used the subset simulation method and FORM-based approximation on the series system reliability.

In the numerical examples, the time-dependent reliability for 100 years (service life of the bridge) was predicted to investigate the effect of corrosion and traffic load. It was confirmed that not only the corrosion which is associated with strengths but also the traffic load is an important factor for time-dependent reliability. In addition, the time-dependent reliability was updated using the data and information obtained from structural inspection and monitoring to identify a future time period that would not satisfy the target level of reliability. As possible maintenance actions of PSC box girder bridges, this study considered filling voids with grout, tendon replacement, and traffic environment control. It was confirmed that the accurate evaluation of the time-dependent reliability during the service life can facilitate establishing an effective risk-informed maintenance strategy. Furthermore, it was noteworthy that not only the repair of the structure but also the traffic environment control to reduce the traffic load effects could be effective as maintenance strategies.

Chapter 6. Conclusions

6.1. Summary and contributions of this dissertation

The dissertation proposed a data-based framework for bridge reliability evaluation and updating considering traffic environment and strength degradation. A comprehensive WIM data-based probabilistic model and a Bayesian updating methodology for bridge traffic loads were developed to estimate the precise traffic load effects over the service life. Furthermore, a new design live load model for long-span bridges which can cover diverse traffic environments was proposed. Finally, the time-dependent reliability of the PSC box girder bridge over its service life was evaluated and updated based on the developed traffic load estimation technique and sophisticated modeling of the corrosion process for strands. It was confirmed that accurate estimation of traffic load effects is essential in the design and condition evaluation of bridges. It is expected that the developed framework will help us to manage the safety and serviceability of the bridge through continuous evaluating and updating of the reliability of the bridge based on data measured during service life. The major findings and contributions of this dissertation are illustrated in Figure 6.1 and summarized as follows:

- While developing and verifying the developed probabilistic model for bridge traffic load using WIM data in Chapter 2, key variables and traffic characteristics, e.g. the difference in headway depending on vehicle types

and lane location, frequency of traffic congestion, which existing studies failed to notice were identified and incorporated into the model.

- The analyses of WIM data revealed that headway depends on traffic volume, driving habits, lane location, and types of front and rear vehicles. These characteristics were elaborately modeled based on the theory of transportation engineering and statistical studies. This study also demonstrated that the headway model is critical for the accurate estimation of traffic loads, especially for short-span bridges.
- Hourly and daily variations of heavy vehicle ratio were observed and considered in the developed model. Correlations among the vehicle characteristic variables (axle weight and distance) were considered through the Nataf model to accurately describe the vehicle characteristic variables.
- Greenshield's model which represents the relationship between traffic volume and speed was observed in the WIM data. Therefore, probabilistic models for traffic volume, speed, and headway were established, separately depending on the congested and free traffic flow. By using five-minute traffic volume rather than one-hour volume, traffic congestion can be modeled with increased accuracy. In addition, the extrapolation using the block maximum method requires accurate daily maximum traffic load samples. To address this, the occurrence frequency of traffic congestion was introduced as an important variable.
- Unlike existing studies that verified the developed model by using hourly or daily maximum traffic load for a short period (one day or one week) and

single-lane bridges, this dissertation computed daily maximum traffic load samples over a longer period (one year) in multi-lane cases and compared them to traffic load values from actual WIM data for more rigorous verification. It was also demonstrated that the developed WIM data-based bridge traffic load model is applicable regardless of span length.

- The numerical examples in Chapter 2 confirmed that the current bridge design codes were conservative due to the multiple presence factor. Furthermore, the parameterized probabilistic models for all variables related to traffic loads enable us to customize the parameters of models to reflect the new information of the traffic environment.
- The proposed updating methodology in Chapter 3 can update the model parameters of the corresponding variable using information that is obtained through traffic investigation and WIM data. Therefore, the methodology can quantify changes in traffic load effects and provides more intuitions.
- The updating examples in Chapter 3 showed that the Bayesian inference-based updating methodology can consider degrees of belief of the prior model and new observations through the hyper-parameter setting. In addition, when there is insufficient data and information to estimate the traffic load effect of a specific bridge, using the existing developed traffic load model based on enough WIM data as a prior model in Bayesian updating can facilitate more accurate estimations of the traffic load effects of a specific bridge.

- While current design live load models can represent only one conservative traffic environment, the design live load model proposed in Chapter 4 can consider various traffic environments because the model was developed based on the traffic data measured in a variety of regions.
- To investigate the characteristics of traffic congestion, the VDF function was used to indirectly estimate the speed using traffic volume. The results confirmed that traffic congestion rarely occurs on long-span bridges in South Korea.
- This study noted that each lane has a different ratio of vehicle types depending on the location of the lanes, which implies that the live load should be estimated differently depending on the location of the lane. To this end, three characteristic lanes (car, middle, and truck lane) were defined. For each characteristic lane, the lane load and multiple presence factors were proposed to consider the disparity of live load among multi-lanes.
- The statistical characteristics (distribution type, bias factor, and coefficient of variation) of live loads and live load effects for KHBDC calibration were investigated.
- To describe corrosion of strands in PSC box girder bridges, variables related to corrosion were investigated with extensive literature reviews and described by probability distributions to consider uncertainty. By referring to the current practice of structure safety inspection, a practical classification of corrosive environment was proposed in Chapter 5.

- An iterative method was proposed for efficient and simple calculation of the flexural strength considering strength degradation due to corrosion. The recently proposed material model of corroded strands was also introduced to consider their actual behavior.
- The numerical examples in Chapter 5 confirmed that traffic load is an important factor in evaluating bridge reliability as well as the strength degradation of members. Time-dependent reliability was evaluated and updated using the data available from the tests in the current practice of structure safety inspection. This allows us to establish maintenance strategies to maintain the target reliability of bridges.

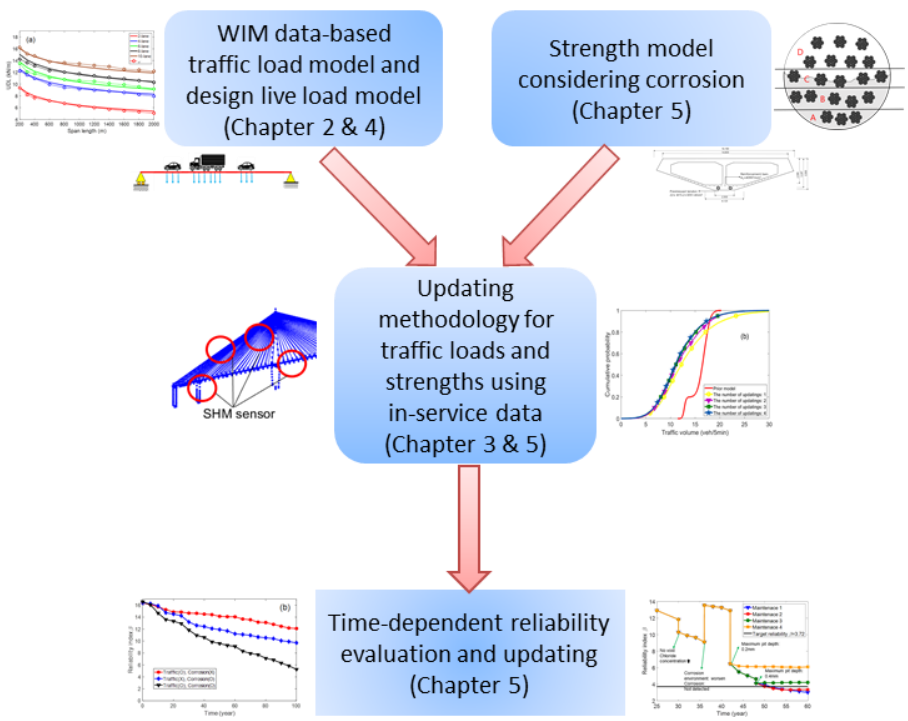

Figure 6.1 Diagram for the main contributions of the dissertation

6.2. Recommendations for further study

To advance and expand the data-based evaluation and updating of bridge reliability which considers traffic environment and strength degradation, the following topics are recommended for future studies:

- When using the data from current WIM systems, there are limitations in that it is difficult to accurately capture the driving pattern of vehicles after passing through the installation point because the WIM system is installed on a certain fixed point on the road or bridge. Therefore, a study is needed to capture the driving patterns of vehicles on bridges using cameras and computer vision technology. Next, based on this, the developed traffic load model can be improved, e.g. optimization of the parameters of the microsimulation models.
- The developed probabilistic model for bridge traffic load can be more rigorously demonstrated and calibrated using the measured structural response such as the measured tension of a cable from tension sensors.
- It requires the large computational cost to estimate the traffic load effects using the currently developed traffic load model in the dissertation. To address this, it is required that the effects of important variables such as traffic volume and heavy vehicle ratio should be evaluated in advance through parametric studies to provide engineers with the traffic load values. This will facilitate convenient estimations of the traffic load effects that

consider the traffic environment of the bridge in designing or evaluating the condition of bridges.

- The developed models and updating methodology for traffic loads in Chapters 2,3, and 4 can accurately estimate traffic load effects of bridges in operation, particularly by employing traffic data and information collected over the service life of bridges. Therefore, it is expected that the developed models and updating methodology for traffic loads will be utilized as a basic tool for the estimation of bridge traffic loads in the current load-carrying capacity evaluation or reliability-based bridge condition assessment.
- As mentioned in Section 4.5.2, it is necessary to study the live loading method depending on the shape of the influence line. In particular, for long-span bridges, where traffic congestion is dominant, the position pattern of vehicles varies depending on the average speed during congestion. For example, in the case of severe congestion (full stop condition), vehicles are tightly spaced in most parts of the bridge, while in the case of average speeds of around 30 to 40 km/h, the part where vehicles almost stop and the other parts where vehicles drive with large headway co-exist due to stop-and-go waves phenomenon. If the influence line has wide beneficial parts that can relieve maximum traffic load effects, the “full stop” condition cannot guarantee the production of the maximum live load values because loading a lot of vehicles on the beneficial parts may excessively reduce the traffic load effect. Rather, in such cases, the stop-and-go waves condition may produce maximum traffic load effects. Therefore, it is necessary to figure

out traffic patterns that can produce maximum traffic load effects for each shape of the influence line.

- To take into account the diverse traffic environments of bridges in the design live load model, a lot of traffic information and data were investigated in the dissertation. However, despite these efforts, to adopt the design live load model proposed in Chapter 4 in the bridge design code in South Korea, broader investigations of the traffic environment of bridges and long-term WIM data measured nationwide are recommended. In particular, it is necessary to thoroughly investigate the occurrence frequency of congestion and the location of heavy vehicles when traffic congestion occurs on multi-lane bridges.
- The reliability evaluation framework and application examples in this dissertation focus on the ultimate limit state. However, the advantage of the developed traffic load model in Chapter 2 is that the traffic load effect can be computed continuously during the desired time duration. Therefore, it is expected that the traffic load effect available for fatigue limit state and serviceability limit state can be obtained from the developed model. Eventually, the developed reliability evaluation framework can be extended to fatigue limit states and serviceability limit states for the design and condition evaluation of bridges.
- The method to consider strength degradation from corrosion of strands has been studied intensively in the dissertation. However, it is necessary to study other strength degradation phenomena to apply the developed framework to

diverse bridge types.

- The framework for time-dependent reliability evaluation and updating developed in Chapter 5 can predict the time span that cannot satisfy the desired performance of bridges and the reliability after taking maintenance actions on bridges. Therefore, based on the framework, the data-informatics-based or machine-learning-based optimization can be performed to identify the best maintenance strategies over the service life of a deteriorating structure under changing environments as a further study.

References

AASHTO (2012). AASHTO LRFD Bridge Design Specifications. Washington, D.C, American Association of State Highway and Transportation Officials.

Adolf, D.M. (1990). Fundamentals of Traffic Flow. Prentice - Hall, New Jersey, Inc. Englewood Cliff.

Aghabayk, K., Sarvi, M., and Young, W. (2012), Understanding the dynamics of heavy vehicle interactions in car-following. *Journal of Transportation Engineering*, 138(12), 1468-1475.

Ahmad, S. (2003). Reinforcement corrosion in concrete structures, its monitoring and service life prediction−−a review. *Cement and concrete composites*, *25*(4-5), 459-471.

Andrieu-Renaud, C., Sudret, B., and Lemaire, M. (2004). The PHI2 method: a way to compute time-variant reliability. *Reliability Engineering and System Safety*, 84(1), 75-86.

Ang H-S, Alfredo. and H. Wilson Tang. (1975). Probability Concepts in Engineering Planning and Design. Vol. I: Basic Principles. Wiley, New York.

Au, S. K., and Beck, J. L. (2001). Estimation of small failure probabilities in high dimensions by subset simulation. *Probabilistic engineering mechanics*, 16(4), 263-277.

Bernardo, J. M. and Smith, A. F. (2009). Bayesian theory (Vol. 405). John Wiley and Sons.

Bilmes, J. A. (1998). A gentle tutorial of the EM algorithm and its application to parameter estimation for Gaussian mixture and latent Markov models. International Computer Science Institute.

Bishop, C. M. (2006). Pattern recognition and machine learning. Cambridge: springer.

Boole, G. (1854). *Laws of thought*, American Reprint of 1854 ed., Dover, New York.

Botev, Z. I. (2017). The normal law under linear restrictions: simulation and estimation via minimax tilting. *Journal of the Royal Statistical Society Series B*, 79(1), 125-148.

BSI (2006). Steel, Concrete and Composite Bridges─Part 2. Specification for loads (BS 5400, Part 2). British Standards Institution, London.

Buckland, P. G. (1981). Recommended design loads for bridges. *Journal of the Structural Division*, 107(7), 1161-1213.

Caprani, C. C., O′ Brien, E. J., and McLachlan, G. J. (2008). Characteristic traffic load effects from a mixture of loading events on short to medium span bridges. *Structural safety*, 30(5), 394-404.

Caprani, C. C., O′ Brien, E. J., and Lipari, A. (2016). Long-span bridge traffic loading based on multi-lane traffic micro-simulation. *Engineering Structures*, 115, 207-219.

Carey, C., Caprani, C. C., and Enright, B. (2018). A pseudo-microsimulation approach for modelling congested traffic loading on long-span bridges. *Structure and Infrastructure Engineering*, 14(2), 163-176.

Celeux, G., and Soromenho, G. (1996). An entropy criterion for assessing the number of clusters in a mixture model. *Journal of classification*, 13(2), 195-212.

ECS (2003). EN 1991-2: 2003 Eurocode 1: actions on structures. Part 2: traffic loads on bridges. Brussels: European Committee for Standardization.

Cowan, R.J. (1975). Useful headway models. *Transportation research*, 9(6), 371-375.

Crespo-Minguillón, C., and Casas, J. R. (1997). A comprehensive traffic load model for bridge safety checking. *Structural Safety*, 9(4), 339-359.

CSA International (2005). CAN/CSA-S6-00 Canadian Highway Bridge Design Code, CSA International, Toronto, Canada.

Darmawan, M. S., and Stewart, M. G. (2007). Spatial time-dependent reliability analysis of corroding pretensioned prestressed concrete bridge girders. *Structural Safety*, 29(1), 16-31.

Der Kiureghian, A. (2005). First- and Second-Order Reliability Methods. In Nikolaidis, E., Ghiocel, D. M., and Singhal (Eds.), *Engineering design reliability handbook.* CRC press.

Ellingwood, B., Galambos, T.V., MacGregor, J. G., and Cornell. C. A. (1980). Development of a probability-based load criterion for American National Standard A58: Building code requirements for minimum design loads in buildings and other structures (Vol. 13). US Department of Commerce, National Bureau of Standards.

El Maaddawy, T., and Soudki, K. (2007). A model for prediction of time from corrosion initiation to corrosion cracking. *Cement and concrete composites*, 29(3), 168-175.

Enright, M. P., and Frangopol, D. M. (1998). Probabilistic analysis of resistance degradation of reinforced concrete bridge beams under corrosion. *Engineering structures*, *20*(11), 960-971.

Enright, B., Carey, C., and Caprani, C. C. (2013). Microsimulation evaluation of Eurocode load model for American long-span bridges. *Journal of Bridge Engineering*, 18(12), 1252-1260.

Enright, B., and O′ Brien, E. J. (2013). Monte Carlo simulation of extreme traffic loading on short and medium span bridges. *Structure and Infrastructure Engineering*, 9(12), 1267-1282.

Franzén, J. (2008). Bayesian cluster analysis. Ph.D. dissertation, Stockholm University, Stockholm, Sweden

FIB. (2006). Durability of post-tensioning tendons. Lausanne, Switzerland: International Federation for Structural Concrete.

Fu, G., Liu, L., and Bowman, M. D. (2013). Multiple presence factor for truck load on highway bridges. *Journal of Bridge Engineering*, 18(3), 240-249.

Fwa, T. F. and Li, S. (1995). Estimation of lane distribution of truck traffic for pavement design. *Journal of transportation engineering*, 121(3), 241-248.

Gauvain, J. L., and Lee, C. H. (1994). Maximum a posteriori estimation for multivariate Gaussian mixture observations of Markov chains. *IEEE transactions on speech and audio processing*, 2(2), 291-298.

Gelfand, A. E. (2000). Gibbs sampling. *Journal of the American statistical Association*, 95(452), 1300-1304.

Gelman, A., Carlin, J. B., Stern, H. S., Dunson, D. B., Vehtari, A., and Rubin, D. B. (2013). Bayesian data analysis. Chapman and Hall/CRC

Glass, G. K., and Buenfeld, N. R. (1997). The presentation of the chloride threshold level for corrosion of steel in concrete. *Corrosion science*, 39(5), 1001-1013.

Gnedenko, B. V. (2018). Theory of probability (6th ed.). London: Routledge.

Gong, C., & Frangopol, D. M. (2019). An efficient time-dependent reliability method. *Structural Safety*, 81, 101864.

Gumbel, E. J. (1958). Statistics of Extremes. Columbia Univ. Press, New York.

Guo, D. and Caprani, C. C. (2019). Traffic load patterning on long span bridges: A rational approach. *Structural Safety*, 77, 18-29.

Guo, T., Chen, Z., Liu, T., and Han, D. (2016). Time-dependent reliability of strengthened PSC box-girder bridge using phased and incremental static analyses. *Engineering structures*, 117, 358-371.

Guo, T., Frangopol, D. M., Han, D., & Chen, Y. (2011). Probabilistic assessment of deteriorating prestressed concrete box-girder bridges under increased vehicle loads and aggressive environment. *Journal of Performance of Constructed Facilities*, 25(6), 564-576.

Hohenbichler, M., and Rackwitz, R. (1982). First-order concepts in system reliability. *Structural safety*, 1(3), 177-188.

Hwang, E. S., Lee, K. T., and Kim, D. Y. (2012). Modelling of truck traffic for long span bridges. *Proc. 18th Congress of IABSE*, IABSE, Seoul, South Korea, 1112-1119.

Hwang, E. S., Nguyen, T. H., and Kim, D. Y. (2013). Live load factors for reliability-based bridge evaluation. *KSCE Journal of Civil Engineering*, 17(3), 499-508.

Hwang, E. S. (2008). Development of live load model for reliability-based bridge design code, Korea Bridge Design & Engineering Research Center, Seoul ,South Korea, (in Korean).

Hwang, E. S. and Kim, D. Y. (2015). Korean highway bridge design code: Vehicular live load model, Korea Bridge Design & Engineering Research Center, Seoul ,South Korea, (in Korean).

Jeon, C. H., Lee, J. B., Lon, S., and Shim, C. S. (2019). Equivalent material model of corroded prestressing steel strand. *Journal of Materials Research and Technology*, *8*(2), 2450-2460.

Kesting, A., Treiber, M., and Helbing, D. (2007). General lane-changing model MOBIL for car-following models. *Transportation Research Record*, 86-94.

Kim, C. H. (2015). Identification of statistical model of vehicular live load in long span bridges using WIM data. MS. thesis, Seoul National University, Seoul, South Korea.

Kim, J. H. (2018). Wind Load Factor Based on Wind Load Statistics for Reliability-Based Bridge Design Codes. Ph.D. dissertation, Seoul National University, Seoul, South Korea.

Kim, J., and Song, J. (2018), Development and validation of a full probabilistic model for traffic load of bridges based on Weigh-In-Motion (WIM) data. *Proc of 6th International Symposium on Life-Cycle Civil Engineering, IALCCE*, Ghent, Belgium, 657-664.

Kim, J., and Song, J. (2019). A comprehensive probabilistic model of traffic loads based on weigh-in-motion data for applications to bridge structures. *KSCE Journal of Civil Engineering*, 23(8), 3628-3643.

Kim, J., and Song. J. (2021). Bayesian updating methodology for probabilistic model of bridge traffic loads using in-service data of traffic environment. *Structure and Infrastructure Engineering*, DOI: 10.1080/15732479.2021.1924797.

Kim, S. H., Choi, J. G., Ham, S. M., and Heo, W. H. (2016). Reliability evaluation of a PSC highway bridge based on resistance capacity degradation due to a corrosive environment. *Applied Sciences*, *6*(12), 423.

Kim, S. S. (2018). Unified code calibration for short- to medium-span and long-span bridges with new vehicular live load model. MS. thesis, Seoul National University, Seoul, South Korea

KISTEC (2019). Safety inspection and safety diagnosis detailed guideline, Jinju, Korea infrastructure safety corporation, South Korea.

KOTI (2018). The Korea transport institute database, Sejong, The Korea transport institute, South Korea.

Kwon, O. S., Kim, E. and Orton, S. (2011). Calibration of live-load factor in LRFD bridge design specifications based on state-specific traffic environments. *Journal of Bridge Engineering*, 16(6), 812−819.

Leahy, C., O'Brien, E. J., Enright, B., and Power, R. T. (2015). Estimating characteristic bridge traffic load effects using Bayesian statistics. *Proceedings of the 12th International Conference on Applications of Statistics and Probability in Civil Engineering (ICASP12)*.

Lee, H. S. (2019). Reliability-based load-resistance factors, Kimoondang, (in Korean).

Lee, J., Lee, Y. J., and Shim, C. S. (2020). Probabilistic prediction of mechanical characteristics of corroded strands. *Engineering Structures*, 203, 109882.

Lee, S. K., and Zielske, J. (2014). An FHWA special study: post-tensioning tendon grout chloride thresholds (No. FHWA-HRT-14-039).

Lee, S. H. (2014). Calibration of the Load-Resistance Factors for the Reliability -based Design of Cable-supported Bridges. Ph.D. dissertation, Seoul National University, Seoul, South Korea.

Lipari, A. (2013). Micro-simulation modelling of traffic loading on long-span bridges. Ph.D. dissertation, University college Dublin, Dublin, Ireland.

Liu, P. L., and Der Kiureghian, A. (1986). Multivariate distribution models with prescribed marginals and covariances. *Probabilistic Engineering Mechanics*, 11(2), 105-112.

Li, F., Yuan, Y., & Li, C. Q. (2011). Corrosion propagation of prestressing steel strands in concrete subject to chloride attack. *Construction and Building Materials*, 25(10), 3878-3885.

Li, Q., Wang, C., and Ellingwood, B. R. (2015). Time-dependent reliability of aging structures in the presence of non-stationary loads and degradation. *Structural Safety*, 52, 132-141.

Lu, N., Beer, M., Noori, M., and Liu, Y. (2017a). Lifetime Deflections of Long-Span Bridges under Dynamic and Growing Traffic Loads. *Journal of Bridge Engineering*, 22(11).

Lu, N., Noori, M., and Liu, Y. (2017b). First-passage probability of the deflection of a cable-stayed bridge under long-term site-specific traffic loading. *Advances in mechanical engineering*, 9(1).

Lu, Q., Zhang, Y., and Harvey, J. T. (2009). Estimation of truck traffic inputs for mechanistic−empirical pavement design in California. *Transportation research record*, 2095(1), 62-72.

Lutomirska, M. (2009). Live load model for long-span bridges. Ph.D. dissertation, University of Nebraska−Lincoln, Nebraska, the United States.

Ma, Y., Wang, L., Zhang, J., Xiang, Y., Peng, T., and Liu, Y. (2015). Hybrid uncertainty quantification for probabilistic corrosion damage prediction for aging RC bridges. *Journal of Materials in Civil Engineering*, *27*(4), 04014152.

MCT (2015). General code for design of highway bridges and culverts. JTG D60-2015, Beijing (In Chinese: China Communications Press) Ministry of Communications and Transportation, China.

Melchers, R. E. (1999). "Structural Reliability Analysis and Prediction", John Wiley and Sons. New York, NY.

MOLIT (2012). The road design manual, Sejong, Ministry of Land, Infrastructure, and Transport, South Korea.

MOLIT (2016a). Korea highway bridge design code (LRFD), Sejong, Ministry of Land, Infrastructure, and Transport, South Korea.

MOLIT (2016b). Korea highway bridge design code (LRFD): Cable-supported Bridges, Sejong, Ministry of Land, Infrastructure, and Transport, South Korea.

MOLIT (2020a). Annual Traffic Volume Report, Sejong, Ministry of Land, Infrastructure, and Transport, South Korea.

MOLIT (2020b). Yearbook of Road Bridge and Tunnel statistics, Sejong, Ministry of Land, Infrastructure, and Transport, South Korea.

Nakamura, S., and Suzumura, K. (2013). Experimental study on fatigue strength of corroded bridge wires. *Journal of Bridge Engineering*, 18(3), 200-209.

Nguyen, V. S., Jeong, M. C., Han, T. S., and Kong, J. S. (2013). Reliability-based optimisation design of post-tensioned concrete box girder bridges considering pitting corrosion attack. *Structure and Infrastructure Engineering*, *9*(1), 78-96.

Nowak, A.S. (1993) Live load model for highway bridge, *Structural Safety*, 13, 53-66.

Nowak, A.S. (1995). Calibration of LRFD bridge code. *Journal of Structural Engineering*, 121(8), 1245-1251.

Nowak, A. S. (1999). Calibration of LRFD bridge design code. NCHRP Report 368. Transportation Research Board, National Research Council, Washington, DC.

Nowak, A. S., Lutomirska, M., and Sheikh Ibrahim, F. I. (2010). The development of live load for long span bridges. *Bridge Structures*, 6, 73-79.

Nowak, A. S., and Szerszen, M. M. (2003). Calibration of design code for buildings (ACI 318): Part 1-Statistical models for resistance. *ACI Structural Journal*, 100(3), 377-382.

O′Brien, E. J., Bordallo-Ruiz, A., and Enright, B. (2014). Lifetime maximum load effects on short-span bridges subject to growing traffic volumes. *Structural Safety*, 50, 113-122.

O′Brien, E. J., and Enright, B. (2011). Modeling same-direction two-lane traffic for bridge loading. *Structural safety*, 33(4), 296-304.

O′Brien, E. J., Lipari, A., and Caprani, C. C. (2015). Micro-simulation of single-lane traffic to identify critical loading conditions for long-span bridges. *Engineering Structures*, 94, 137-148.

O′Brien, E. J., Schmidt, F., Hajializadeh, D., Zhou, X. Y., Enright, B., Caprani, C. C., Wilson, S., and Sheils, E. (2015). A review of probabilistic methods of assessment of load effects in bridges. *Structural safety*, 53, 44-56.

O'Connor, A., and O′Brien, E. J. (2005). Traffic load modelling and factors influencing the accuracy of predicted extremes. *Canadian journal of civil engineering*, 32(1), 270-278.

O'Hagan, A., and Forster, J. J. (2004). Kendall's advanced theory of statistics, volume 2B: Bayesian inference. Arnold.

Papaioannou, I., Betz, W., Zwirglmaier, K., & Straub, D. (2015). MCMC algorithms for subset simulation. *Probabilistic Engineering Mechanics*, 41, 89-103.

Pillai, R. G., Trejo, D., Gardoni, P., D. Hueste, M. B., & Reinschmidt, K. (2014). Time-variant flexural reliability of posttensioned, segmental concrete bridges exposed to corrosive environments. *Journal of Structural Engineering*, 140(8), A4014018.

Raiffa, H. and Schlaifer, R. (1961). Applied statistical decision theory.

Ruan, X., Zhou, J., Shi, X., and Caprani, C. C. (2017). A site-specific traffic load model for long-span multi-pylon cable-stayed bridges. *Structure and Infrastructure Engineering*, 13(4), 494-504.

Sajedi, S., Huang, Q., Gandomi, A. H., and Kiani, B. (2017). Reliability-based multiobjective design optimization of reinforced concrete bridges considering corrosion effect. *ASCE-ASME Journal of Risk and Uncertainty in Engineering Systems, Part A: Civil Engineering*, 3(3), 04016015.

Schneider, R., Thöns, S., and Straub, D. (2017). Reliability analysis and updating of deteriorating systems with subset simulation. *Structural Safety*, *64*, 20-36.

Sivakumar, B., Ghosn, M., and Moses, F. (2011). Protocols for collecting and using traffic data in bridge design (NCHRP Report No. 683). Transportation Research Board, Washington D.C.

SMFMC (Seoul Metropolitan Facilities Management Corporation). (2017). Synthesis report: Academic service contract related with maintenance of PSC box girder bridges in Seoul jurisdiction. [In Korean.] Seoul: SMFMC.

Song, H. W., and Saraswathy, V. (2007). Corrosion monitoring of reinforced concrete structures-A. *Int. J. Electrochem. Sci*, *2*, 1-28.

Song, J., and Der Kiureghian, A. (2003). Bounds on system reliability by linear programming. *Journal of Engineering Mechanics*, 129(6), 627-636.

Song, J., W.-H. Kang, Y.-J. Lee, and J. Chun (2021). Structural system reliability: a state-of-the-art review on theories and applications. *ASCE-ASME Journal of Risk and Uncertainty in Engineering Systems, Part A: Civil Engineering*, 7(2), 03121001.

Srinivas, S., Menon, D., and Meher Prasad, A. (2006). Multivariate simulation and multimodal dependence modeling of vehicle axle weights with copulas. *Journal of transportation engineering*, 132(12), 945-955.

Stewart, M. G. (2010). Reliability safety assessment of corroding reinforced concrete structures based on visual inspection information. *ACI Structural Journal*, *107*(6), 671.

Straub, D., Schneider, R., Bismut, E., and Kim, H. J. (2020). Reliability analysis of deteriorating structural systems. *Structural safety*, 82, 101877.

Tabatabai, H., Titi, H., and Zhao, J. (2017). WIM-based assessment of load effects on bridges due to various classes of heavy trucks. *Engineering Structures*, 140, 189-198.

Thoft-Christensen, P. (1998). Assessment of the reliability profiles for concrete bridges. *Engineering structures*, *20*(11), 1004-1009.

Treiber, M., Hennecke, A., and Helbing, D. (2000). Congested traffic states in empirical observations and microscopic simulations. *Physical review E*, 62(2).

Tu, B., Dong, Y., and Fang, Z. (2019). Time-dependent reliability and redundancy of corroded prestressed concrete bridges at material, component, and system levels. *Journal of Bridge Engineering*, 24(9), 04019085.

Val, D. V., and Melchers, R. E. (1997). Reliability of deteriorating RC slab bridges. *Journal of structural engineering*, *123*(12), 1638-1644.

Van der Spuy, P., Lenner, R., de Wet, T., and Caprani, C. (2019). Multiple lane reduction factors based on multiple lane weigh in motion data. *Structures*, 20, 543-549.

Virmani, P. Y., and Ghasemi, H. (2012). Literature review of chloride threshold values for grouted post-tensioned tendons. US Federal Highway Administration, FHWA-HRT-12-067.

Vrouwenvelder, A. C. W. M., and Waarts, P. H. (1993). Traffic loads on bridges. *Structural Engineering International*, 3(3), 169-177.

Wang, C., Zhang, H., and Li, Q. (2017). Time-dependent reliability assessment of aging series systems subjected to non-stationary loads. *Structure and Infrastructure Engineering*, *13*(12), 1513-1522.

Wang, F. Y., and Xu, Y. L. (2019). Traffic load simulation for long-span suspension bridges. *Journal of Bridge Engineering*, 24(5).

Wang, Z., & Wang, P. (2012). A nested extreme response surface approach for time-dependent reliability-based design optimization. *Journal of Mechanical Design*, 134(12).

Witczack, M. W., and El-Basyouny, M. M. (2004). Guide for mechanistic-empirical design of new and rehabilitated pavement structures Appendix GG-1: Calibration of permanent deformation models for flexible pavements (NCHRP Project 1-37A). Transportation Research Board.

Yang, D. Y., Teng, J. G., & Frangopol, D. M. (2017). Cross-entropy-based adaptive importance sampling for time-dependent reliability analysis of deteriorating structures. *Structural Safety*, 66, 38-50.

Yoo, C. H., Chul Park, Y., and Kim, H. K. (2018). Modeling corrosion progress of steel wires in external tendons. *Journal of Bridge Engineering*, 23(12), 04018098.

Youn, S. G. (2013). Experimental evaluation for ultimate flexural behaviors of PSC beams with a corroded tendon. *Journal of the Korean society of civil engineers*, 33(3), 843-854. (in Korean).

Yu, Y., Cai, C. S., He, W., and Peng, H. (2019). Prediction of bridge maximum load effects under growing traffic using non-stationary Bayesian method. *Engineering Structures*, 185, 171-183.

Yu, Y., and Cai, C. S. (2019). Prediction of extreme traffic load effects of bridges using Bayesian method and application to bridge condition assessment. *Journal of Bridge Engineering*, 24(3).

Zhou, J., Shi, X., Caprani, C. C., and Ruan, X. (2018). Multi-lane factor for bridge traffic load from extreme events of coincident lane load effects. *Structural Safety*, 72, 17-29.

Zhou, J., Ruan, X., Shi, X. and Caprani, C. C. (2019). An efficient approach for traffic load modelling of long span bridges. *Structure and Infrastructure Engineering*, 15(5), 569-581.

Zhou, J., Chen, Z., Yi, J. and Ma, H. (2020). Investigation of multi-lane factor models for bridge traffic load effects using multiple lane traffic data. *Structures*, 24, 444-455.

Zhou, X. Y., Schmidt, F., Toutlemonde, F., & Jacob, B. (2016). A mixture peaks over threshold approach for predicting extreme bridge traffic load effects. *Probabilistic Engineering Mechanics*, 43, 121-131.

Zivkovic, Z. (2004). Improved adaptive Gaussian mixture model for background subtraction. *Proc. 17th International Conference on Pattern Recognition*, IEEE, Cambridge, UK, 2, 28-31.

초 록

김지환

건설환경공학부

서울대학교 대학원

교량은 사용수명동안 다양한 환경으로부터 여러 종류의 하중이 재하되며 노후화 및 열화 현상으로 인한 강도 저하 등의 상태 변화를 겪는다. 따라서 이러한 상태 변화를 지속적으로 관찰하고 이를 반영하여 교량의 신뢰도를 평가하는 것은 교량 유지관리에 있어 필수적이다. 여러 종류의 하중 중에서 강풍, 지진 하중 등의 재난으로부터 발생하는 하중을 제외한 일반적인 사용환경에서 가장 불확실성이 큰 하중 중 하나는 차량 활하중이다. 그러므로 확률론적 방법론을 통해 불확실성을 고려하여 차량 활하중을 정확하게 산정하는 것은 교량의 설계 및 상태 평가에 중요하다. 그러나 대부분의 연구들은 교량 부재의 강도저하를 고려하기 위해 부식 및 노후화 과정을 정교하게 모델링하는 반면 차량 활하중효과는 상대적으로 소홀하게 추정해왔다. 따라서 본 논문에서는 교량 부재의 강도뿐만 아니라 부재에 가해지는 차량 활하중효과도 정교하게 추정하여 신뢰도 평가를 수행하는 것을 목표로 한다. 이를 위해 본 학위논문은 구체적으로 교통환경에 따른 차량 활하중 변화 및 강연선의 부식으로 인한 휨 강도저하에 초점을 맞추어 PSC 박스 거더 교량의 사용수명동안 신뢰도를 평가하고 업데이트하는 프레임워크를 제안하였다.

먼저, 교량의 다양한 교통환경을 반영하여 차량 활하중을 산정하기 위하여 국내 세 지역(김천, 선산, 왜관)의 고속도로에서 1년동안 수집된 WIM 데이터를 기반으로 교량 차량 활하중 확률 모델을 개발하였다.

교통환경을 나타내는 WIM 데이터를 분석하여 핵심 랜덤 변수를 선정하고 확률론적 분석과 교통공학 이론에 기초하여 확률 모델을 구축하였다. 정체 교통 상황 시, 차량의 속도 및 차로 변경을 고려하기 위하여 마이크로 시뮬레이션 모델을 도입하였다. 수치 예제를 통해 개발된 모델은 엄밀하게 검증이 되었으며 설계기준의 다차로재하계수가 보수적임을 확인하였다. 또한 개발된 모델의 주요 변수들은 파라미터화 되어있기 때문에 주요 교통환경 변수의 변화가 차량 활하중효과 산정에 미치는 영향을 정량적으로 평가할 수 있음을 간단한 파라미터 스터디를 통해 확인하였다.

두번째로 시간에 따라 변화하는 교통환경에 주목하여 이를 지속적으로 고려하여 차량 활하중효과를 업데이트할 수 있는 베이지안 추론 기반 차량 활하중 업데이트 방법론을 제안하였다. 가우시안-역감마 분포, 베이지안 선형회귀, 깁스 샘플링을 이용하였으며 사전 분포의 믿음의 정도와 새 관측값의 정확도를 고려한 하이퍼파라미터 설정 방법을 제안하였다. 업데이트 예제를 통해 제안한 업데이트 방법론은 검증되었으며, 개발된 방법론을 이용하면 교통환경의 변화가 교량의 차량 활하중효과 미치는 영향을 정량적으로 평가할 수 있고 교통정보가 부족한 특정 교량(제2진도대교)의 차량 활하중효과를 더 정확하게 추정할 수 있음을 보였다.

세번째로 국내 장경간 교량의 교통환경을 반영한 새로운 설계 차량 활하중 모델을 제안하였다. 이를 위해 국내 장경간 교량들의 교통환경을 조사하고 2개의 중요 변수(중차량, 교통 정체)에 대해 교통환경 분류를 제안하였다. 각 교통환경에 대해 정체 교통류 시뮬레이션을 하여 차량 활하중 샘플들을 계산하고 이를 바탕으로 설계 차로하중 모델과 다차로재하계수를 제안하였다. 케이블교량의 영향선을 통해 차량 활하중효과를 산정하여 도로교설계기준-케이블교량편으로부터 산정된 차량 활하중효과 값과 비교하였다. 비교 결과는 현재 설계기준의 차량

활하중 모델이 보수적임을 보여준다. 이뿐만 아니라 단경간 교량부터 장경간 교량까지 적용가능한 통합 설계 차량 활하중 모델을 최종적으로 제안하였고 활하중과 활하중효과의 통계 특성을 계산하였다.

마지막으로 앞서 개발된 교량 차량활하중 산정 기법들을 이용하여 차량 활하중효과를 정확히 산정하고 강연선의 부식을 정교하게 모델링하여 강도저하를 고려한 PSC 박스 거더의 시간의존 신뢰도를 평가해보았다. 이를 위해 불확실성을 가진 여러 변수들을 고려하여 강연선의 부식을 모델링하고 부식환경 분류를 제안하였다. 적용 예제로 화양조발대교의 두 단면(정모멘트, 부모멘트)을 선정하였다. 대상 교량 주변의 교통 정보와 가정한 교통환경 변화 시나리오를 기반으로 대상 단면의 차량 활하중효과(휨 모멘트)를 추정해 보았고 거더의 휨 강도는 부식을 고려한 반복법을 통해 산정하였다. 극한한계상태1을 신뢰도 계산 시 한계상태로 이용하였으며 총 22개의 랜덤변수가 신뢰도 평가에 사용되었다. 시간의존 신뢰도를 효율적으로 계산하기 위해 Subset simulation과 최근 제안된 FORM과 샘플링 기반 방법론을 결합한 구조 신뢰성 방법을 사용하였다. 교량의 총 수명 100년동안의 시간의존 신뢰도를 평가하여 부식과 차량하중이 신뢰도에 미치는 영향을 분석하였다. 이를 통해 PSC 박스 거더 교량 신뢰도 평가 시 강연선의 부식뿐만 아니라 차량 활하중 역시도 중요한 요소임을 알 수 있었다. 또한 검사 및 모니터링을 통해 얻은 데이터와 정보를 이용하여 신뢰도를 업데이트해보았고 이 결과를 토대로 목표 신뢰도 수준을 만족시키기 위한 유지보수 전략을 수립할 수 있었다.

본 논문에서 제안된 교통 및 부식 환경을 고려한 데이터 기반 교량 신뢰도 평가 및 업데이팅 프레임워크는 교량 성능평가 기술 고도화 및 최적화된 유지보수 의사결정에 기여할 것으로 기대된다.

주요어: 교량 신뢰도 평가, Weigh-In-Motion, 차량 활하중, 교통하중, 시간 의존 신뢰도, 베이지안 업데이팅, 설계 활하중 모델, 도로교설계기준(한계상태설계법), 다차로재하계수, 교통환경, 데이터 기반, 강도저하, 강연선 부식, PSC 박스 거더교.

학번: 2015-22922